Optimization and Analysis of the Laser Isotope Separation Technique SILEX and Ensuing Proliferation Ramifications

By

Aaron Taylor Baldwin

B.S. Electrical Engineering
Valparaiso University, 2014

Submitted to the Department of Nuclear Science and Engineering
In Partial Fulfillment of the Requirements for the Degree of

Master of Science in Nuclear Science and Engineering

at the

Massachusetts Institute of Technology

June 2016

Signature of the Author: Signature redacted
Aaron Taylor Baldwin
Department of Nuclear Science and Engineering

Certified by: Signature redacted
R. Scott Kemp, Ph.D.
Norman C. Rasmussen Assistant Professor of Nuclear Science and Engineering at MIT
Thesis Supervisor

Certified by: Signature redacted
Charles W. Forsberg, Ph.D.
Principal Research Scientist, Department of Nuclear Science and Engineering
Thesis Reader

Accepted by: Signature redacted
Ju Li, Ph.D.
Battelle Energy Alliance Professor of Nuclear Engineering
Chair, Department Committee on Graduate Students

Optimization and Analysis of the Laser Isotope Separation Technique SILEX and Ensuing Proliferation Ramifications

By

Aaron Taylor Baldwin

Submitted to the Department of Nuclear Science and Engineering
on April 28, 2016 in Partial Fulfillment of the
Requirements for the Degree of Master of Science in
Nuclear Science and Engineering

ABSTRACT

SILEX is a molecular isotope separation technique that takes advantage of the differing energies of molecular excitations between different isotopes of uranium. This process occurs within a jet of supersonic gas, the gas includes both uranium hexafluoride and a carrier gas, and reportedly allows for high separation factors relative to other isotope-separation processes. Industry interests have argued that it could be readily commercialized. This topic is of particular interest because laser isotope separation technology has seen an increase in interest and funding over the last decade. This suggests some study of the risks that such a technology poses to society may now be in order. To inform policymakers about the risks inherent to a particular enrichment technology, it is necessary to understand the theoretical underpinnings of the technology before one can analyze the impact of the technology. Positions expressed in the current literature are ill-informed and range from deep opposition, citing concerns that SILEX poses greater proliferation risk than centrifuge or gaseous diffusion technology, to claims by scientists that it is not possible to use the technology to produce greater than 50% enriched U-235. A rigorous and holistic view of the technology will better inform policy by improving the accuracy of claims and identifying realistic solutions to problems the technology may pose. This thesis will seek to provide this deeply technical and holistic analysis of the technology, and will use the results to interpret the economic and proliferation impact such a technology will have on the global nuclear enterprise. The holistic analysis in this thesis will present several important conclusions: 1) the enrichment factor of SILEX is not quite as large as proponents suggest; 2) asymmetric cascade designs will be required; 3) SILEX may not be cheaper than centrifuge facilities; 4) SILEX will not be viable without improvements in laser technology; and 5) international policies may be the most effective means of curtailing enrichment schemes like SILEX.

Thesis Supervisor: R. Scott Kemp
Title: Norman C. Rasmussen Assistant Professor of Nuclear Science and Engineering at MIT

Acknowledgements

I want to thank my research advisor Dr. Scott Kemp for his support, extensive knowledge, numerous insights and valuable suggestions that helped to mold my conception of policy issues as they interact with enrichment technologies.

I want to thank Dr. Jeff Eerkens for his lifetime of work in laser isotope separation, and the valuable knowledge that he has shared during this project.

I want to thank the MacArthur Foundation for their financial support for this project, and their interest in completing detailed analysis of the enrichment process known as SILEX.

I want to thank my parents, Rich and Lisa Baldwin, for their support and encouragement throughout my education.

And finally, I want to thank the Department of Nuclear Science and Engineering for affording me the opportunity to join this top-tier community of learning and research.

Table of Contents

List of Figures

List of Tables

Part 1: Laser Isotope Separation

1.1. Introduction

The purpose of this research is to evaluate the laser isotope separation process known as SILEX (Separation of Isotopes by Laser Excitation). This evaluation will use a proposed design of the system found in current literature, which leaves some aspects of the design unexplored. The analysis done in this thesis will focus on two aspects of the design, the fluid dynamics involved in the supersonic flow of uranium hexafluoride gas, as well as the larger design of an enrichment facility, and associated proliferation concerns. Using the information from current literature a simulation is created to determine the optimal characteristics of the enrichment process. The results of this simulation will be used to develop a fluid dynamics model of SILEX using CD-Adapco's STAR-CCM+ modeling package. Then using the combined results from the fluid dynamics simulation and the physics simulation (from physics developed in [13, 15]) it will be possible to design an industrial-scale enrichment plant based on the design variables discovered through the simulation process.

Once the specifications for a cascade have been developed it will be possible to create several economic estimates of the cost of such a facility. These analyses will include an estimate of the impact on the localized cost of electricity as well as the impact on the nuclear fuel cycle cost. An estimate of the cost of each enrichment unit and the facility at large will be needed as a precursor. The difficulty of engineering a cascade of this design will impact the proliferation potential of the technology, and will engender an important discussion about enrichment control and the likelihood of weapons production. It is important to note that these broad policy questions do not have concrete answers, but using scientifically based predictions of the technology to inform policy is in the author's mind the best way to proceed. The final section of this thesis will discuss policy in broad strokes and attempt to identify methods to control and handle proliferation as well as make comparisons to other enrichment technologies.

Laser isotope separation technology has seen an increase in interest and funding over the last decade. This suggests some study of the risks that such a technology poses to society may now be in order. To inform policymakers about the risks inherent to a particular enrichment technology, it is necessary to study the theoretical underpinnings of the technology and analyze

the impact of the technology. Given a holistic view of the technology, and any characteristics deemed lacking, policy can be informed, and be able to make more realistic claims and create more apt solutions for risks that such a technology may pose. The positions in the current literature range from deep opposition to the technology, citing concerns that SILEX poses greater proliferation risk than centrifuge or gaseous diffusion technology [40], to claims by scientists that it is not currently possible to use the technology in production of greater than 50% enriched U-235 [34]. Literature and reports from companies like Global Laser Enrichment (GLE), suggest that the enrichment factor[1] of the system could be greater than two and even as large as five, compared to factors of 1.1–1.5 typically found in gas centrifuges. The simulations described in this thesis will attempt to address these concerns and answer the open questions about this technology. Using these answers a more informed view of the technology can be developed, which will further help to inform and instruct policy and security decisions in the sphere of international relations.

The existing gaps in the literature that need to be addressed focus primarily on the best operating conditions for the SILEX process. This is likely due to the classified nature of much of the SILEX process, which was deemed such by the Department of Energy when agreements between the U.S. and Australia allowed Global Laser Enrichment (GLE) to develop the technology in the United States. However, literature about the SILARC and SILEX process does exist. This is primarily from the researcher Jozef W. Eerkens, and several of his papers discuss the predicted physics and molecular behavior of particles in such an enrichment process [13, 14, 15, and 75]. These papers make suggestions on combinations of gases and temperatures that will yield high enrichment factors, but there is no quantitative optimization scheme to find the best operating conditions for a given gas mixture. There is also little discussion on the practical side of constructing a cascade of SILEX units for enrichment purposes; this is another gap that will be addressed as part of this thesis. Lastly, the projections of cost for LIS facilities have generally been vague, if not optimistic, in literature, and claims that SILEX will be cheaper than centrifuges have little quantitative backing. This is a third aspect of the technology that will be analyzed, and a more accurate depiction of the costs associated with such a facility will be attempted. It is

[1] The enrichment factor represents the ratio of relative abundance of a material between the input and output within a stage of an enrichment process. Relative abundance is equal to the natural abundance (or atomic percent) N, divided by 1-N. In short, R=N/(1-N).

important to note that this projection is intended to provide a more accurate estimation, but the prediction of large-scale project costs by nature are highly uncertain.

Such predictions and projections will be important components of the evaluation in this thesis. Although this thesis will be fairly broad in scope, it is important to note which areas are not analyzed as part of this thesis. There is no experimental attempt to verify the theoretical underpinnings of the molecular theory developed by J.W. Eerkens. The theory is assumed to be correct in so far as it applies to the simulations that are discussed. Other regimes for separation of different elements will not be described (such as for plutonium purification), as the work focuses solely on the use of separation techniques for uranium. No experimental verification of the enrichment capacity, nor the operational capability of an industrial cascade is undertaken. The work is primarily focused on developing a theoretical understanding of the characteristics of a SILEX system, based on accepted models of design and chemical engineering theory.

When beginning to analyze laser enrichment technologies it is important to keep in mind the four categories for effective laser enrichment posed by E.W. Becker (inventor of the Becker nozzle separation process). These categories are as follows:

1. The absorption spectrum shows a sufficient isotope shift.
2. A light source of appropriate wavelength, mono-chromaticity, and intensity is available.
3. Selective excitation can be extended to a permanent separation of the isotopes via a physical-chemical follow-up procedure.
4. The selectivity of the entire process is not significantly impaired by nonspecific physical or chemical processes [44].

These criteria affect every form of laser separation that has been identified in the past and keeping in mind these tenets, the success or failure of both past and present technologies can be better understood.

1.2. History of Laser Isotope Separation Research in the United States

Laser isotope separation research began soon after the discovery of the laser in the 1960s. However, it was not until the 1970s that powerful enough lasers were built to begin considering them for use as part of a separation technology. Laser intensity is significant because of the photon density that enables excitation, higher density enables higher excitation, and thus higher

throughput per unit capital. Laser enrichment research originated at Los Alamos National Lab in 1971, where small quantities of uranium were enriched using laser excitation [43]. Two different approaches were considered in the 1970s for using lasers to selectively excite certain isotopes; these general approaches were named AVLIS (Atomic Vapor Laser Isotope Separation) and MLIS (Molecular Laser Isotope Separation). The research and development task was divided between Lawrence Livermore National Laboratory (LLNL) and Los Alamos National Lab (LANL) to develop AVLIS and MLIS respectively. LLNL was successful in the late 1980s at producing significant enrichments using AVLIS techniques [14]. The AVLIS technique is based on differences in atomic energy levels between ^{238}U and ^{235}U. The first step of the AVLIS process requires uranium vapor to be produced using electron sputtering of metallic uranium, and the isotope selective excitation process (and subsequent ionization) of U-235 occurs by multi-step photon absorption. Several laser wavelengths are used in the process, all of which are in the visible spectrum. Then the ^{235}U ions are collected by a negatively charged collector plate placed above the gaseous uranium [15].

The physics behind electron excitation spectroscopy of uranium was well understood during AVLIS development, which likely contributed to its early success [14]. The development of the "process science, technology, and hardware was [apparently] so impressive" [24] that in 1985 the Department of Energy determined that LIS techniques had the best potential to provide a lower cost and more environmentally acceptable method for enrichment than other alternatives (i.e. gaseous diffusion plants or the centrifuge). This decision eliminated significant DOE interest in the research and development of a US centrifuge technology[2]. The first tests using full-scale components and systems began in the early 1990s [24]. At nearly the same time the Energy Policy Act (1992) transferred enrichment responsibility to the then quasi-government agency known as USEC (United States Enrichment Corporation). During this transfer of responsibility the AVLIS research project was placed on standby until July of 1994, when USEC gave permission for the project to continue into the development stage. Research continued on the AVLIS project through the late 1990s at LLNL where a commercial pilot plant was constructed and tested. The pilot facility was able to undergo continuous cycles of operation, ran for approximately 400 hours at a

[2] The current American Centrifuge Project centrifuges built by USEC, the AC-100, are loosely based on this 1985 design, the design which was abandoned in favor of laser enrichment research [1].

time, and produced enriched uranium at nearly the same cost as gaseous diffusion plants. Around $2 billion dollars was invested in the project, in total, to develop AVLIS technology and build a full-scale pilot plant [24] (Figure 1 shows the demonstration facility that was constructed at LLNL). However, funding for future development of the technology was stopped by the United States Enrichment Corporation (USEC) after discovering that it was unlikely to be economically viable due to high capital costs.

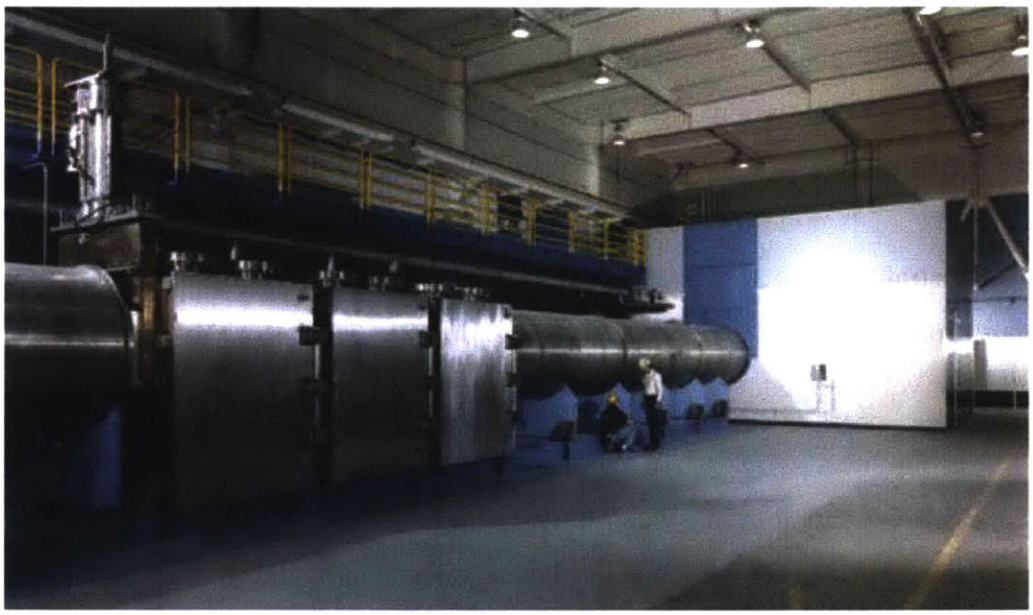

Figure 1. AVLIS demonstration facility at Lawrence Livermore National Lab.

MLIS techniques were also researched in detail in the United States; LANL began research on Molecular Obliteration Laser Isotope Separation (MOLIS) in the 1970s. Several other MLIS techniques have also been proposed over the years, beginning with CRISLA (Chemical Reaction Isotope Selective Laser Activation) or CHEMLIS (Chemical Laser Isotope Separation). The MOLIS technique involves the selective excitation and dissociation of UF_6 through the following reaction process:

$$^{235}UF_6 + nh\nu \rightarrow {}^{235}UF_5 + F$$

Following this dissociation CH_4 is added to scavenge the fluorine and inhibit the recombination of UF_6. This process requires several 16μm laser photon absorptions, a process called multi-photon dissociation (MPD). The absence of high power 16μm IR lasers required a Raman conversion of

a 10μm wavelength laser from a pulsed CO_2 laser [15]. The $^{235}UF_5$ can then precipitate and be filtered from the gas stream [43].

The CRISLA or CHEMLIS process of inducing an accelerated chemical reaction occurs by combining UF_6 with a slow co-reactant that can be accelerated by irradiating the gas using isotope selective vibrational laser excitations. Another proposed CHEMLIS scheme sought to use selective excitation and dissociation of metastable $^{235}UF_5$:X, where X was some form of halogen (i.e. Cl or Br). Neither of these CHEMLIS schemes were able to produce significant enrichments and were subsequently abandoned in favor of other MLIS schemes[3] [15]. CRISLA was later renamed Condensation Repression of Isotope Selective Laser Activation (CRISLA-2 or SILARC), which is the nearest precursor to SILEX and uses an alternative MLIS separation technique. SILEX (Separation of Isotopes by Laser Excitation) is a similar process to CRISLA-2, and was developed in Australia in the 1990s. After this point no new methods have been proposed and although many countries began research efforts into developing LIS technologies, no competitive technology has of yet emerged.

Today few economically viable LIS technologies remain, and all remaining options use MLIS techniques. SILEX technology has been licensed in the United States, and the licensee of the technology, GLE (Global Laser Enrichment), has received approval from the Nuclear Regulatory Commission (NRC) to construct a facility in Wilmington, NC [14]. Proponents of SILARC or CRISLA-2 technology (a nearly identical process to SILEX) claim that this methodology can be more economically competitive than SILEX because of lower capital costs [15]. The following section will describe the scientific process behind each of these two historical laser separation techniques.

1.3. Molecular Laser Isotope Enrichment

Molecular laser isotope separation (MLIS), where the absorption spectrum of the UF_6 molecule is the target for laser excitation rather than atomic electrons. However, the absorption spectrum of UF_6 is vastly more complicated than that of atomic uranium, as was used in the AVLIS technique, and thus complicates the separation method. The UF_6 molecule can undergo transitions

[3] The CHEMLIS process was able to produce some minor levels of enrichment, but it was not competitive with other enrichment technologies and the chemical process involved complicated procedures that limited the speed of the process [15].

between several vibrational and rotational states, which do not exist when dealing with solely atomic uranium [66]. The uranium hexafluoride molecule is an octahedron, where the uranium is at the center and the fluorines are equidistant from the center at ninety degrees from each other in the traditional octahedral Lewis structure.

The UF_6 molecule is able to vibrate in six different modes, of these modes only two have a movement that incorporates the uranium atom in the center of the structure, as seen in Figure 2. The movement of the uranium atom is necessary to create an isotopic shift in the absorption spectra to differ the U-238 from the U-235 [66]. The most useful mode for laser enrichment purposes, ν_3, is where the uranium atom and the fluorine atoms above and below it move up and down, while the other four fluorine atoms remain fixed in their plane. The normal modes of vibration can be seen in Figure 2.

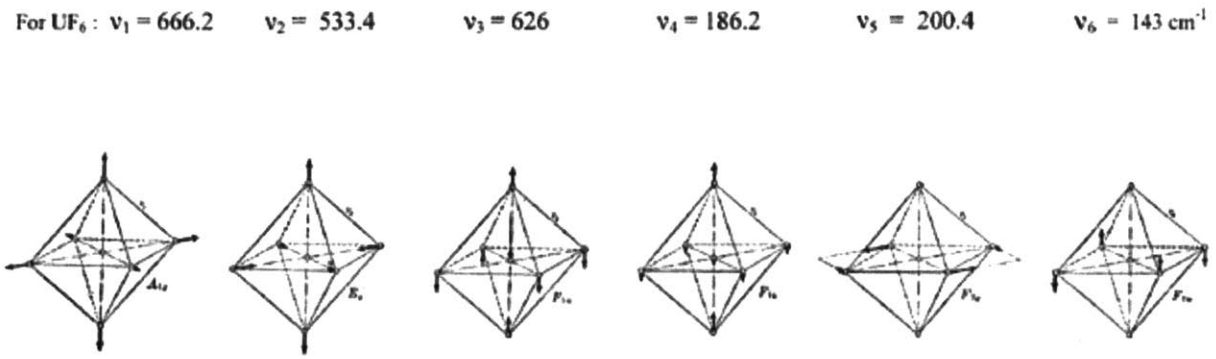

Figure 2. Six normal vibration modes of octahedral UF_6 molecules [66, 67]. The vibration modes of interest for laser separation are ν_3 and ν_4 because the four fluorine atoms in the plane move in identical directions.

Each of these different modes can be created by transitions in the vibrational quantum number, which increases by unity, or by change in the rotational quantum number, which can change by plus or minus unity. Peaks on the spectra represent transitions from different rotational quantum levels. Using the spectra, certain conditions can be applied to find the optimal location for $^{235}UF_6$ absorption, i.e. the location of highest ratio of cross-section. The key is to find locations on the spectra where a $^{235}UF_6$ absorption maxima occurs at the same place as a $^{238}UF_6$ minima. The difficulty lies in the fact that at standard temperature and pressure (STP) the spectra of the two molecules overlap significantly. This issue is due to the fact that at STP very few of the molecules

are in their ground state, which is necessary for a predictable spectrum and excitation to a specific vibrational state. Doppler broadening plays a significant role in this cross-section overlap and as temperature increases broadening does as well. The excited states that these molecules occupy at STP have absorption spectra that significantly overlap with $^{238}UF_6$. However, at lower temperatures the population of ground state molecules increases significantly[4] (as seen in Figure 3) and the absorption spectra of $^{235}UF_6$ and $^{238}UF_6$ begins to become better defined (due to the convergence of molecules from many states to the ground state and reduced Doppler broadening), thus creating a region of discernibility that is advantageous at some narrow line spacing [66].

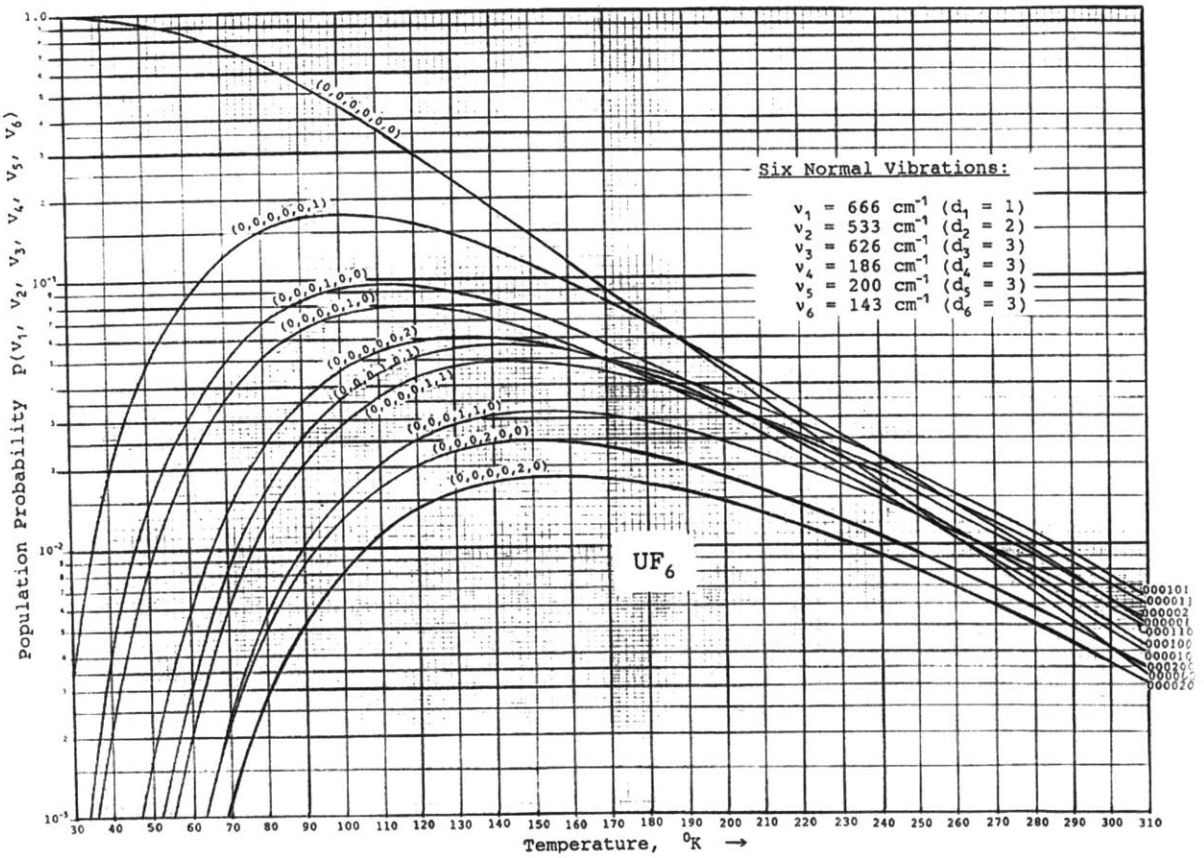

Figure 3. Population of UF_6 in each energy state given temperature [67]. The relevant state is {0,0,0,0,0,0}, which represents the ground state, the graph shows a probability of 0.99 for molecules to be in this state at temperatures below 60 K. This is important because the larger the population the more efficient the laser excitation process can be at enabling ν_3 excitations.

[4] Using the Stefan-Boltzmann equation the ratio of $N_2/N_1=\exp(-(E_2-E_1)/kT)$ can be found for the two lowest molecular energy states for UF_6. If the ratio is analytical computed, using NIST values; the value is equal to .001626, which is in agreement with the population probability at 30 K shown in Figure 3. The figure suggests .002% of the molecules are in the first excited state which is only slightly more than the analytical estimate.

Using the information in the spectrum of $^{235}UF_6$ and $^{238}UF_6$ at lower temperatures a target region can be identified that has both good isotopic separation and also corresponds to a manufacturable laser wavelength. The LIS process would also need to be able to cool the UF_6 to low temperatures in practice: usually to below 50 K to maximize the population of molecules in the ground state, and according to Figure 3, and footnote 4, such a temperature will result in a ground state population of >99%. Such temperatures can be reached through supersonic expansion of UF_6 diluted in a carrier gas, where the rapid cooling of the high gamma monoatomic gas helps to cool the UF_6. In the SILEX process, a supersonic nozzle is used to adiabatically expand the gas which lowers the temperature enough to maximize the ground state population [66] for appropriate lasing conditions within the core of the flow.

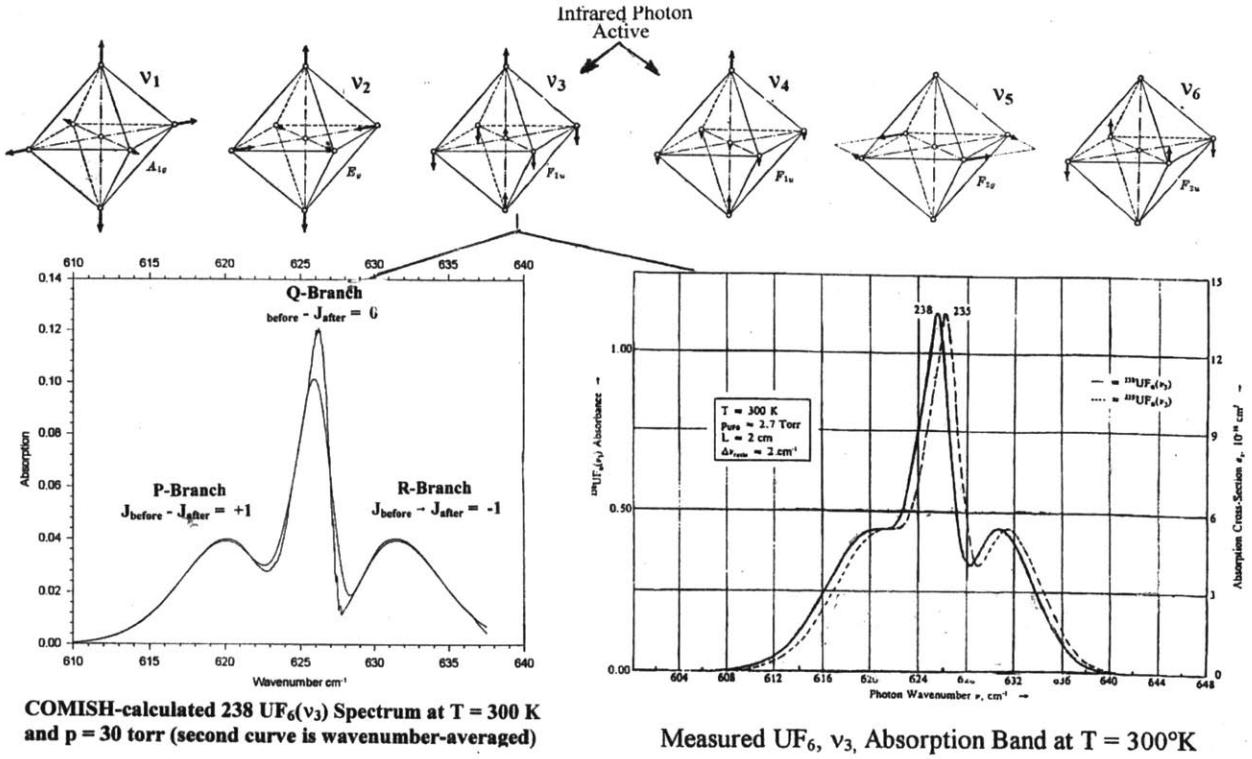

Figure 4. Main Spectral Features of Octohedral UF_6 Molecules [67]. These two graphs show the theoretical and measured effects of doppler broadening on the spectrum of UF_6 istopes; at 300 K the overlap is so advanced that photon absorption at ν_3 enabling seperation is highly improbable.

Excitation of supersonically cooled $^{235}UF_6$ molecules is possible through the absorption of laser photons by the molecule while it occupies the ground state. The photon source, an infrared

laser, is required to produce a wavelength resonant with a ν_3 transition. In the case of SILEX, a 16μm laser is required. The spectrum point of highest cross section is what determines the required wavelength (see also Figure 6). However, a difficulty arises in manufacturing a laser that is capable of producing that particular wavelength at an intensity that will make the process economical. Two main categories of lasers exist, continuous and pulsed wave. The continuous laser is one which the output power is considered steady when averaged over a significantly long time period (nanoseconds) [74]. The pulsed laser category refers to any laser that is not able to operate in continuous mode and produces optical power in pulses at some particular duty cycle, the pulse repetition rate for these lasers can range from femtoseconds to seconds. The prefered type of laser for an enrichment system would be one that can operate continuously, providing a simpler path to exciting a continuous stream of molecules, reducing stress on optical components, and eliminating the need to pulse the supersonic flow. By contrast, a pulsed laser decreases the total irradiation time and decreases the excitation efficiency. This is primarily an engineering consideration that simplifies the separation apparatus, rather than improving the physical phenomena.

Several types of lasers exist that produce light in the infrared spectrum, which is the desired area of operation for the SILEX process. A CO or CO_2 pumped continuous CF_4 laser is one option, however the lasing line is at 615.1 cm^{-1} rather than the 627.7 cm^{-1} that matches up with the $^{235}UF_6$ absorption spectrum. Such a laser cannot be shifted using alternative processes like Raman conversion because a physical medium to produce the up-scatter is not available in the applicable range [15]. Another set of options includes the hydrofluoric laser driven cadmium-tellerium laser (OPO) and the PbSnTe semiconductor laser, both of these are capable of generating a 16 μm wavelength [67]. However, the power output, or laser intensity, is much too small to be of practical use in a enrichment facility. The laser power in these devices does not scale linearly, and are designed mainly for opto-electronic applications in semiconductors. Based on recent advances in the study of the Weyl point[5], photonic crystals may become capable of producing scalable,

[5] The Weyl point is a singular energy spectrum location of a "massless" particle and a characteristic of a Weyl semimetal, a specifically engineered solid state crystal that under low energy excitation produces Weyl fermions. These fermions are robust electrons, meaning there is a non-dependent capability to tune energies, thus a high degree of mobility. Single-mode lasers, at a large scale, would be a useful application of such phenomena [73].

configurable laser assemblies that meet the criteria for an enrichment plant, but it may be decades before such research comes to fruition [73].

Another possible option is the free-electron laser (FEL), an electron accelerator that is capable of producing the widest spectrum of lasing wavelengths, but even though this laser can produce high intensities and the correct lasing wavelength, its operational requirements present some difficulty to implement in a LIS scheme. FELs require electron accelerators (and shielding), which requires power from a klystron and the use of many vaccuum pumps [84]. Such a facility is large and likely to be prohibitively expensive. Physically large lasers, in general, are difficult to build because the larger a laser becomes the greater the number of modes that light can follow, which makes isolation of a particular wavelength increasingly difficult[6]. Although some of the lasers described in this section produce approprate lasing lines, no viable contender exists that meets both criteria of intensity and wavelength.

The current method of choice is to use the CO_2 laser, a well-known laser design that can incorporate very high intensity and which operates at a 10.6μm wavelength. This wavelength can be shifted to 16μm using a process known as Raman conversion. Raman conversion is the process of inelastic scattering of a photon to produce new photons at a different wavelength; typically Raman conversion is best suited to energy ranges in the infrared. Raman scattering occurs when a molecule in its ground state (or a low energy state) absorbs the energy of an incident photon. This results in the molecule moving to a higher energy state. The molecule will then relax back to its ground state, thus releasing a photon that represents the difference in energy between its excited state and ground state. The energy of this new photon is lower than the primary photon, and thus the wavelength is longer ($E=hc/\lambda$). In order to produce photons of 16μm wavelength from a CO_2 laser with initial wavelength 10.6μm (E=0.11698eV) a Raman scattering event must take place, but an intermediary material is needed to provide the conversion. Thus after the CO_2 laser production unit a Raman cell is placed containing the media that is capable of producing these secondary 16μm photons. The media that is likely used in the SILEX process is known as para-hydrogen [14].

[6] This is with the exception of FEL undulators [83].

Parahydrogen refers to H_2 with a particular nuclear spin state. This is a singlet state where the spins of the two atoms are in opposing directions. The parahydrogen, as a singlet state, is non-degenerate and produces the required photon energies at de-excitation from a rotational state. Parahydrogen is known for its excellent optical properties, and modern techniques allow for solid pH_2 deposition on surfaces within vacuum environments. The particular Raman conversion process used in SILEX was developed by Dr. R.L. Byer and his associates at Stanford University [85] (Raman Effect for Intense Focused Laser Beams passing through Cold Para-Hydrogen Gas):

$$h\nu_L(980\ cm^{-1}) + H_2 \rightarrow h\nu_L(626\ cm^{-1}) + H_2(\varepsilon_{rot}=354\ cm^{-1})$$

$$[10.2\mu m \rightarrow 980 cm^{-1};\ 16\mu m \rightarrow 626\ cm^{-1}\ (\nu=1/\lambda)]$$

Figure 5 shows an example of the construction of such a laser and the components that make it up, which is a fairly complicated setup.

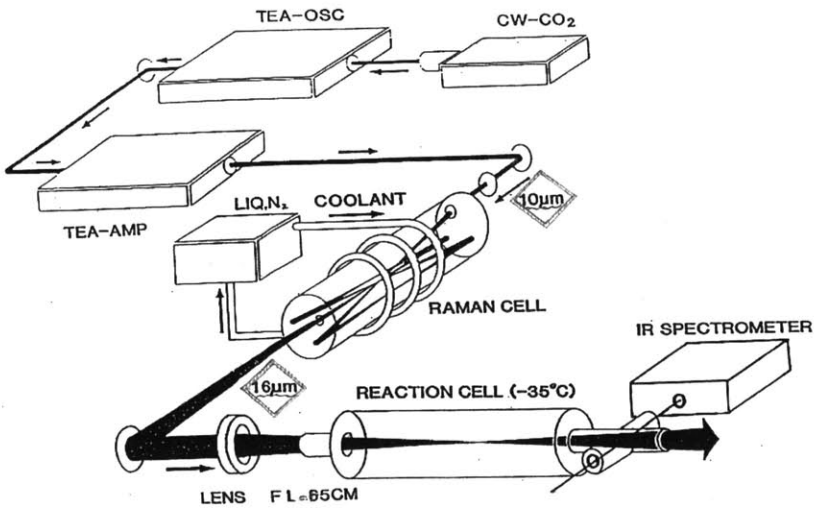

Figure 5. Raman Conversion and Production of 16μm CO_2 Laser [67]. The continuous wave CO_2 laser goes through an oscillator and amplifier and is then passed through the Raman cell, which excites the parahydrogen. The resulting wavelength is the required 16μm

The reaction cell shown in this figure provides an schematic representation of what the laser stage of the system would look like. The laser itself is pulsed at a repetition rate of around 300 Hz [34], which irradiates the supersonic flow of UF_6 and carrier gas traveling through the reaction cell. This slow repetition rate (in comparison to the pulse length) decreases the excitation

efficiency of the system, contributing to a low duty cycle (one of the main problems with the SILEX system). One possible solution to the slow pulse rate would be to have many lasers operating at slight offsets to ensure a more continuous irradiation of the supersonic flow. Another option would be to pulse the supersonic flow syncronously with the laser. Another problem is the CO_2 lasers are only 1% efficient and the Raman conversion process is about 25% efficient (in terms of photons available for excitation after conversion). This combination of low efficiencies contributes to a higher capital cost that may challenge the commercial viability of the SILEX system.

In addition to the MLIS process known as SILEX, the process known as SILARC or CRISLA-2 incorporates many of the same physical processes to achieve enrichment. The essential difference is the vibration mode being excited by laser absorption. In this case, the $3\nu_3$ band is used (the third excited level of the ν_3 branch), and at around 100 K overlaps with a CO laser line at 5.3μm, this can be seen in Figure 6.

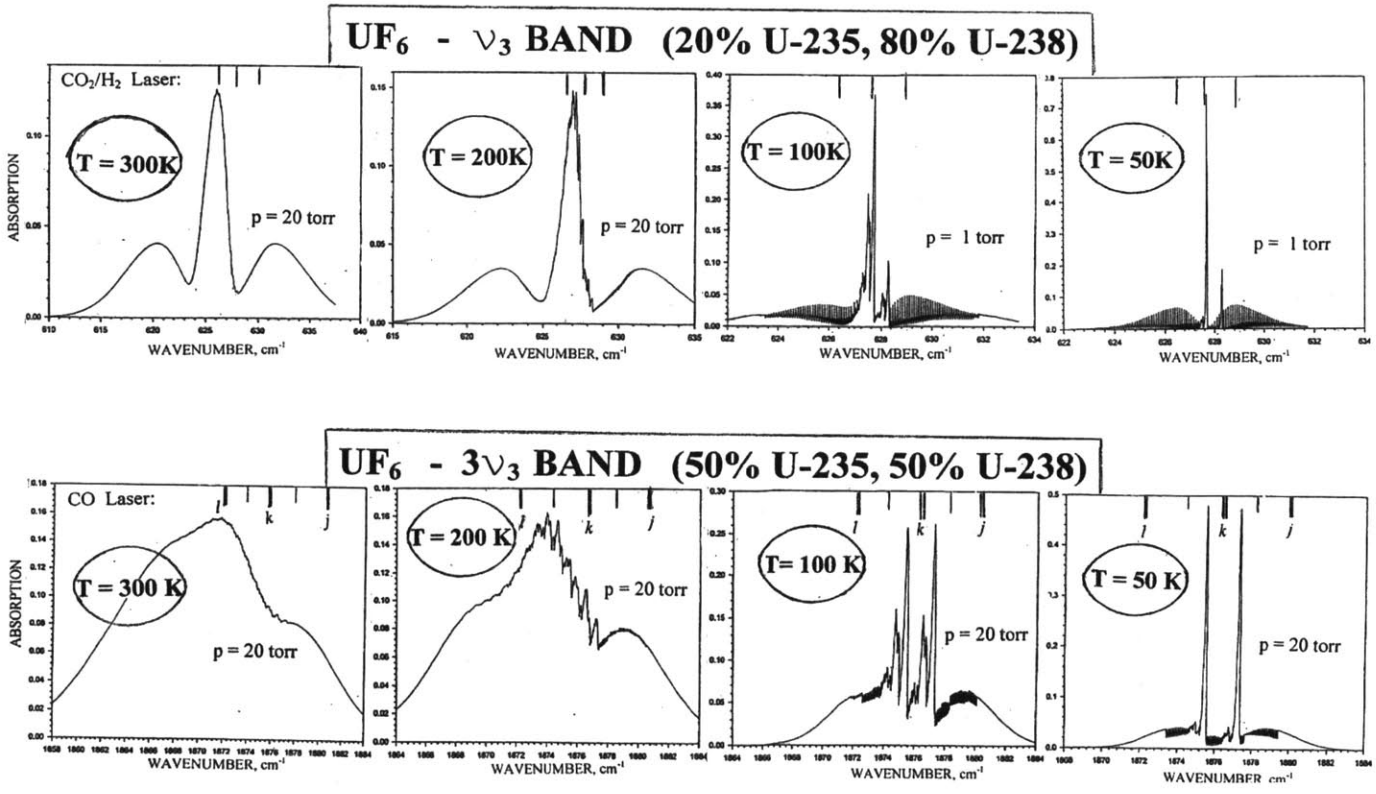

Figure 6. Cross-sections for SILARC/ SILEX excitations, (lasing lines are at top of graph) [67]. The top set of graphs describe the lasing bands and spectrum for SILEX ν_3 excitation, the lower set show the temperature dependent spectrum for SILARC and $3\nu_3$ excitation.

The carbon monoxide laser is a continuous laser, and no conversion process to another photon energy is necessary. The hope is that this laser would mitigate many of the engineering complexities associated with pulsed 16μm lasers. However, the cross section for $^{235}UF_6$ excitation at the $3\nu_3$ band is a factor of 10^4 smaller than the corresponding cross section for the SILEX process at 16μm [14]. Although the cross section is smaller, the continuous lasing capability as well as slightly higher core gas temperatures make the system easier to construct and operate. The continuous capability might allow the SILARC process to compete with SILEX even though its cross-section is considerably smaller.

1.4. Enrichment Physics Overview

For both the SILEX or SILARC process, the key molecular dynamics processes take place after the laser excitation stage. These effects are responsible for creating physically separated streams of enriched and depleted gas. At the macroscale a supersonic jet of gas moving through a low pressure media has different regions of flow with different pressures, temperatures, densities, and isotopic abundances. The excited molecules of $^{235}UF_6$ and other molecules (mainly the carrier gas) begin to cluster or condense at the low temperature of the expanding gas (Figure 7). The length of the chamber must be short enough to proclude full condensation, and is determined by the speed of the gas and the average time for condensation to occur. A representative chamber and flow for a single stage of the enrichment process is shown in Figure 7. The temperatures inside the gas flow can reach below 30 K, which drives a process called dimerization.

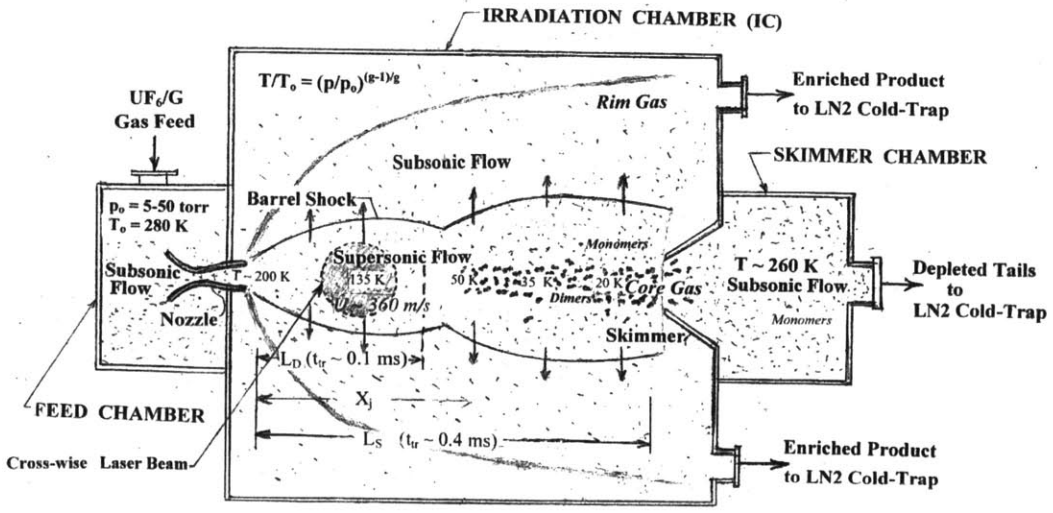

Figure 7. Depiction of Enrichment Process [67]

Dimerization is the initial stage of condensation of a gas, where particles begin to form bonds with each other, these bonds can be covalent or intermolecular. Intermolecular forces (VanderWaals) modeled by the Lennard-Jones potential describe the interaction that takes place [13]. The dimer is a set of two particles, it can either be a heterodimer, like UF_6:Ar, or a homodimer, like UF_6:UF_6. It is the inhibition of dimer formation by selective excitation of one isotope that drives the separation process. As dimers begin to form in the gas flow, either one of two processes can be used to create separation, depending on the particle that is excited. The enrichment system can be designed to excite $^{235}UF_6$ monomers by laser activation, or to excite $^{235}UF_6$:G dimers. In either case the result leads to an excited $^{235}UF_6$ paired with a molecule of carrier gas. It is important that a high percentage of the gas flow is carrier gas (95-99%) to maintain useful phenomena at the molecular level, more will be discussed in the following section about the consequences of isotope scrambling (i.e. negative effects resulting from a dimer of the form $^{235}UF_6$: $^{238}UF_6$).

Once a dimer has been created with an excited $^{235}UF_6$ particle it undergoes a process of rapid dissociation as the vibrationally excited $^{235}UF_6$ transfers its energy into translational motion, a process called VT conversion. The resulting monomers have higher kinetic energy, and the partitioning of energy depends on the mass of the carrier gas (the heavier the carrier gas, the higher the velocity for the uranium-bearing particle). The conversion probability (s^{-1}) of the excited particle also depends on the carrier gas used and the temperature, Figure 8 shows these relationships.

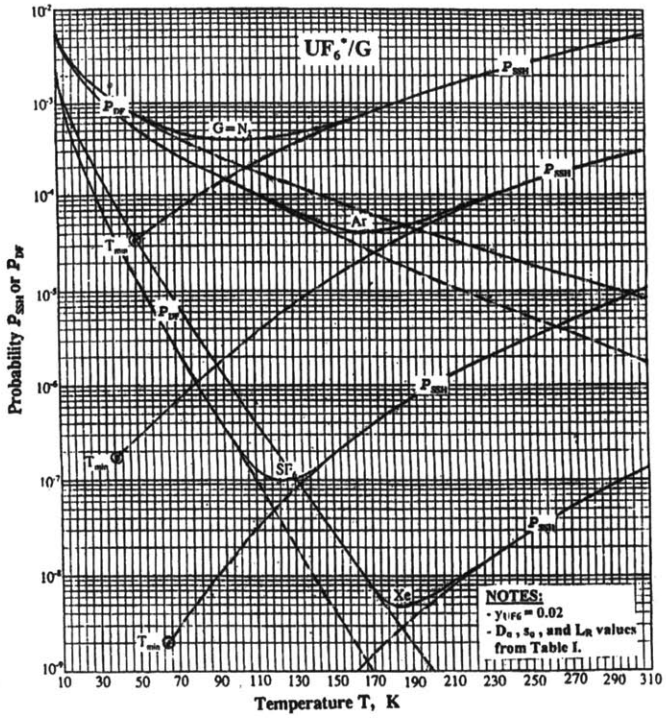

Figure 8. VT Conversion Probability given Temperature and Carrier Gas [67]

During dissociation the UF_6 recoils and becomes more likely to appear in the outer regions or escape the supersonic gas flow. Thus the gas on the outside of the flow becomes enriched to a higher percentage of $^{235}UF_6$ and can be separated from the rest of the gas flow through the use of a stationary skimmer at the end of the chamber (Figure 7). The molecular progression required has three distinct stages: laser excitation, dimer formation, VT dissociation (for monomer excitation) or alternatively dimer formation, laser excitation, VT dissociation (for dimer excitation). The process is outlined in Figure 9 below for both types of processes, using a carrier gas of Xenon. The times are significant because of the length of time that it takes for the gas to flow through the irradiation chamber.

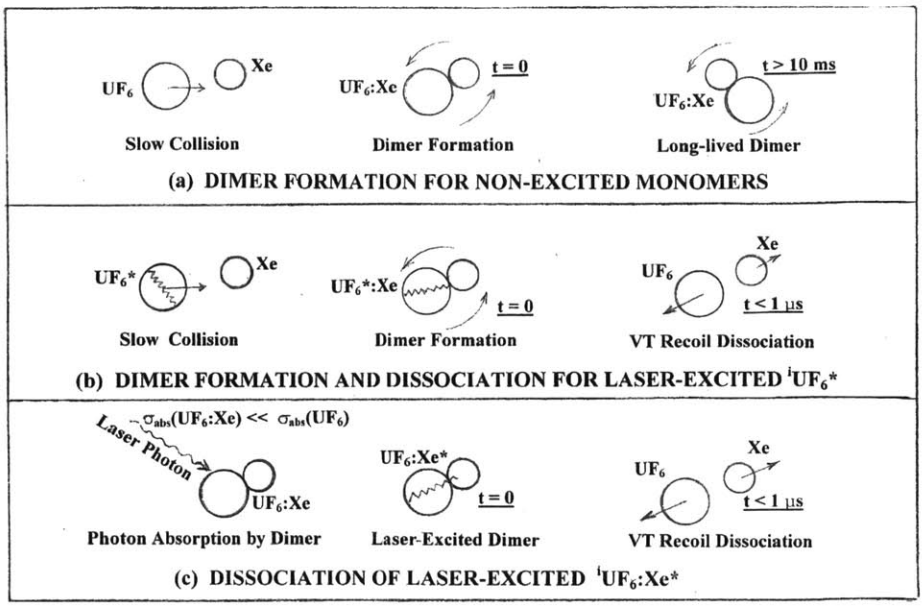

Figure 9. Dimerization process for excited and non-excited monomers [67]

However, this simple cycle does not relate the entirety of the reactions that can (and do) occur within the supersonic flow. When the monomer $^{235}UF_6$ is first excited there are several types of interactions that can affect the future enrichment yield. Spontaneous emission of a photon is a probable event that can de-excite the $^{235}UF_6$ monomer and halt dissociation if a dimer were to form. Collisions between molecules also occur, these collisions may form dimers, or may be primarily elastic encounters. Of particular interest are collisions between molecules of uranium hexafluoride but of different isotopes. The formation of dimers between uranium isotopes, where the $^{235}UF_6$ molecule is excited, can cause isotope scrambling, a process which leads to the transfer of energy to the $^{238}UF_6$ through a direct specular resonant vibrational-vibrational energy transfer (see Appendix 5.5). In order to minimize isotope scrambling a high percentage of the isotopic composition of the gas must be an inert carrier gas. It is important to also note that not all particles will necessarily form dimers within the flow, the time that it takes the gas to travel from one side of the irradiation chamber to the skimmer is ~1ms. Dimers that are formed also collide with one another, and can cause each other to dissociate through elastic collistions. Also of note, not all $^{235}UF_6$ will be excited by the laser, the cross-section is on the order of 10^{-18} cm^2. These are all contributing factors to loss of enrichment potential within the system.

In addition, after the VT dissociation of the $^{235}UF_6$:G dimer, the epithermal $^{235}UF_6$ molecule must diffuse to the outer portion of the gas stream where it can "escape the jet." In essence the

molecule does not "escape the jet" entirely, it just escapes to the region of the flow outside of the cylinder of flow that is represented by the input of the skimmer, which separates the gas exiting the irradiation chamber. Thus, radial diffusion is the only means of diffusion that is of interest for computing escape populations. For each type of molecule (excited, non-excited, epithermals) there is a particular rate of diffusion out of this region of the jet stream. The epithermal migration rate of $^{235}UF_6$ is particularly relevant for enrichment factor calculations. This is because particles that have undergone VT dissociation will be above thermal energies, which are molecules of $^{235}UF_6$. This diffusion rate will be higher than other particles because the velocity of these particles is higher, due to increased translational energy. However, the diffusion of dimers also occurs, along with thermal monomers (which may or may not be previously excited epithermals, depending on the number of collisions) and these rates must also be taken into account. The populations of each of these molecular groups must be computed and used to determine the diffusion rates of particles outside the cylinder preimposed by the skimmer orifice. The enrichment factor and product cut can be computed using the diffusion rates of the different populations of molecules. It is also possible for multiple cycles of dimerization and dissociation to occur within the irradiation component of the flow. The speed of dimerization is less than a microsecond, and flow moves through the irradiation zone within a few microseconds. Also, later on the previously excited epithermal monomers may also rethermalize and again form dimers. However, these dimers will not dissociate again, due to the lack of vibrational excitation, but will still have a higher probability of already diffusing farther out of the center of the flow.

For information about the development of the equations that govern the physics processes that were discussed qualitatively within this section, see [13] or [75]. Also, a mathematical overview of [13] and of the equations described in [75] is provided in Appendix 5 of this thesis. These are the equations that were implemented in the simulations that were used to characterize the SILEX process and will be described in chapter 2.

1.5. Additional Light Scattering Concerns (Rayleigh and Mie Scattering)

Several physical phenomena affect the efficiency of the laser irradiation process. When the laser must pass through many consecutive flows, there is the danger that a significant portion of the photons are lost through reflection processes. Therefore, it is important to identify whether scattering on the supersonic flow, through the processes of Rayleigh and Mie scattering, has any

deleterious effect on the process. Mie scattering is the phenomena responsible for the low light penetration through media such as clouds. Scattering of light takes place when the wavelength is comparable in size (within an order of magnitude) to the particle that it interacts with. In the case of SILEX, the particle size of both UF_6 and the carrier gas is less than 10 Å in monomer form, whereas the wavelength is 16um. Therefore, the likelihood of Mie scattering on the supersonic flow is nearly nonexistent. However, Rayliegh scattering plays a larger role. Rayliegh scattering describes the elastic scattering of photons by particles that are much smaller than the wavelength of the light, which describes the SILEX conditions. The following equations quantify the contribution that the Rayleigh phenomenon makes to light removal from the system. The intensity I of the light, with wavelength λ, R distance to the particle, particle diameter d, and scattering angle θ, is:

$$I = \mathrm{I}_0 \frac{1+\cos^2\theta}{2R^2} \frac{2\pi^4}{\lambda^4} \left(\frac{n^2-1}{n^2+2}\right)^2 \frac{d^6}{2^6}$$

The Rayleigh scattering cross-section, the more useful equation for the SILEX process, is shown in the equation below, where n is the refractive index of the medium.

$$\sigma_s = \frac{2\pi^5}{3} \frac{d^6}{\lambda^4} \left(\frac{n^2-1}{n^2+2}\right)^2$$

Under the consideration that 95-98% of the flow is composed of a carrier gas, it is reasonable to use a noble gas, like Xenon, for the calculation of the cross-section. This is because noble gases are chemically inert, have specific-heat ratios and most importantly do not have infrared transitions. However, it is important to note that the actual cross-section will be slighty larger than the estimate using the carrier gas. The diameter of the UF_6 is larger than the carrier gas, Xe, by a factor of 1.71, which multiplies the cross-section by approximately twenty-five. The refractive index for Xenon is n=1.0008306, and the index for UF_6 is roughly equivalent [79]. The resulting Rayleigh cross-section for Xenon, using parameters λ=16μm and d=3.8 Å, provides a cross-section of $2.8659*10^{-37}$ cm^2. The cross-section for pure UF_6 is comparable. This cross-section when multiplied by the photonic production of a 1kW laser, ($\sim 10^{20}$ photons/s*cm^2), is on the order of 10^{-17} photons lost per second. This makes it clear that there is no significant deleterious contribution to the process due to Rayleigh scattering. This fact will be invaluable in the engineering design of a single SILEX enrichment unit.

Part 2: Engineering and Design Analysis

2.1. Optimal Conditions for SILEX Process

In order to determine the best conditions for operation of a SILEX system it was necessary to vary the inital parameters of the physics process and solve for the separative power of the device, and the ensuing enrichment factor and product cut. This could most easily be accomplished by developing a MATLAB simulation that incorporated all the physics equations that were described in the previous section. Furthermore, the simulation would also need to vary parameters such as excitation temperature, carrier gas pressure, and carrier gas type to determine the conditions which maximized the product cut and the enrichment factor. Such a program was created, and can be found in its entirety in Appendix 1. The best case operating conditions were found to be an enrichment factor of 1.712, a product cut of 0.21, mole fraction of 0.02 $^{235}UF_6$, with a carrier gas of Xenon at partial pressure .035 torr, at a minimum gas expansion temperature of 30 K, and a reservoir temperature of 300 K. The temperature and pressure operating conditions are used as parameters in the design the supersonic nozzle. A more detailed description of the MATLAB code is described in the following paragraphs along with optimal conditions for several different carrier gases (holding the ratio of UF_6 to carrier gas constant).

The purpose of the MATLAB simulation is to use the physics described in [13] to model the operational parameters and determine the optimal operating conditions (i.e. separative work, enrichment factor, product cut). The MATLAB simulation is the preliminary step to the STAR-CCM+ simulation, this is because target values for nozzle design are determined within this code. The MATLAB code falls short on determing some of the characteristics of the supersonic flow, such as the lasing location (zone of minimum temperature). This is where STAR-CCM+ fills the gaps, using the optimal pressures and target minimum flow temperature found in the MATLAB simulation to determine the flow characterictics. These variables are used to design the nozzle based on the input and output pressures required to create a zone of the required temperature. The MATLAB code only determines the minimum temperature and the outlet pressure flow values, then STAR-CCM+, based on these parameters, will produce a more reliable depiction of the flow behavior and provide a likely lasing location.

Within the MATLAB code, based on the physics described in [13, 75], some preliminary assuptions were made. The first assumption was the excitation scheme, where monomer excitation was chosen over dimer excitation. The power of the laser was another assumption, a 1kW laser was used. The laser power has some affect on the enrichment factor; however, a doubling of power corresponds to only a 2% increase in enrichment and no corresponding increase in cut, and as power is further increased there are diminishing returns. While the higher laser intensity does cause more excitated monomers, the population of epithermals is not directly related to the number of excited monomers [13], thus the low impact on enrichment factor. Two other variables were held constant, the length of the irradiation chamber (at 20cm) and the radius of the flow (at 1 cm), these were simply operational choices that only affect the general behavior (size, number of mach discs) of the supersonic flow.

The only other variables that were held moderately fixed were the molar ratio of UF_6 to carrier gas and partial pressure of the carrier gas. These were moderately fixed because they were found through an independent iterative optimization process. It was suggested by [13] that the molar ratio should not exceed 5% UF_6, then by iterating through several test cases a value of 2% was found to be the best operational value for any combination of gases. The same was done for the carrier gas partial pressure. These variables then became fixed values in the final simulation. Finally, by iterating through different values of minimum temperature and carrier gas the optimal conditions were found; these conditions can be seen in Table 2. Using the program found in Appendix 1, it was possible to run this optimization code to maximize the variables of interest.

These variables were the separative power (δU), enrichment factor (R_p/R_f), and the product cut. These variables are dependent on one another, so it was necessary to find the optimal balance for both, given the carrier gas, to determine the best operating conditions (that condition being the optimal point of separative work, ΔU). In Table 1 the maximum enrichment factors are displayed for each carrier gas, as well as the other variables of interest. The carrier gas pressure was fixed at the value of 0.05 torr because after this point the increase in pressure only led to diminishing returns in enrichment factor, which made little difference to the maximum value. The most notable point about this table is the low product cuts which occur at these "maximum enrichment factors," such low cuts would make production infeasible and require more complex cascades.

Table 1. Maximum Enrichment Values

	Product Cut	Enrichment Factor (N_p/N_f)	Enrichment Factor (R_p/R_f)	Minimum Flow Temperature (K)
Xenon	0.015	1.95	1.937	29
Argon	0.012	1.81	1.80	23
Sulfur Hexafluoride	0.009	2.142	2.123	27
Nitrogen	0.0078	1.854	1.843	20
Hydrogen	0.006	1.708	1.699	14
Helium	0.002	1.617	1.610	7

It is important to note that the maximum enrichment values are not the best means of optimizing the process, the product cut is the other variable of interest, and the closer its value is to 0.5 the better; this variable determines the type of cascade (asymmetric vs. symmetric) that will be needed to produce the desired results. Therefore, it is necessary to determine what the optimal conditions are to maximize both the enrichment factor and the product cut. Because so many input variables exist, it was necessary to first run the simulation found in Appendix 1 for multiple values of carrier gas pressure. Once determined empirically[7] the optimal carrier gas pressure was held constant at 0.035 torr for different optimization runs for each carrier gas. Table 2 shows the final results of the MATLAB code.

Table 2. Optimal for Different Types of Carrier Gas (pg=.035 torr=0.5 Pa)

	Product Cut	Separative Work (ΔU)	Enrichment Factor (N_p/N_f)	Enrichment Factor (R_p/R_f)	Minimum Core Temperature (K)
Xe	0.2045	45.15	1.712	1.703	30
Ar	0.2128	30.28	1.569	1.562	28
SF_6	0.2061	35.20	1.626	1.619	35
N_2	0.2095	19.76	1.464	1.459	29
H_2	0.2078	7.387	1.285	1.282	24
He	0.2155	.8406	1.094	1.093	19

[7] Empirically in this context means the pressure was determined by entering pressures at a large step size and running the program to find the best general value for high enrichment values. There is a general pressure zone of high enrichment stability, but outside values of ~0.1-0.01 torr, there is a significant impact on cut and enrichment.

The value of the enrichment factor determined here is one of the most important conclusions of this study. It is significantly lower than estimates proposed by proponents of LIS, and out of the 2-5 hypothesized range [15]. This is due to several constraints on the system, from physical phenomena to engineering design choices. In terms of physical constraints, as was discussed earlier, the laser does not excite every single particle of $^{235}UF_6$. The excitation rate was one of many variables computed as part of the MATLAB program, and was equal to $\sim 10^6$ excitations/s, a fairly low value, but representative of the excitation cross-section. Other physical effects like spontaneous de-excitation, elastic collisions, isotope scrambling, and diffusional losses represent the factors that affect the final isotopic output. The engineering design is constrained by the product cut, a value which should be close to either 0.25 (for asymmetric design) or 0.5. In order to ensure a high product cut it is necessary to sacrifice enrichment factor (hence the decrease from factors >2 to 1.5-1.8) because the two variables are dependent on one another. The resulting maximum factor, using Xenon, comes out to 1.703, which is still 20-50% higher than centrifugal units. Using these best case operating conditions, the temperature and pressure information was then transferred to a simulation of the fluid dynamics performed using the computational tool STAR-CCM+.

2.2. Optimal Aerodynamics with Carrier Gas (STAR-CCM+)

2.2.1. Nozzle design and application

In order to begin studying the fluid dynamics associated with SILEX process it is first necessary to discuss the engineering design behind the supersonic nozzle. The nozzle design is important because it regulates (1) the speed of the flow and (2) the flow shape as it expands. The velocity of the gas determines other characteristics like the temperature, density, and pressure throughout the supersonic flow. All of these characteristics are variables that need to be controlled, in order for the appropriate conditions to be tailored for the SILEX process. From the MATLAB simulation it is known that the flow needs to have a region with temperature at least 30 K, and that the carrier gas to be used is Xenon at molar abundance 0.98. STAR-CCM+ was used to facilitate the design of a nozzle and to validate that the nozzle produced the correct internal flow temperature, pressure conditions, and flow rate according the optimal characteristics, found in MATLAB, that would produce the best conditions for enrichment.

A supersonic nozzle, or de Laval nozzle, expands a gas from a high-pressure reservoir with a fixed temperature into a low-pressure expansion chamber. In the SILEX process, the expansion chamber is also the irradiation chamber. This chamber pressure, or backpressure, is regulated by pumps attached to the outputs of the vessel. The pressure differential is what creates the supersonic flow.

The nozzle is attached to the gas reservoir and begins converging, or decreasing in cross-sectional area, to a point of smallest radius. Due to the conservation of mass, the mass flow is constant at all points within the nozzle. According to fluid dynamics the mass flow rate, m-dot, is equal to the product of the velocity, the density, and the cross sectional area of the flow. As the cross-sectional area of the nozzle becomes smaller and smaller the velocity and density must both increase in order to conserve the mass flow rate. However, because of the effects of compressibility the density cannot increase ad infinitum, but reaches a saturation point where it cannot get any larger. At this point, the flow going through the nozzle becomes choked at Mach 1 and becomes irreversible. Ideally, this also becomes the waist-point for the nozzle, so as to maximize flow through the choked region. As the nozzle expands, the pressure and density of the gas decrease drastically as the velocity increases to supersonic speeds (once again to conserve the mass flow rate). A phenomenon known as oblique shocks causes the flow to drop in pressure non-linearly as the gas continues to expand. These shocks are also known as Mach discs.

2.2.2. Note on the Formation of Shock diamonds (Mach Discs)

Mach discs are due to the formation of standing waves in a supersonic, compressible gas flow. This flow pattern can be found in supersonic jet engines, or in flows traveling through a supersonic nozzle. Mach discs are shock fronts (abrupt density changes) that arise from standing pressure oscillations caused by a mismatch of exit pressure of the supersonic flow and the pressure of the ambient medium surrounding the flow. They are interesting to uranium enrichment because the pressure and density gradient that occurs normal to the flow direction. Inside the flow different layers of temperature gradient ensure particular energy states of particles, as was discussed previously. The flow either becomes expanded or compressed by oblique shock waves that occur at an angle to flow, once this angle becomes 180 or 0 degrees a shock wave normal to the flow causes the formation of a normal shock wave [68]. This location is where the shock diamond pattern occurs. At the normal shock wave the flow becomes compressed to such an extent that it

undergoes expansion in the next stage to form an expansion fan. At some point the expansion pressure reaches the ambient pressure which causes a reflection of the flow from the outer edge, called a contact discontinuity. The reflected flow begins to compress again, this time creating a compression fan. The flow will again reach a point where a normal shock wave occurs. This pattern of compression and expansion continues until turbulent shear forces at the edge of the flow (contact discontiuities) force the pattern to dissipate. The length of the flow pattern depends on the medium through which the supersonic flow is traveling, if the gaseous medium is at extremely low pressure and density then the shear force (force due to friction) is minimized and the flow can continue to form many additional Mach discs [68]. A depiction of this flow pattern is shown in Figure 10 below. Understanding this phenomena was relevant to understanding the flow behavior within STAR-CCM+ and understanding the expected behavior of supersonic flows for use in enrichment applications.

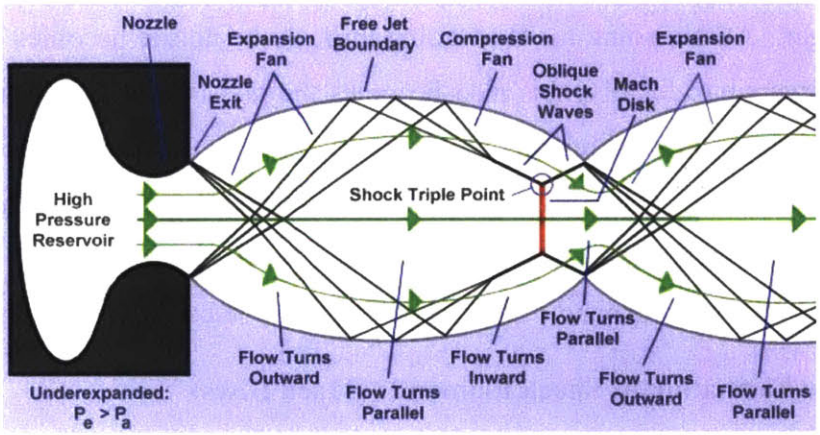

Figure 10. Mach disc formation and behavior [68]

2.3. STAR CCM+ Designs and Simulation Results

In order to verify, and extend the research done in [14], a fluid dynamics model was developed to test and understand the behavior of the supersonic flow within the irradition vessel of the SILEX system. After designing models of the nozzle, irradiation chamber, and outlets within the STAR-CCM+ software, it was possible to simulate the relevant fluid dynamics. Several parameters had to be defined and created within the model, this included the construction of the CAD nozzle and system as well as defining the relevant regions of the system. These regions included the stagnation inlet (the exit of the reservoir tank), the pressure outlet-which is the exit of the irradiation chamber (outlet pressure defined by the MATLAB result of .035 torr), and the body

(or boundaries/walls) of the model. At the same time a mesh of the system was created, using advanced options it was possible to decrease the size of the mesh in regions where fine detail was more important. One such region is the area where the flow diverges and converges as it moves through the nozzle. Another region where detail is significant is the main body of the flow until it reaches the skimmer. Using the surface mesher and the hexagonal mesh option a mesh of approximately 50000 cells was created. One example of the mesh is shown in Figure 12; however, several different simulations were created with different nozzles and chamber shapes, which caused the number of cells and shape to differ between simulations. Several different simulations of different characteristics, i.e. carrier gas, isotopic abundance, nozzle shape, pressure differential, were used to characterize the flow and the available options for an entity interested in developing a SILEX facility. The subsequent sections will detail several of the simulations that were run and the results of each respective model.

2.3.1. SILEX Conditions Nozzle 1

In the following simulation the following conditions were observed. The model described within this section, see Figure 11, is composed of a converging-diverging nozzle with a throat diameter of one centimeter, and a output diameter of two centimeters, the skimmer on the right side of the irradiation chamber is also two centimeters in diameter. The simulation can run using an axial symmetric solver, which cuts the model in half along the x-axis (the system is symmetric along the x-axis). The geometry of the system, or the CAD model, is shown below in Figure 11. It is important to note that the extended size of the outlets is not a depiction of reality, only a necessity to eliminate recirculation effects that are taken into effect in the simulation. These effects are allowed to occur in the simulation, even though they may not exist in reality, and can cause errors in the simulation. Therefore, it is necessary to elongate the outlets so that any recirculation can be minimized that may reach the primary supersonic flow. In reality a pump would maintain the outlet pressure and draw in the gases without recirculation occuring, but in STAR-CCM+ the only information that can be entered into the program is the pressure at the outlet, not if recirculation (or gases re-entering) the simulation is allowed.

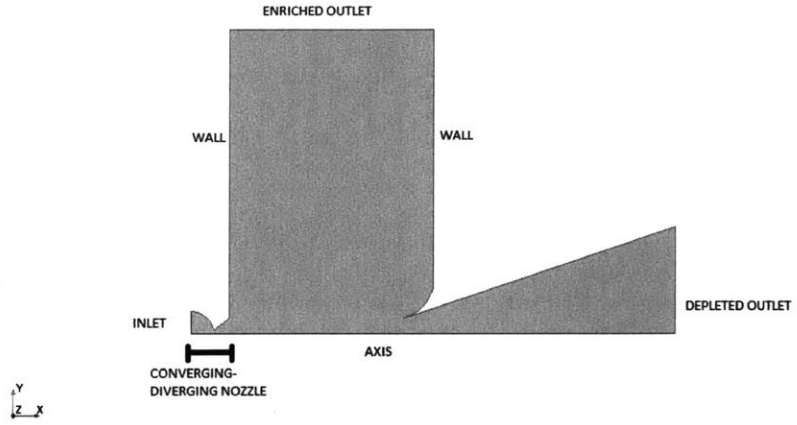

Figure 11. CAD Model of Nozzle Output and Irradiation Chamber

Figure 12 shows a representation of the computational mesh that was superimposed upon the model. The mesh is composed of polygons and hexagonal mesh cells with the highest density of cells in the main supersonic flow region. The smaller the cells the more refined the simulation will be in that region. Small cells are used in regions of interest; large cells are used at the outlets and away from boundary conditions to reduce computational effort. The total number of cells used in this mesh was 50,000.

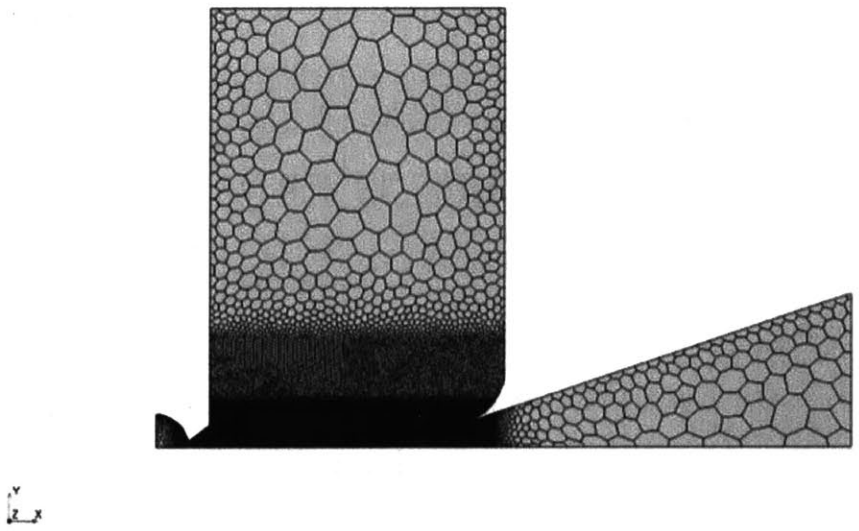

Figure 12. Mesh for Supersonic Nozzle Model and Irradiation Chamber

The physics conditions that were applied to this simulation included models intended for supersonic flow, given that the flow was at high speed and had a Reynolds number greater than 10^3, these included: the K-Omega turbulence solver, the axisymmetric model, coupled flow, coupled energy, non-reacting gas, multi-component gas, Reynolds-Averaged Navier-Stokes, SST (Mentor) K-Omega, and steady-state flow. Using these physics models, as suggested by CD-Adapco for low-mach supersonic flows [80], the flow was appropriately characterized.

The boundary values associated with this particular model consisted of a definition of a region as the wall (a non-permeable surface), the boundaries in this case were the walls of the model as shown in Figure 11. The output of the simulation was defined as the region where the gases exit the skimmer, both on the left side and top of the model, as is shown in Figure 11. The initial conditions were partially taken from the MATLAB simulation discussed earlier. The conditions taken from MATLAB included the exit pressure, 0.5 Pa, the carrier gas of Xenon, and the required minimum temperature of the flow. This temperature and the exit pressure were used to calculate the reservior pressure. Several different simulations were run with this particular nozzle model, they gradually increase in specificity with regards to the gas mixture characteristics. In the first run, Xenon was held at a molar concentration of 100%; using only Xenon is believed to provide a close estimate to the behavior of the true Xe+UF_6 mixture because such the Xe typically constitutes 95–98 mole percent of the gas). The use of only Xenon in the initial trial portrays an initial picture of the flow characteristics, but more specific simulations will also be described in the following sections. The pressure within the reservoir is 200 Pa, and the exit pressure (not the ambient pressure in the irradiation chamber) is 0.5 Pa. The temperature within the reservoir chamber, which is not depicted in Figure 15 is assumed to be 300 K or room temperature. The radius of the throat of the nozzle is 0.5 cm and the radius of the nozzle outlet and skimmer is 2 cm; these parameters are kept constant through all the simulations described in this document.

The pertinent results of this simulation are shown in the following three figures, which show the results after 4500 iterations. Figure 13 depicts the pressure across the system, which as intended shows an inlet pressure of 200 Pa and and low, near-vaccuum outlet pressure of .00101 Pa. This figure yields no more information than a verification that the boundary and pressure conditions are applied correctly and the nozzle functions as theoretically predicted. The pressure

differential determines the speed of the flow, and the location of shocks, which in turn determine the temperature of the flow. The temperature is a critical value to achieve a large ground-state population and will determine where the laser should irradiate the gas.

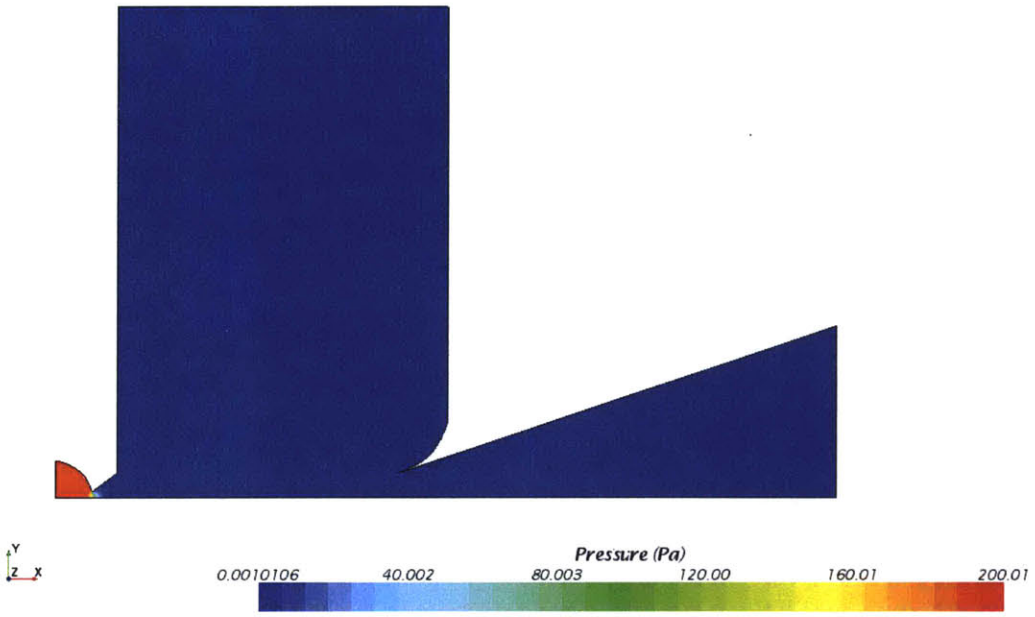

Figure 13. Absolute Pressure across Supersonic Flow

Figure 14 shows the mach speed of the flow as it travels throughout the irradiation chamber and through the skimmer. The mach cell that is seen at the exit represents the zone of highest speed flow and subsequently the zone of lowest temperature. A secondary mach cell can be seen near the entrance of the skimmer, this cell is only traveling at around Mach 2 at the center. The predictions of [13] suggests that only a few Mach cells will exist within the flow, which agrees with the results of this simulation. The speed of the flow is also relevant because it determines the average time which the molecules spend in the irradiation chamber and if there is enough time for the processes highlighted in molecular phyics section to occur. These processes include: spontaneous emission, dimerization, dissociation, and clustering. The amount of time that a given section of the flow spends inside the low temperature, low-pressure irradiation chamber has a signficant impact on the eventual enrichment factor. In this case the velocity matches closely to the theoretical value, so processes like clustering are significantly inhibited due to their comparatively long timescale.

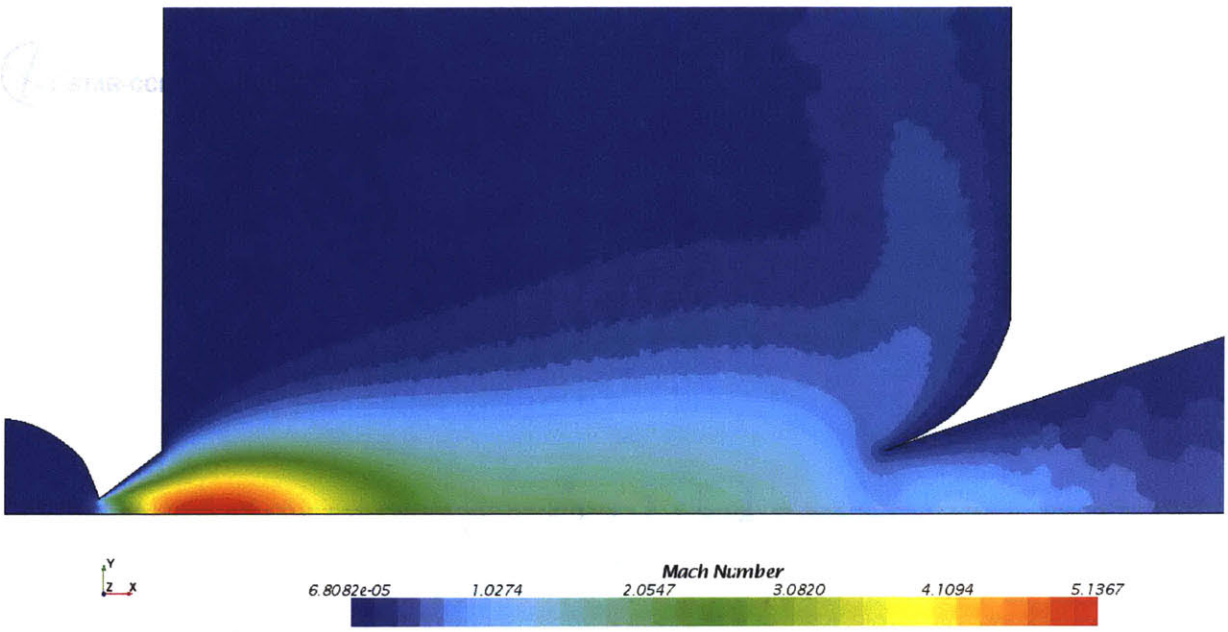

Figure 14. Mach Number of Flow through the SILEX system

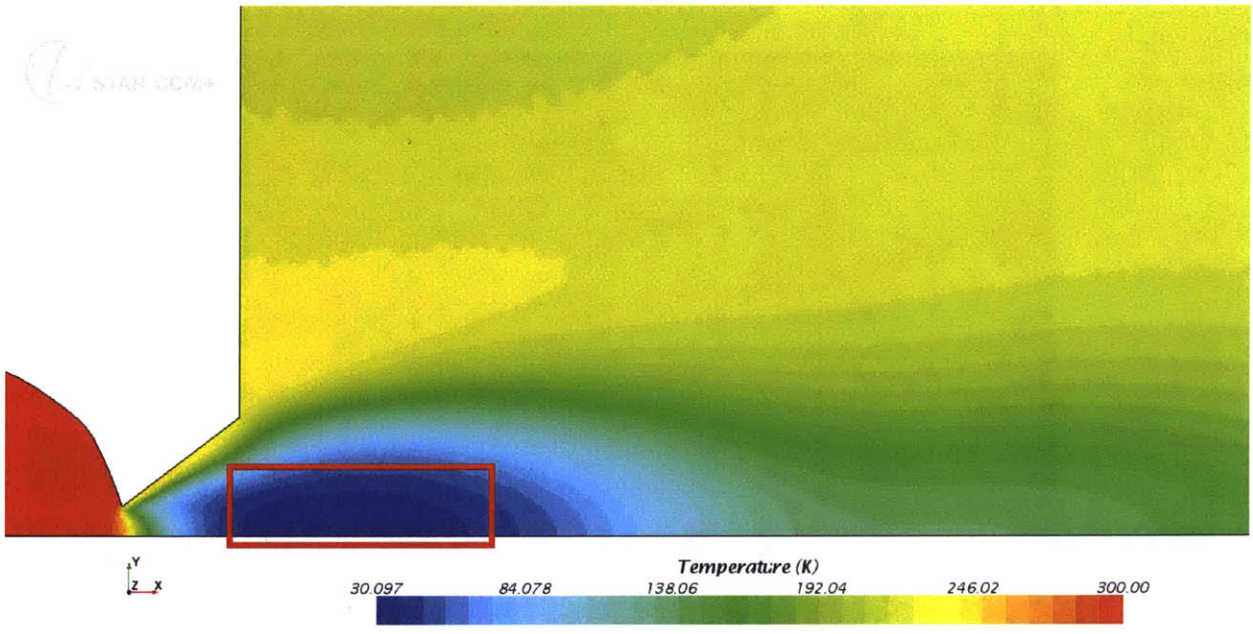

Figure 15. Temperature at Nozzle Exit

Figure 15 gives the gas temperature and describes the region that can be efficiently excited by the laser. Given the operating conditions from the MATLAB simulation, the temperature of the carrier gas Xenon that minimizes the doppler broadening overlap of the cross-sections of $^{235}UF_6$ and $^{238}UF_6$ is 30 K. Therefore, given the temperature at the center of the mach cell, as provided by Figure 15, it is possible to determine that the key irradiation region is cross-wise (or normal to the flow) at the center of the cell from approximately the nozzle exit to 2 cm within the irradiation chamber. This region is highlighted in red on the figure. Multiple lasers could be used to penetrate the length of this irradiation zone as it is a fairly large region of temperature conformity. This simulation model gives a fairly good indication of the behavior of the flow, and provides engineering information for a generic SILEX unit.

The above calculations were made under the assumption the gas is pure Xenon. It is important to also verify that a gas mixture of approximately 98% Xe and 2% UF_6 provides similar results.

2.3.2. SILEX Nozzle Model 2 (Inclusion of Uranium Hexafluoride)

The change made to this model of the flow was the addition of UF_6 to the flow composition. By molar fraction 2% of the flow is comprised of uranium hexafluoride in this simulation. The mach speed of the flow is shown in Figure 16.

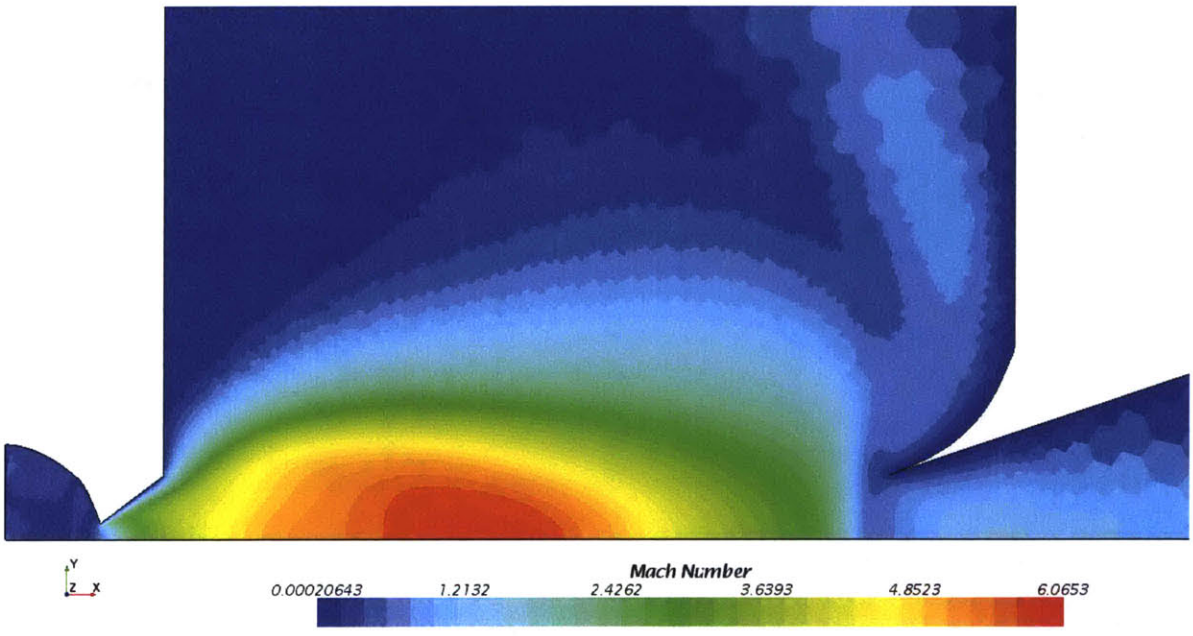

Figure 16. Mach number for supersonic flow with the incorporation of uranium hexafluoride in addition to xenon.

The temperature profile shown in Figure 17, shows a similar region at 30K, although it has been displaced by about 3 cm. The irradiation zone, with this further information should be fixed farther away from the nozzle output. This result is important because a model using only Xenon would lead engineering design to misappropriately place the irradiation zone too close to the nozzle and decrease the efficacy of the enrichment process. However, it is important to note that the results of the simulation provide an estimate or a first guess for the irradiation zone, the precise final irradiation location would have to be experimentally developed.

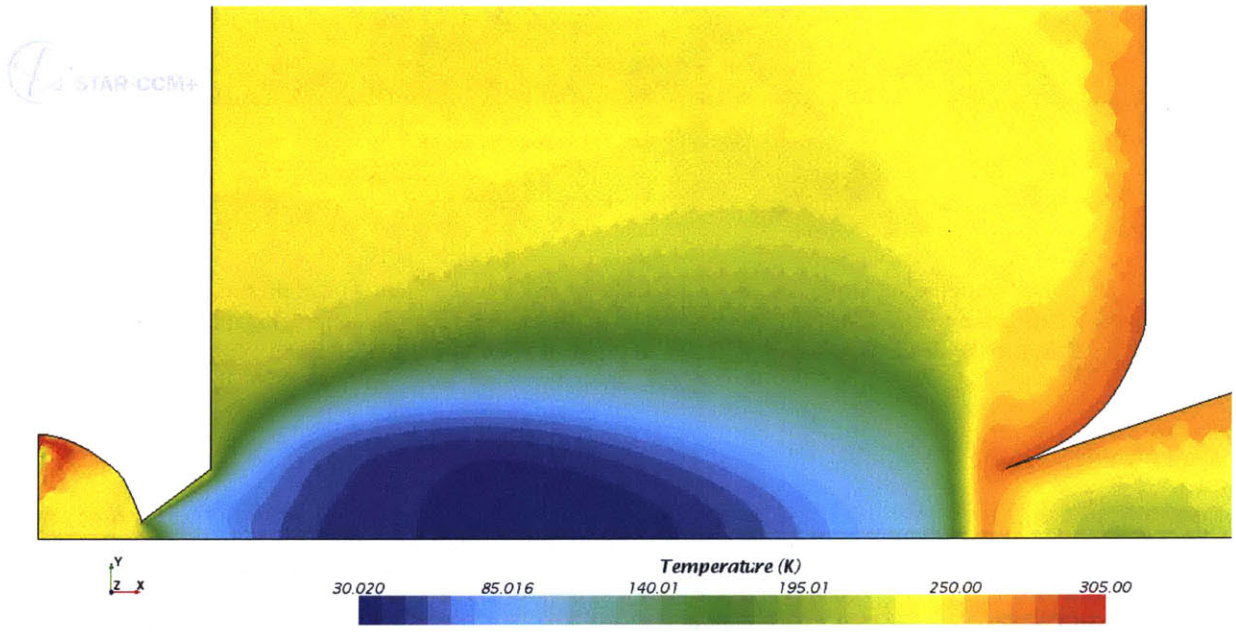

Figure 17. Temperature profile (K) for the supersonic flow of uranium hexafluoride and xenon

Figure 18 shows the concentration of UF_6 within the system. The concentration of UF_6 is highest at the exit of the nozzle and in the first third of the irradiation chamber, increasing from 2% pre-expansion to 18% post-expansion. This confirms the concentration of UF_6 in the irradiation zone is sufficient for laser excitations. However, it also suggests the probability of isotope scrambling may be higher in the irradiation zone because of the increased rate of $^{238}UF_6$-$^{235}UF_6$ collisions in that region of the flow. Additionally, there is increased risk of homogenous dimers (UF_6 :UF_6, rather than UF_6:Xe) which may affect the enrichment performance.

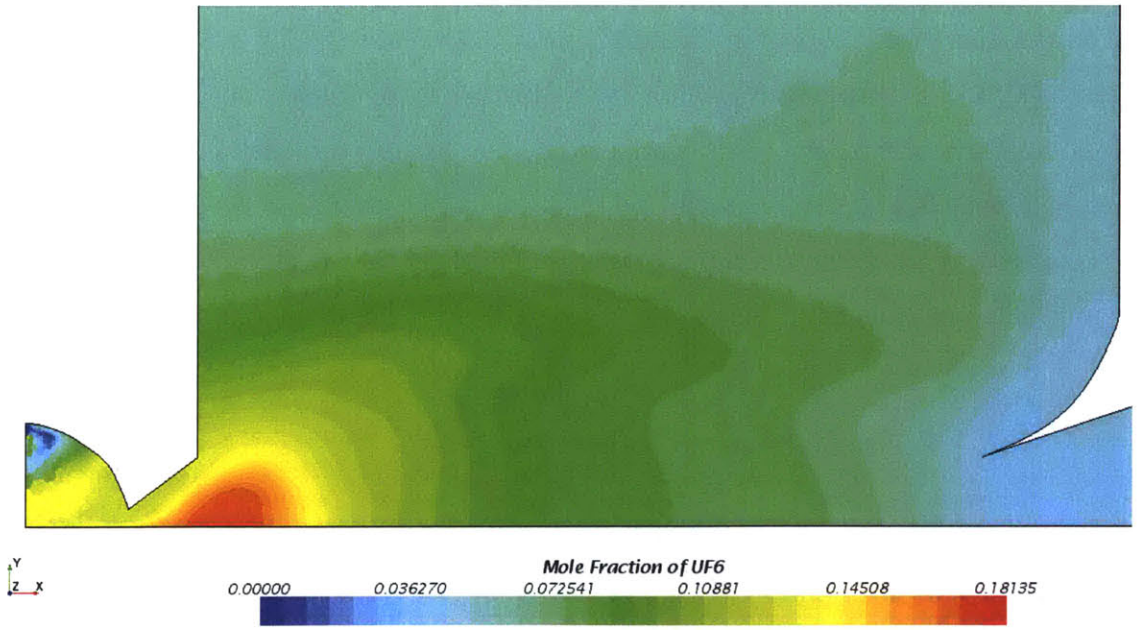

Figure 18. The molar fraction of uranium hexaflouride is shown in the plot above. The highest concentrations of UF_6 are seen in the diverging portion of the laval nozzle and at the exit into the irradiation chamber. The high mole fraction of UF_6 closer to the center of the flow is likely due to thehigher diffusion speed of the lighter Xe gas.

Finally, Figure 19, shows the pressure conditions of the simulation. The pressure at the outlets would need to be maintained by vacuum pumps to move the tails (depleted stream) and heads (enriched stream) of the flow to the subsequent stages in the cascade. The output pressure was maintained in the region at 0.1-0.5 Pa, as the pressure affects the speed of the flow, and in turn affects the temperature of the irradiation zone. While pressures in the system are within ranges readily attainable by vacuum pump under static conditions, there may be some difficulty in designing pumps that can operate at this pressure and still maintain the necessary flow rates. This will determine the maximum flow that can be incorporated into a single irradiation vessel with major implications for the capital cost of the system.

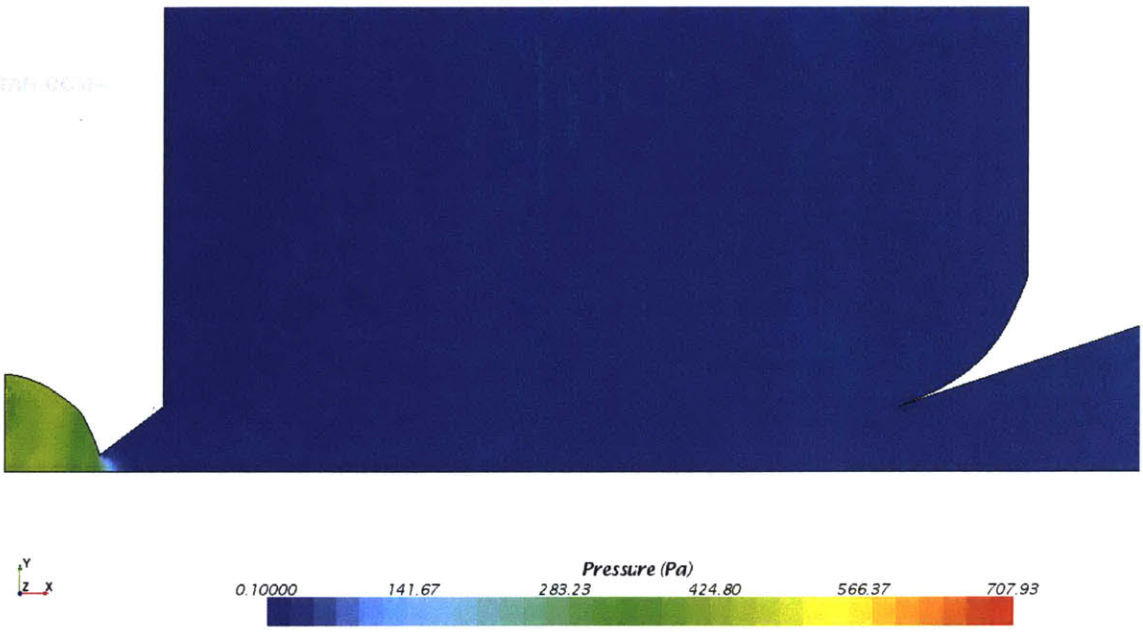

Figure 19. Absolute pressure of SILEX system

This simulation model provides a good indication of the behavior of the flow, and provides engineering information for a generic SILEX unit. However, the flow dynamics alone will produce some separation of isotopes even without laser irradiation. This can be modeled by including two gasses: $^{235}UF_6$ and $^{238}UF_6$ into the model.

2.3.3. SILEX Model 3: Inclusion of $^{235}UF_6$ and $^{238}UF_6$ to Model Becker Nozzle Behavior

This model uses the same chemical mixture of uranium hexafluoride and xenon as the previous simulation, but incorporates two isotopic species for UF_6 where 0.72 percent of UF_6 is of uranium-235, equivalent to natural uranium. Similar to the two previous simulations the mach speeds and temperature profile are comparable. The mach speed, shown in Figure 20, is at maximum around Mach 6.28, which is similar to the previous SILEX simulations. The velocity profile is nearly identical to the previous simulation and is of the expected form (according to the behavior of general mach flows).

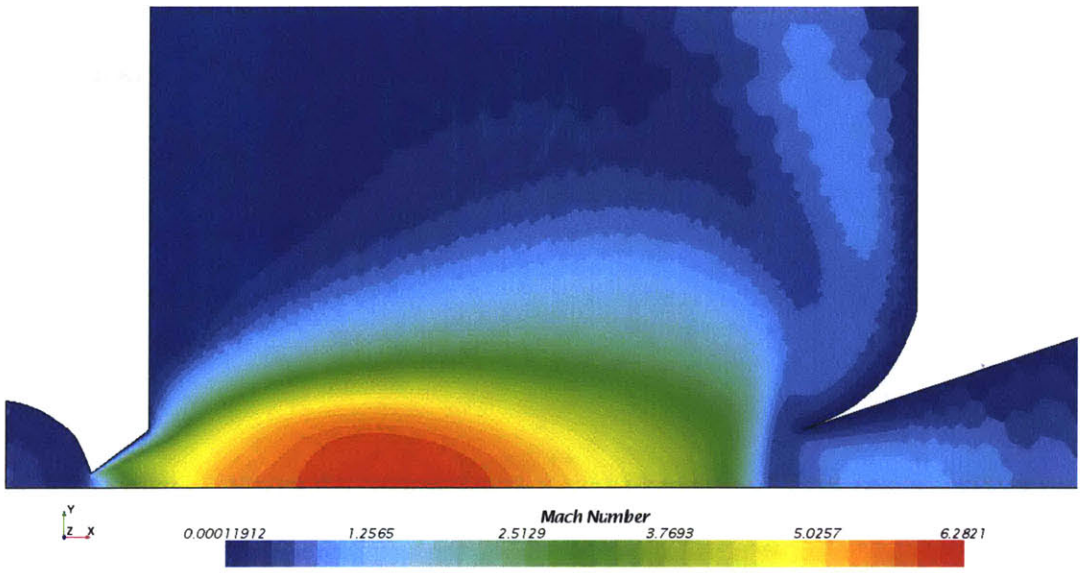

Figure 20. Velocity profile in terms of mach number for supersonic flow incorporating isotopic difference in uranium hexafluoride.

The next diagram, Figure 21, shows the temperature profile of the flow. This profile is similar to the previous simulation; and although the size of the irradiation zone is slightly larger, the location and shape of the zone is comparable. Using this information it is clear that precision in the placement of the laser irradiation zone is important, and that these simulations provide a reasonable estimation of the location.

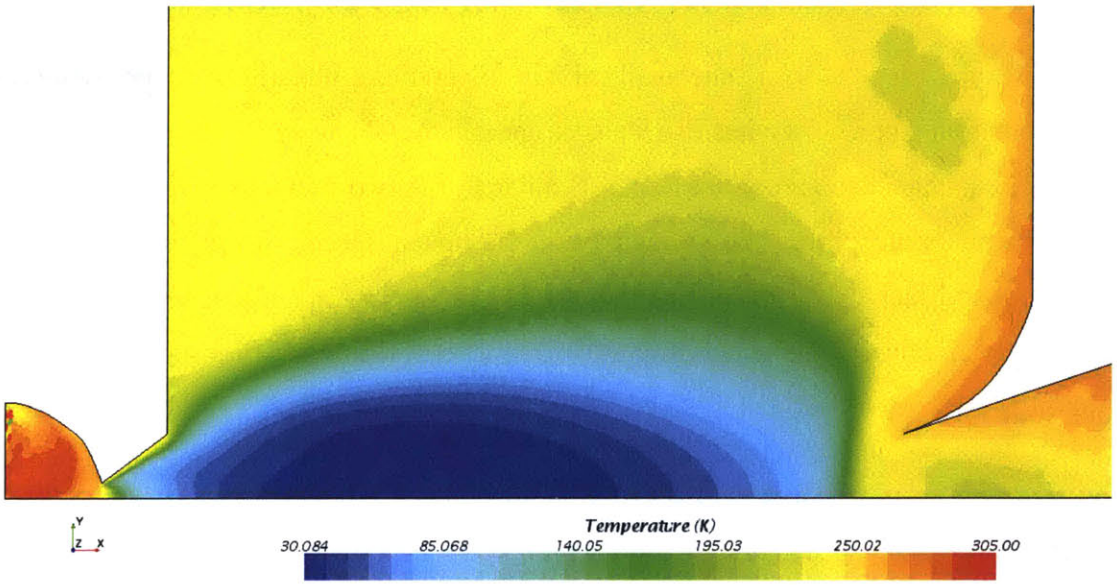

Figure 21. Temperature profile of supersonic flow with the inclusion of isotopic differences

The information provided by the STAR-CCM+ simulations is useful for engineering design and laser placement within the SILEX system. The incorporation of optimal operating parameters, determined by the MATLAB physics program, provides a clearer picture of the operating conditions that constrain the engineering design of the enrichment facility. Using the information provided by these simulations, a theoretical enrichment facility can be designed using cascade theory, which will be described in the following section. This will in turn be useful in answering important policy questions in reference to economic and proliferation issues related to SILEX.

Part 3: Cascade Overview and Derivation

3.1. Ideal Cascade Construction and Derivation of Generic Cascade Parameters

The basic premise of ideal cascade construction is that material balances (or isotopic compositions) of the flow of a medium from stage to stage are not mixed with material of different composition. The mixing of unequal enrichments results in an entropy that counteracts the process of enrichment. In a traditional cascade, the tails exiting from one stage may be introduced into the feed of a previous stage, and to be considered ideal these flows must be identical in terms of their isotopic mole fractions. The ideal nature of these cascades imposes a boundary condition on the mathematics that can be used to solve for the number of stages and mass flows necessary to achieve production of a certain specified product composition and amount.

An ideal symmetric cascade is one in which the tails are introduced to the feed of the immediately previous stage, and the product is fed into the immediate subsequent stage. Separating elements compatible with symmetric cascades must typically have a product cut in the range 0.40-0.50. However, for SILEX, a symmetric cascade design may not be optimal. It was previously determined in section 2.1 that the optimal product cut is approximately 0.20, suggesting a non-ideal cascade. This is similar to the Becker nozzle process, developed in the 1950s, which had a similarly low product cut (~0.25). For these processes an asymmetric, ideal cascade can be constructed, for example, a two-up one-down cascade, where the output (product) of a single stage (N) becomes the feed for a stage that is two levels up (N+2), and where the tails goes to the stage below (N-1). A diagram of such a cascade process is shown in Figure 22. The mathematical formulism that characterizes an asymmetric cascade of this type was published by Olander [77]. The following section describes the mathematical theory in greater detail for both the ideal symmetric cascade (used for gaseous diffusion and centrifuge processes), and the two-up one-down non-symmetric process.

3.1.1. Ideal Symmetric Cascades

In order to qualify as an ideal cascade, two conditions must be satisfied:

1. The separation factor at the output or heads (β) must be constant between stages.
2. The heads and tails that are mixed together from separate stages must have the same isotopic composition.

These conditions are the basis for the mathematical formulism that describes a cascade. The theory of cascades was developed by K. Cohen and is described in greatest detail in *The Theory of Isotope Separation* [69]. Only relevant derivations will be shown, but the author suggests using either Cohen [69] or Benedict, Pigford, & Levy [66] for further explanation of the derivation. Several factors are key in the description of a cascade. The heads factor (β) represents the ratio of isotopic abundance between the product stream of a stage and the feed stream. The tails factor (γ) represents the factor of isotopic abundance between the waste stream and the feed stream. The overall separation factor (α) is the ratio of isotopic abundance between the waste and product streams. All of these factors are in terms of isotopic abundance where N is the molar fraction and A (abundance) is equal to N/(1-N). The factors are described in terms of molar fractions and abundances here:

$$\alpha = \frac{x_p}{1 - x_p}\left(\frac{1 - x_w}{x_w}\right) = \frac{A_p}{A_w}$$

$$\beta = \frac{x_p}{1 - x_p}\left(\frac{1 - x_f}{x_f}\right) = \frac{A_p}{A_f}$$

$$\gamma = \frac{x_w}{1 - x_w}\left(\frac{1 - x_f}{x_f}\right) = \frac{A_w}{A_f}$$

It is important to note that authors tend to swap notations for these factors and it is important to be aware what each symbol describes in a particular context. In an ideal cascade the factors (γ-tails factor, α-stage separation factor) have the following relationship:

$$\beta = \sqrt{\alpha} = \gamma$$

The minimum number of stages in the cascade is equal to the following expression, where x_p, x_w, and α represent the isotopic abundance of the product, tails and stage separation factor respectfully:

$$n = \frac{2\ln\left[\frac{x_p(1-x_w)}{(1-x_p)x_w}\right]}{\ln(\propto)} - 1$$

And the number of stages in the stripping section (the section where tailings move through in order to satisfy the second condition of cascade operation), where x_f represents the isotopic abundance of the feed:

$$n_s = \frac{\ln\left[\frac{x_f(1-x_w)}{1-x_f}\right]}{\ln(\beta)} - 1$$

The number of stages in the enriching section can be described as:

$$n - n_s = \frac{\ln\left[\frac{x_p(1-x_f)}{(1-x_p)x_f}\right]}{\ln(\beta)}$$

The material, or flow rate in any given stage, n, can be determined as well, first the material flow in the enriching section:

$$\frac{N_{i+1}}{P} = \frac{1}{\beta - 1}\left[x_p(1-\beta^{i-n}) + (1-x_p)\beta(\beta^{n-i}-1)\right]$$

and in the stripping section:

$$\frac{M_j}{W} = \frac{1}{\beta - 1}\left[x_w\beta(\beta^{j}-1) + (1-x_w)(1-\beta^{-j})\right]$$

Using these equations a cascade can be mapped out in terms of the required throughput per stage, these equations have been put together to form a general MATLAB program to calculate the shape and size of an ideal symmetric cascade given parameters such as the required product composition and the stage separation factor of the technology. This program is found in Appendix 2, and is useful for analysis of gaseous diffusion and centrifuge technologies, and will be useful for comparisons made in the next major section.

The last important way to describe a cascade is in terms of its separative work. Separative work describes the total work done by the cascade to provide a certain amount of output at a particular composition. The units are defined as SWU (separative work units). In essence

separative capacity provides a measure of the rate at which a particular cascade is performing separation [66]. However, it is important to note that it does not represent the physical output product (kg/s) of the cascade. The expression for separative work for an ideal symmetric cascade is given as:

$$S = W(2x_w - 1)\ln\left(\frac{x_w}{1-x_w}\right) + P(2x_p - 1)\ln\left(\frac{x_p}{1-x_p}\right) - F(2x_f - 1)\ln\left(\frac{x_f}{1-x_f}\right)$$

Which is composed of the value function:

$$V(x) = (1-2x)\ln\left(\frac{1-x}{x}\right)$$

And the general expression for separative work:

$$Separative\ Work\ (SW) = Product * V(x_p) + Waste * V(x_w) - Feed * V(x_f)$$

It important to note also, that

$$F = P + W \text{ and } F = P\left[\frac{x_p - x_w}{x_f - x_w}\right]$$

3.1.2. Ideal Non-Symmetric Cascade: Two-Up One-Down Cascade

Cascades that operate at product cuts significantly lower than ½ can no longer take advantage of the symmetry provided in a traditional ideal cascade. For product cuts around ¼ to 1/3, like those in the SILEX process, or the Becker nozzle system, it is necessary to redesign the cascade in a non-symmetric form, while still maintaining the ideality of the system (i.e. there is no mixing between differing compositions). A two-up one-down cascade feeds material from the output of a stage to a location two stages above it, and the waste of a stage is sent to the stage below it. An example of this system is shown in Figure 22. The secondary output Q, is due to the two-up design, which forces the second to last stage to provide an output that does not feed to the next stage. The composition of this output is equal to $x_q = x_p/\gamma$. Like the traditional symmetric cascade there are distinct sections for stripping and enriching within the cascade.

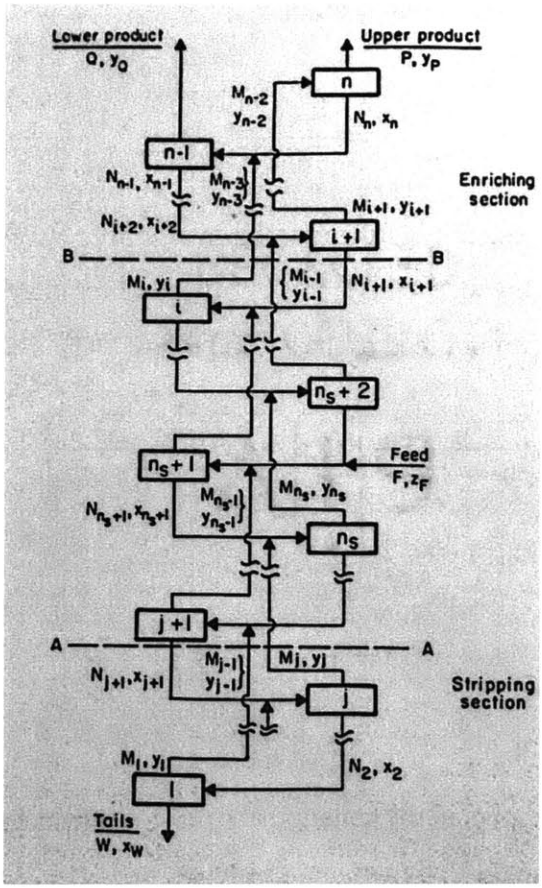

Figure 22. Example of a two-up one-down asymmetric cascade [66].

The derivation of the appropriate equations for such a cascade were determined by Olander [77]. The results of the equations are shown below, beginning with the calculations of the heads separation factor (β) and the tails separation factor (γ):

$$\beta = \alpha^{\frac{2}{3}}$$

$$\gamma = \alpha^{\frac{1}{3}}$$

Like the traditional symmetric cascade there are distinct sections for stripping and enriching within the cascade. The number of stages in the stripping section is described as:

$$n_s = \frac{\ln\left(\frac{x_f}{x_w}\right)}{\ln(\gamma)} - 1$$

And the number of stages in the enriching sections is:

$$n_e = \frac{\ln\left(\frac{x_p}{x_w}\right)}{\ln(\gamma)} - 2$$

The expression for separative capacity is determined in a similar way to the symmetric cascade described above, the only difference is the inclusion of the Q term as is seen in the expressions below, where Q represents the output feed of the second to last stage as is seen in Figure 22 above:

$$SWU_{2U1D} = W(2x_w - 1)\ln\left(\frac{x_w}{1-x_w}\right) + P(2x_p - 1)\ln\left(\frac{x_p}{1-x_p}\right) + Q(2x_q - 1)\ln\left(\frac{x_q}{1-x_q}\right) - F(2x_f - 1)\ln\left(\frac{x_f}{1-x_f}\right)$$

$$F = P + W + Q$$

$$Fx_f = Px_p + Wx_w + Qx_q$$

In order to find the flow rates shown in the equation above, it is necessary to provide some relations between the variables using the following expressions:

$$r = \left(\left(\frac{1}{\gamma(\gamma+1)}\right) + \left(\frac{1}{\gamma(\gamma-1)(2\gamma+1)}\right) - \left(\frac{1}{(\gamma-1)(\gamma+2)}\right)\right)\left(\left(-\frac{1}{\gamma+1}\right)^{n_S-1}\right) - \left(\left(\frac{1}{(\gamma-1)(2\gamma+1)}\right)\left(\left(\frac{1}{\gamma}\right)^{nS}\right)\right) + \left(\frac{1}{(\gamma-1)(\gamma+2)}\right)$$

$$s = \left(\left(1 - \left(\frac{\gamma^2}{(\gamma-1)(2\gamma+1)}\right) + \left(\frac{1}{(\gamma-1)(\gamma+2)}\right)\right)\left((-(\gamma+1))^{n-nS}\right)\right) + \left(\frac{\gamma^{n-n_S+2}}{(\gamma-1)(2\gamma+1)}\right) - \left(\frac{1}{(\gamma-1)(\gamma+2)}\right)$$

$$t = \left(\left(\left(-\frac{\gamma}{(\gamma-1)(2\gamma+1)}\right) + \left(\frac{1}{(\gamma-1)(\gamma+2)}\right)\right)\left((-(\gamma+1))^{n-nS}\right)\right) + \left(\frac{\gamma^{n-n_S+1}}{(\gamma-1)(2\gamma+1)}\right) - \left(\frac{1}{(\gamma-1)(\gamma+2)}\right)$$

Then using these three variables the flow ratios for the product and waste flows can be shown to be equal to the following expressions:

$$\frac{Q}{P} = \frac{\left(r\left((\gamma^{n+2}) - (\gamma^{n_S+1})\right) - s(\gamma^{n_S+1} - 1)\right)}{t(\gamma^{n_S+1} - 1) - r(\gamma^{n+1} - \gamma^{n_S+1})}$$

$$\frac{W}{P} = \frac{t(\gamma^{n+2} - \gamma^{n_S+1}) - s(\gamma^{n+1} - \gamma^{n_S+1})}{t(\gamma^{n_S+1} - 1) - r(\gamma^{n+1} - \gamma^{n_S+1})}$$

These equations have been implemented within a MATLAB code for the purpose of designing both a weapons cascade and a traditional cascade using the SILEX process, which will be discussed in detail, in comparison with other enrichment technologies in the section 3.2. These MATLAB codes can be found in Appendices 3 and 4 respectively. The mathematical results of the simulation will be useful in developing cascades for diffusion, centrifugal, and laser enrichment and for comparison based on difference in enrichment factor.

3.2. Comparisons of Enrichment Technology

Several modes for isotope separation exist today as a result of extensive research during the last few decades in the pursuit of a means to enrich the uranium isotope U-235 for energy and defense purposes, where most modern forms are based on ideal, symmetric cascades. One of the earliest forms of enrichment technology was called gaseous diffusion, historically this methodology was responsible for the majority of enriched uranium production in the United States. Gaseous diffusion uses barriers made of porous membranes to separate molecules of different isotopic mass. The holes in the porous membrane are smaller than the mean free path of UF_6. Using a pressure differential between the sides of the membrane allows for some of the gas to diffuse from the higher to the lower pressure side. This side is slightly higher in abundance of $^{235}UF_6$ because the mean speed of $^{235}UF_6$ is slightly higher than $^{238}UF_6$. These particles have equivalent kinetic energies on the feed side of the membrane, but because the masses differ slightly the lighter particles, the $^{235}UF_6$, have higher velocity and thus higher incidence against the membrane, which allows for slightly higher transmission among this isotopic group. Roughly half of the feed material flows through the membrane into the lower pressure chamber. Due to the fact that the kinetic energies are equivalent the mean free speeds of the molecules are equal to the inverse square root of the masses. These values contribute to the calculation of a separation factor,

α, per stage, where the fraction of $^{235}UF_6$ passing through the membrane over the fraction remaining behind provides an indication of the separation. This factor is represented by the ratio of the mean free speeds of the molecules, as seen here.

$$\alpha = \sqrt{\frac{M_{238\mathrm{UF}_6}}{M_{235UF_6}}} = \sqrt{\frac{352.0412}{349.0343}} = 1.0043$$

This value of alpha is so small that it requires many stages to reach a desired enrichment level; for example, using natural uranium as a feed product (0.72% U-235) and producing reactor grade uranium (4.95% U-235) with an industry standard tails composition (0.2% U-235) it will take 1517 stages. The ideal cascade that would produce these specifications would have 919 enriching stages and 598 splitting stages and would have the shape shown in Figure 23.

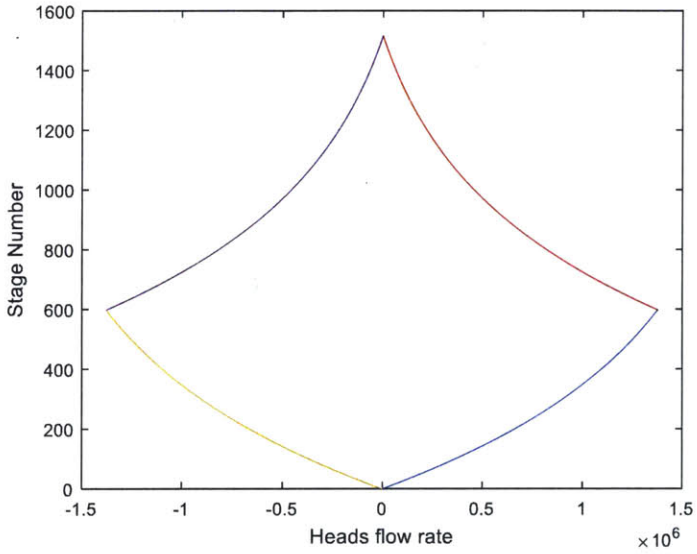

Figure 23. Stage vs. Flow Rate for Industrial Power Applications with Gaseous Diffusion

Another example to consider would be in the production of weapons grade uranium (>90% U-235). Using similar tails and feed composition as the previous example the resulting cascade, producing 95% U-235, would require 4267 stages. Of these stages 3669 are in the enriching section and 598 in the stripping section. The below diagram, Figure 24, depicts the cascade necessary for this level of enrichment.

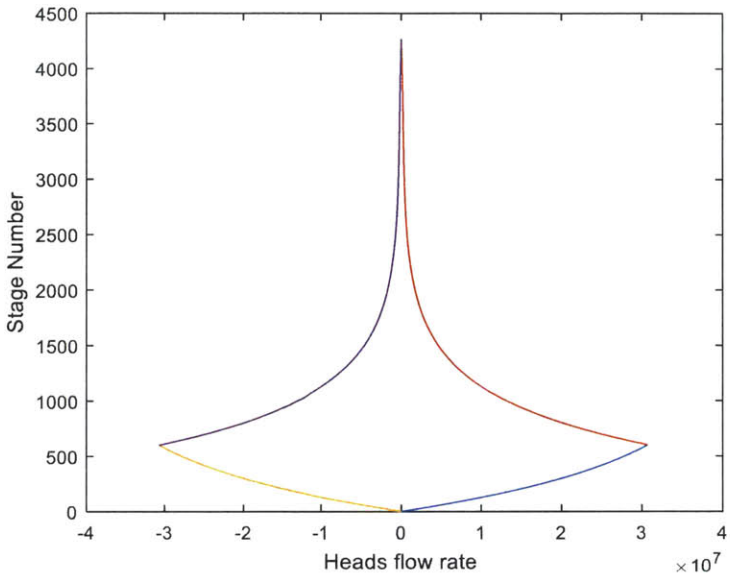

Figure 24. Stage vs. Flow Rate for Weapons Production using Gaseous Diffusion

The size of these cascades can be used to infer the cost and power necessary to produce a given amount of uranium. The costs for gaseous diffusion have a larger impact on the fuel cycle than other enrichment technologies, one such cheaper technology is the centrifuge.

The centrifuge is the most popular means of enrichment in the market today. The centrifuge has replaced gaseous diffusion as the dominant technology in the enrichment market, and likely is the top competitor to new laser enrichment technologies. The first gaseous centrifuge for uranium enrichment was proposed and built by engineer, Gernot Zippe [1]. This centrifuge is comprised of a rapidly rotating cylinder with a high strength to density ratio, the material used inside the centrifuge has low reactivity with fluoride compounds (this can be done by lining with chemically inert materials). The rotation of this bowl subjects the UF_6 gas inside it to extreme centrifugal accelerations. Thus the pressure in the outer region of the rotating cylinder is vastly greater than at the center axis and ensures that the concentration of $^{238}UF_6$ is significantly higher than at the inner radius of the container. Using scoops and rotating baffles placed at the top and bottom of the rotating container a longitudinal countercurrent flow can be induced. This will ensure that the gas at the bottom of the centrifuge is higher in abundance of the lighter $^{235}UF_6$ and the top higher in $^{238}UF_6$. A diagram illustrating the construction of such a centrifuge is seen in Figure 25.

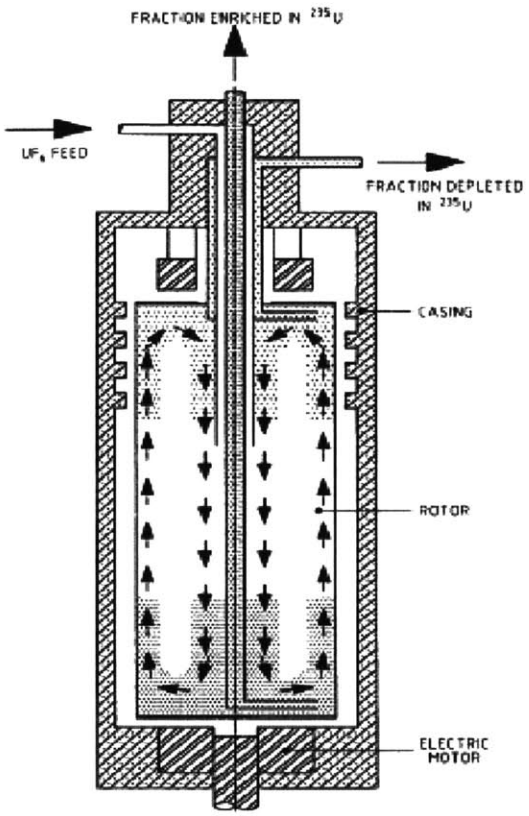

Figure 25. Zippe type gas centrifuge

A similar analysis can be done with centrifuges to determine the enrichment factor of these devices; however, given the variety of centrifuge designs through the last several decades the enrichment factor varies between 1.04 and 1.40 (depending on size and criticality[8]) [78]. So, taking an average enrichment unit to be capable of enacting an enrichment factor of 1.20, for every stage, the ideal cascade shape and flow regime can be created for two separate production capabilities. These two capabilities use the same values as the industrial and weapon examples that were calculated previously for gaseous diffusion.

[8] Centrifugal criticality refers to the range of operation of the device. When operating a centrifuge certain regions of velocity are termed critical rotational frequencies. Operating at these resonant frequencies will destroy the device. There are two options to solve this problem, operate at speeds below the first critical resonant frequency; hence the term sub-critical centrifuges. Or, one can operate in between critical frequencies; thus the designation super-critical centrifuge. The latter is more difficult to operate because during start-up and shut-down these frequencies must be quickly bypassed. The benefit to operating super-critical centrifuges is the increase in separative work capacity.

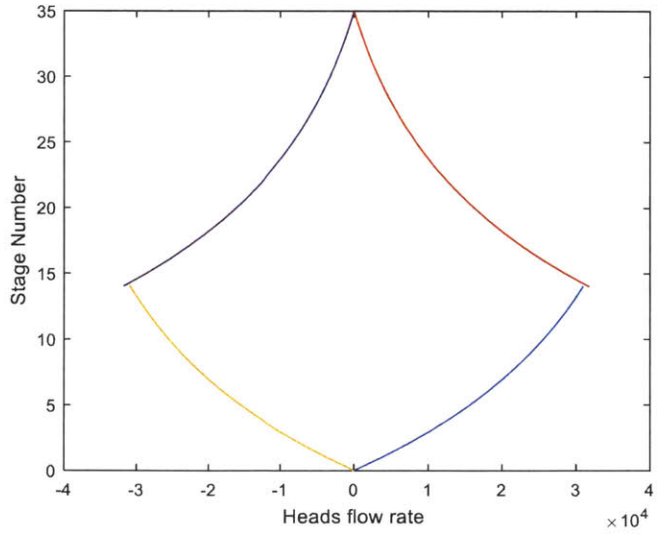

Figure 26. Centrifuge cascade for producing reactor grade U-235

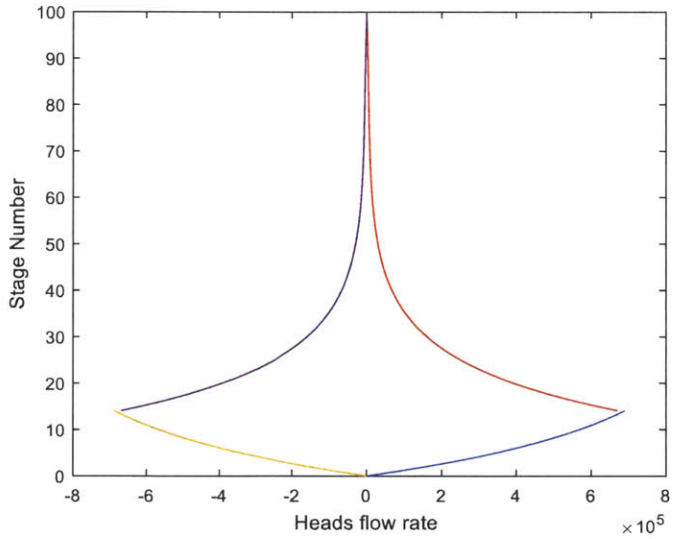

Figure 27. Weapons production cascade for gaseous centrifuge

The number of stages necessary for private sector power generation grade enriched uranium (4.95%) was 35, 22 of which would be used in the enriching section and 13 in the stripping section. For the weapons production centrifuge cascade a total of 99 stages would be needed, 13 stages would be used in the stripping stage and 86 in the enrichment section. The required number of stages for the gaseous centrifuge plant is drastically reduced in comparison to a gaseous diffusion plant. This makes it evident that the greatest competitor for a novel enrichment technology is the gaseous centrifuge.

In comparison to the centrifuge, the SILEX process, assuming that the theoretical projections are fairly accurate, would have an industrial production cascade that looks something like Figure 28. This is operating at an enrichment factor of 1.712, using Xenon as the carrier gas, and a product cut of 0.21.

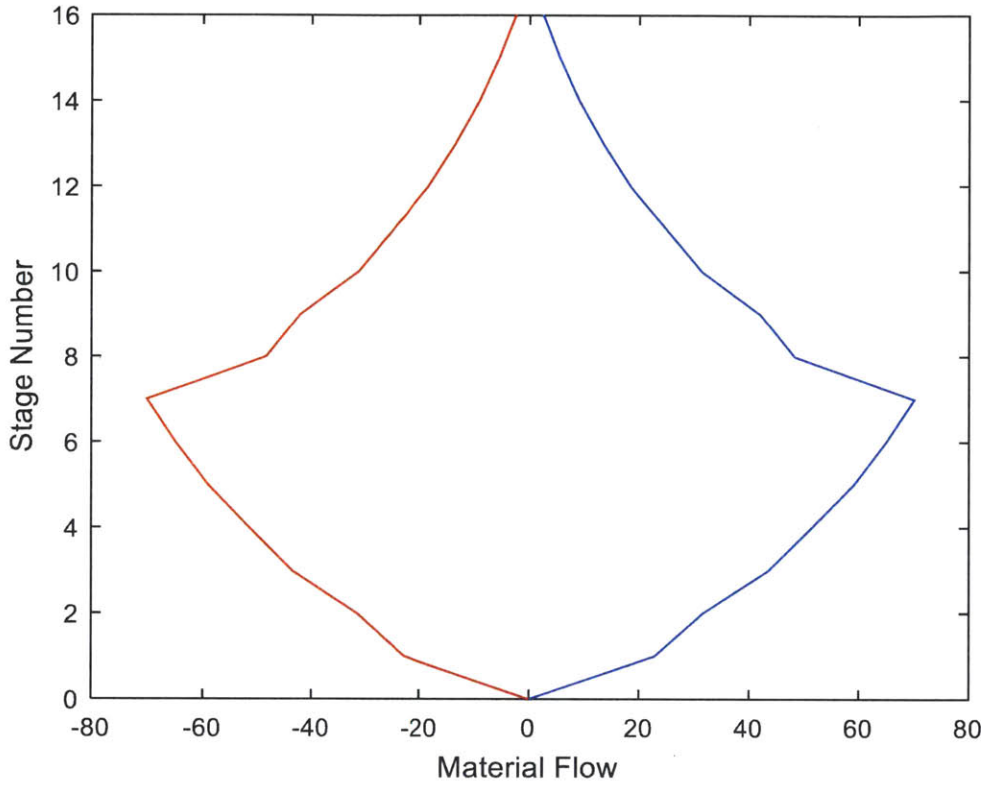

Figure 28. Industrial production of reactor grade fuel using SILEX

The reactor grade enrichment process requires only a total of 16 stages, with 10 enriching stages and 6 stripping stages. These stages are composed of the two-up one-down ideal cascade structure as was discussed in the previous section for product cuts at ~0.25. The bumps that appear in Figure 28 are caused by a different throughput for each integer stage, so the low number of stages emphasizes the bumps because there is no calculation for non-integer stages, say stage 7.5, otherwise the cascade would look smooth. The following diagram, Figure 29, shows the construction of such a cascade for reactor fuel production. The two-up one-down cascade is particularly interesting because there are two products at different levels of enrichment. These could be blended together, but with a loss of separative work. However, different levels of enrichment in power rods is typical. It would make economic sense to produce two different levels

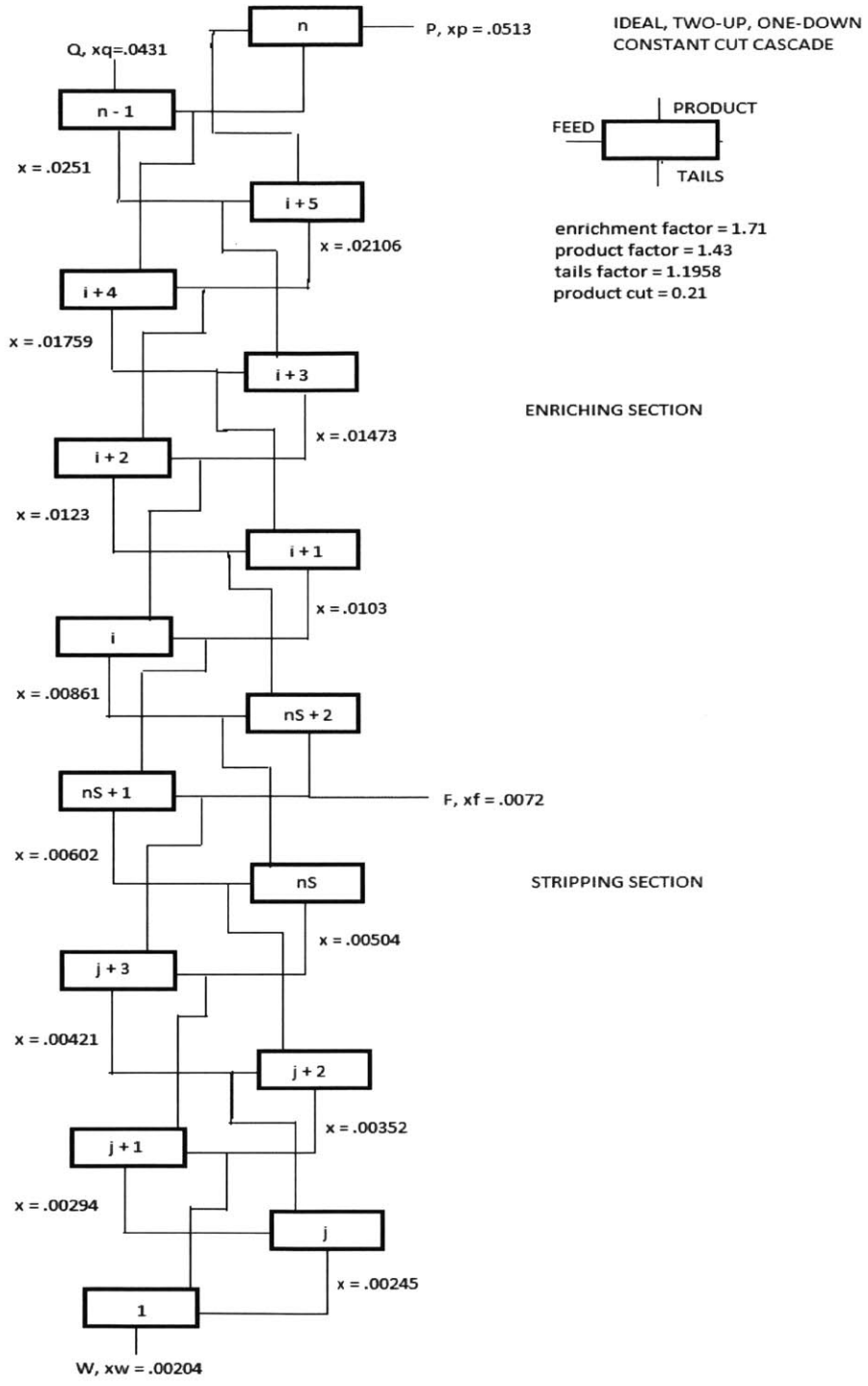

Figure 29. Ideal, Two-Up, One-Down Constant Cut Cascade

of enrichment instead of having to down-blend some of the fuel for LWRs. This means there may be an interesting economic advantage with this type of cascade; that is in its ability to conserve

potentially lost separative work. The next important cascade design to consider is one which produces weapons quality HEU. Before the cascade can be determined, it is necessary to evaluate the likelihood that the molecular-dynamics associated with the process will be able to produce a consistent enrichment factor (α). If α varies, the process could become more complicated as it scales to weapons production. Note that the enrichment factor is described as R_p/R_f, and whether this value is more or less constant is pertinent for design considerations and scalability. Using the MATLAB simulation for molecular dynamics and excitations (in Appendix 1) iterating over different initial isotopic abundances the effect was determined. The graph below shows the relationship between the enrichment factor (R_p/R_f) and the isotopic abundance of the feed material.

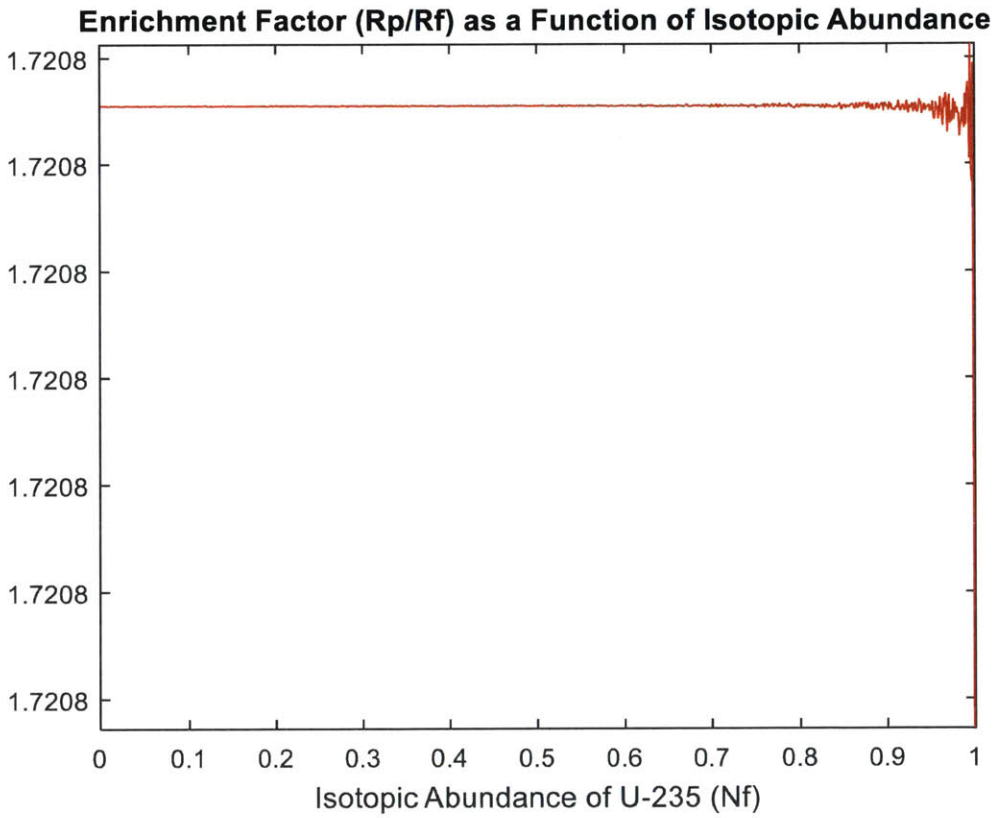

Figure 30. Enrichment Factor versus Isotopic Abundance of Feed

This graph indicates that the enrichment factor can be considered constant across a cascade, under the assumptions of the MATLAB model, even up to the region where the feed is in excess of 50% U-235. The numerical instability seen in high initial abundance feed is due to the fact that the computation of enrichment factor is determined in part by a denominator that includes dependency on N_f and the value is unstable as the denominator approaches zero. This is significant

for proliferation and weapons production concerns associated with the SILEX technology, assuming the theory proposed in [13, 75] is correct. For a weapons grade facility, with a desired output of 95% enriched U-235, the design is therefore not effected by any substantial instability. As the enrichment factor oscillates only as enrichment increases above 0.90, and at 0.95 there is only a negligible difference in enrichment factor (<.001). Using these design parameters a cascade for the production of weapons grade (95% enriched U-235) uranium is shown in Figure 32.

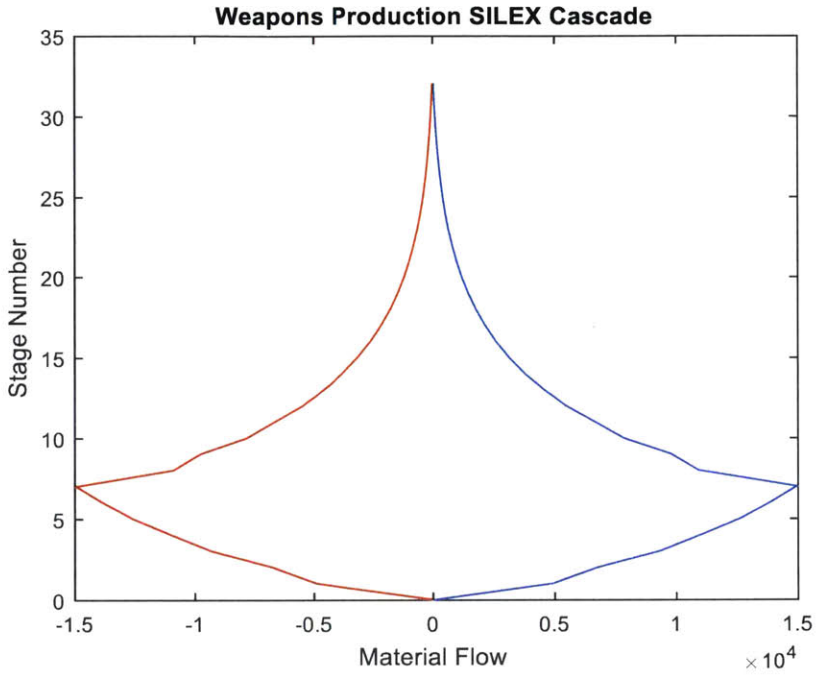

Figure 31. Weapons production cascade using SILEX

The cascade in Figure 31 is designed to produce 50 kg of product on a yearly basis, basically the amount needed to produce a bare sphere critical mass of uranium; equivalent to one nuclear warhead using a simple gun-type weapon design. This design can be altered to produce more product, the only change would be in the number of units in any given stage. The number of stages in this two up one down cascade is 32, with 6 stripping stages and 26 enriching stages. The MATLAB program that computed the cascade parameters can be found in Appendix 4 below. The weapons cascade still has a significantly smaller number of stages than an equivalent centrifuge facility (32%); however, the physical size of each unit is much larger in the SILEX facility than a single centrifuge. The size of each unit (containing an array of nozzles), will be determined in the next section, determines throughput and by extension how much separative work

can be performed per unit. The theoretical design of SILEX weapons production cascades will be useful for comparison to existing technologies when analyzing proliferation considerations. In terms of industrial enrichment production it is especially useful for companies to be aware of cost savings that may be present with new technologies. Economic analyses for the purpose of cost estimation of SILEX facility construction and operation are examined in the following section.

Part 4: Economic and Engineering Analysis

Overview

In order to provide an effective comparison of SILEX technology to alternative enrichment schemes, and to see if there is an industrial competitive edge, it is useful to estimate the costs associated with the construction of a SILEX facility. First, the cost associated with the development of a single enrichment unit must be determined. Using this information it is possible to then calculate the cost and size of the facility given the material balances that are computed as part of the LEU SILEX cascade that was designed in the previous section. The enrichment plant developed in this analysis will adopt a standard 1 MSWU/year (most commercial plants are in the MSWU range) size for comparison to other technologies. Using this 1 MSWU/year capability, it is possible to compute the requisite material flow rate per stage within the cascade. These material balances determine the number of nozzles that will be needed per stage. The material balances will allow an estimation of the components needed within the cascade to provide the production capability required. Once the capital cost of a SILEX enrichment facility is determined, the levelized cost of SWU can be computed assuming a forty-year plant lifetime. This levelized cost can be used to estimate the impact on the fuel cycle cost and the price of electricity, all of which are valuable means for understanding the economic advantage (or disadvantage) of this particular enrichment technology.

4.1.1 Engineering Model for a Single SILEX Unit

In order to make a commercial scale SILEX facility feasible, it is necessary to improve the flow rate for a single stage of the enrichment cascade. A single nozzle has the capability of creating a flow of rate 0.693 kg/s[9], which would mean a vast number of units required if only one nozzle was used per unit, and a correspondingly large number of lasers and other components. As determined in section 1.5, the cross section for Rayleigh scattering is insignificant, which means the laser can penetrate and irradiate multiple parallel jets of supersonic gas in sequence. Similar parallelized designs were adopted for the development of the Becker nozzle enrichment process

[9] This value was given by the results of the STAR-CCM+ simulation.

[66]. The number of nozzles used in a single unit depends on considerations like the capacity of the vacuum pumps used in the unit, and the cost of materials and manufacturing.

For the engineering model described in this document, an array of 40x40 nozzles is considered, the size of the panel of nozzles on one side of the irradiation chamber would thus have surface area of ~6.25m^2 (2.5x2.5m) assuming spacing of 2 cm between nozzles and a 1 cm diameter nozzle output. Note that between levels of flows, a sheet of metal must separate each row of flows from mixing with the flows above and below it. Following proposed designs like the one shown in Figure 33 below, partially taken from [14], will provide a representative technical model on which to base economic estimates. Note that Figure 33 shows only three flows; however, the number of flows would continue to be spaced side by side for as many flows as required.

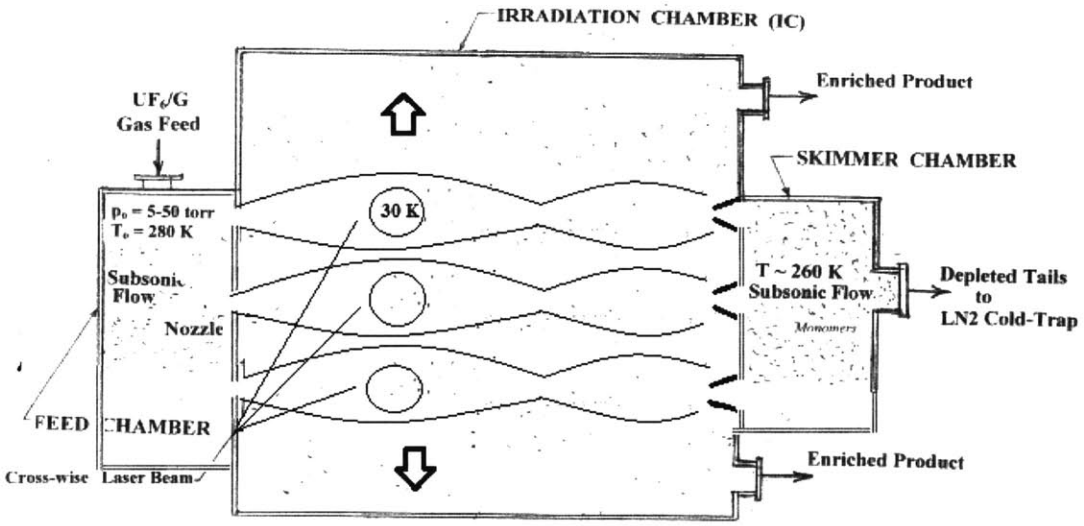

Figure 32. Engineering 2-D Model of the nozzle array and Irradiation Chamber

4.1.2. Estimate of Capital Costs

The single unit cost can be determined by computing the costs for the separate materials that will be used within the design. The alloy that should be used in the design of the irradiation chamber and reservoir must not react with UF_6. The alloy can be determined from materials identified by Oak Ridge National Laboratory and other publically available studies. The NRC requires, in Appendix C to Part 110 (Illustrative List of Gaseous Diffusion Enrichment Plant Assemblies and Components under NRC Export Licensing), the following:

> "All surfaces which come into contact with the process gas are wholly made of, or lined with, UF_6-resistant materials. For the purposes of this appendix, the materials resistant to corrosion by UF_6 include copper, copper alloys, stainless steel, aluminum, aluminum oxide, aluminum alloys, nickel or alloys containing 60 percent or more nickel and fluorinated hydrocarbon polymers." (10 CFR 110 Appendix C [81])

In keeping with these guidelines for gaseous uranium hexafluoride it is important to incorporate the requirements into the engineering model. Most stainless steel alloys are not resistant to corrosion by UF_6, but a material such as Monel (Alloy 400), is less susceptible to stress corrosion cracking as well as interaction with fluorides. This alloy is primarily composed of copper and nickel (97-98%), with the remaining composition from small amounts of Manganese, Silicon, Carbon, and Sulfur in order of weight [82]. Monel is often used in enrichment facilities as an alloy of choice. However, this alloy is fairly expensive, so the cost to make a pressure vessel and irradiation chamber may be fairly high. However, there is an allowance in the federal regulation for lining structures with the material, as opposed to using solid alloys.

This would be preferable for large vessels like the irradiation chamber and the low pressure feed tank of the unit. The nozzle plate would likely be made from solid Monel, as well as all the piping that would take the enriched and depleted feeds to the appropriate stages. Pumps may also need to incorporate the alloy. Any seals would likely be made of Teflon, a non-reactive fluoropolymer, which is resistant to UF_6, and was also incorporated in gaseous diffusion plants [76]. The estimated costs for Monel fabrication and manufacturing are listed in Table 4 below. Note that these are back of the envelope calculations (using rough estimates from online suppliers) and do not reflect exact estimates from manufacturing entities. The volume of material needed was a rough estimate based (10 m^3) on the size and thickness of the irradiation chamber (1.3 m^3 and 2cm thick), nozzle plate, reservoir tank, and piping needed. This value is likely to be an overestimate, especially of the thickness, but a good rule of thumb for near-vacuum chambers is 1/100 the size of the maximum diameter of the vessel. The distance across a row of nozzles is ~1m, so a thickness of ~1 cm to minimize buckling is likely reasonable. Any extra material will likely be used as 1mm sheets between the rows of supersonic flows and in the output piping. Note that because there is no complete engineering design it would be better to overestimate the material cost assumption.

Table 3. Manufacturing and Material Costs for a Single SILEX unit

Direct Materials Costs			
Material	COST ($/kg)	Density (kg/m^3)	Volume (m^3)
MONEL	$30	8800	10
	TOTAL COST	$2,640,000	
MONEL LINED			
MONEL	$30	8800	2
Stainless Steel	$10	7850	8
	TOTAL COST	$1,156,000	
Direct Labor Cost			
Nozzle Plate	9500		
Welding	100000		
Product/Tails	100000		
Feed Chamber	10000		
	TOTAL COST	$219,500	
Manufacturing Overhead Cost			
Admin, etc.	30000		
Machining	10000		
	TOTAL COST	$40,000	
FINAL ESTIMATE		$1,415,500	per unit

The direct labor cost includes the manufacturing cost for welding and using machining tools to drill nozzles into the plate as well as fabricating the piping and output and input mechanisms. Manufacturing a plate with spaced nozzles using a CNC Mill, due to Monel's increased hardness, puts estimates at around $10,000 for that piece alone. Assuming one-thousand man hours spent welding and fabricating other parts at $200 an hour, assembly costs are estimated to be around $100,000-200,000. These rough estimates were found using a manufacturing estimation tool found at the website cited in [86]. Indirect labor costs amount to paying administrative fees and also account for the wear and tear on machining equipment. Administrative fees would likely decrease as the number of components being produced increases, but for the sake of simplicity, the value will remain encapsulated within the unit cost.

The cost of the laser system is not included in the capital cost, because these systems will likely need constant rejuvenation. They are included in the operating and maintenance costs, below; pumps and control equipment are also incorporated into this cost. Thus, the cost to construct a single SILEX separating unit, absent the laser system, is roughly 1.5 million dollars. This estimate is based on the use of lined Monel steels and minimizing the use of the nickel based

alloy where it is not necessary. This cost will likely decrease if aluminum parts were incorporated in non-fluoride atmosphere containing components, as well as decreasing the amount of Monel that would be needed. If the unit is solely constructed from Monel the cost roughly doubles; the material required determines the majority of the cost. In order to determine the capital cost for an entire plant's worth of separators, it is now necessary to find the number of units needed in a 1 MSWU/year cascade.

The material balances, number of nozzles, and number of enrichment units are shown in Table 3 for each stage within the cascade. The number of nozzles per unit is assumed to be 1600 (a 40x40 array[10]). The material values in the output section were calculated using the MATLAB code in Appendix 3 for each stage using a rate of 1 MSWU production per annum. The nozzles needed per stage are based on the throughput of a single nozzle of 0.693 kg/s, based on the flow rate given by the STAR-CCM+ simulation. Given this information it is possible to calculate the number of units needed per stage using a 40x40 array of nozzles in a single unit. The area displaced by each stage is estimated by using the diameter of the nozzles (1 cm) and spacing between them (2 cm) to estimate the cubical volume occupied by a single unit. That area is then multiplied by a factor of three to compensate for free space around the units and administrative warehouse space. The material balances calculated in MATLAB are based on a two-up, one-down cascade and the stage parameters are found using the equations described in section 3.1.2. The total number of nozzles was found by taking the required flow, converting the value to kg/s, and then dividing by the flow rate of a single nozzle.

[10] The array can "theoretically" be any number of nozzles, given the transmission probability of the laser (see section 1.5); however constraints due to required pumping power and overall size of the unit, the decision to make the array larger than 40x40 is to increase the nozzle plate area greater than 1.5 m^2. It is important to note that this is engineering assumption and increased research and development of the unit itself could require decreasing or increasing the number of nozzles used. This estimate is used primarily as a starting point in the creation of a rough engineering design on which to base economic conclusions.

Table 4. From the output per annum (a result of the 1 MSWU cascade calculation in MATLAB), the number of total units and the area displaced are determined. Stage 1 is the lowest stage of the tails portion of the cascade, and stage 16 is the output (see Figure 28 for a visualization of the cascade; although, note that the material moving through each stage changes based on SWU requirements).

Stage #	Output (kg/yr)	Nozzles/Stage	Units/Stage	Area Displaced (m^2)
16	31867	1529	0.96	34.39
15	70308	3372	2.11	75.88
14	115540	5542	3.46	124.70
13	171250	8214	5.13	184.82
12	234320	11239	7.02	252.89
11	317510	15230	9.52	342.67
10	399950	19184	11.99	431.64
9	533950	25612	16.01	576.26
8	616410	29567	18.48	665.25
7	893070	42837	26.77	963.84
6	827670	39700	24.81	893.25
5	752560	36097	22.56	812.19
4	655930	31462	19.66	707.91
3	555350	26638	16.65	599.36
2	402190	19292	12.06	434.06
1	291260	13971	8.73	314.34
Totals	6869135	329487	205.93	7413.45

The total number of units needed within a 1 MWSU facility is approximately 206 for this particular engineering design. This value will be useful in computing the capital cost of constructing the cascade. Capital costs other than the cascade must also be estimated. The area displaced by the cascade provides the information necessary to begin an estimate of other construction costs.

4.1.3. Facility Cost Estimates

Facility size estimates, indicate around 5 acres is needed per 1 MSWU. This is comparable to the land area of the 6 MSWU GLE Wilmington plant, which will occupy an area of 24 acres [22]. The average cost of land in the United States is $3,020 an acre, which will add a cost of around $75,000 to the facility, assuming a 25-acre parcel. The cost to build a warehouse over the cascades depends on the security and engineering requirements. The average conventional warehouse cost is about $50-80 per square foot [87]. The building will likely be on the upper end of the cost spectrum due to NRC requirements. The warehouse itself adds roughly $20 million to the project. Another sunk cost is the price to license the facility with the NRC. Although this is

much cheaper than trying to license a nuclear power plant, several expensive iterations of licensing are required. The majority of the cost of licensing is from an environmental impact statement that the NRC must approve for the site of the facility. The licensing cost, depending on the number of iterations of documents, will be around half a million dollars, using the average cost of $280/hour per professional [22] in addition to extraneous licenses for transportation and storage of uranium hexafluorides, plus the cost for the preparation of relevant documents by the owner of the facility [81]. The estimate for NRC licensing costs is conservative, and assumes that fewer iterations of environmental documentation will be required (as of 2016, both Areva and URENCO have gone through the process in the U.S.), as well as meeting operating standards early on. The NRC now allows dual operating and construction licensing for enrichment facilities, which may also help cut down costs. Note that in some countries there is little to no licensing cost for an enrichment facility. An estimate of these plant wide costs is listed below, note that the estimate for the warehouse construction includes the cost of structural engineering associated with the design.

Table 5. Cost estimates for facility-wide costs

Licensing Cost			
Cost/hr	Hours at NRC	Cost of Preperation	Licensing Fees
280	400	300000	3000
	TOTAL COST	$415,000	
Area of Facility (*3 machinery)		ft^2	acres
22240.3402		239393.0449	5.495
Dimensions (square) m		feet	
149.1319557		489.2780854	
Land Expenses (acres *avg land cost-$3020/acre)			
TOTAL COST	$75,500		
Warehouse Expenses ($80 per ft^2*area of facility)			
TOTAL COST	$19,151,444		
ADDITIONAL PLANT COSTS TOTAL		$19,641,944	

Using these estimations and the material flow through the cascade (calculated in MATLAB, found on Table 3) it was possible to create the following worksheet, Table 6, for analysis of the total cost of a building a SILEX enrichment facility. The engineering and personnel costs reflect the manpower required for cascade design, fabrication, and management of the facility. The values for cascade construction, engineering, and personnel costs are estimates based on the cost to build AREVA's 6.6 MSWU facility in Idaho; at $0.5B/MSWU. The construction costs (cost of general materials and manpower) represent roughly 20% of this total cost. The

construction costs also encapsulate the estimate of costs of the extra technology required in any enrichment plant, such as loading stations, monitoring equipment, and other low cost additions. A five-year construction timeframe, with twenty full-time engineers and twenty managers yields ~$20,000,000 in expenses (with an average salary of $100,000).

Table 6. Total estimated cost for construction of operating SILEX facility

TOTAL COST WORKSHEET	
Cascade Cost	$291,593,000
Plant Costs	$19,641,944
Engineering	$10,000,000
Cascade Const.	$100,000,000
Personel	$10,000,000
TOTAL ESTIMATE	$431,234,944

4.1.4. Operating and Maintenance Cost Estimate

Because I anticipate lasers will likely be replaced frequently, this expense is considered as part of the operating and maintenance costs in Table 7. The initial estimate of the laser systems depends on the complexity involved; if, for instance, a Raman conversion process is used then the cost is much higher than estimated here. However, because of the issues with low duty cycle I assume that the facility will be built with a single step lasing process, where a CW laser at 16μm is used, where the cost might be lower. Although no such laser yet exists, I believe this is a reasonable assumption for a commercial full-scale production facility, as a more complex laser could be cost prohibitive as indicated by the lack of progress made by GLE in Wilmington in the last ten years. The cost of a laser system is assumed to be ~$40,000/kW [89]. Assuming one laser per unit, and 207 active units, the total cost is around ten million dollars. An average lifetime of each laser system is assumed to be 3-4 [89] years, adding a base cost of three million a year in laser related expenses to the operating and maintenance costs.

4.1.5. Estimation of Levelized Cost of SWU

The process of calculation within Table 7 begins by calculating the revenue, based on the cost/SWU, next the operating costs are deducted from this value, and then payments are made on both the debt and equity that was used to finance the facility. The levelized cost/SWU is manipulated until the remaining debt and equity is equal to zero at the end of the plant lifetime for

a particular levelized cost value. Assuming a plant lifespan of forty years, near-continuous operation (~24/day), borrowing equally split between equity (at 13.5% return) and loans (at 4% interest), rate of taxation of 19%, and an inflation rate of 3%. The levelized cost per SWU is found to be $39.72.

Table 7. Levelized cost of separative work for SILEX facility

SILEX Facility at 1 MSWU/yr f = 0.5, r_i =0.03, r_b=0.04, r_e=0.135								
Levelized cost ($/SWU)=	39.72							
Period	1	2	3	4	5		39	40
Price, p ($/SWU)	39.721	39.721	39.721	39.721	39.721		39.721	39.721
Revenue, R(n) (million $)	39.7	40.9	42.1	43.4	44.7		122.1	125.8
Fuel + O&M cost, (Cfuel(n) + Lasers+Co&m(n)) (million $)	3.6500	3.7960	3.9478	4.1058	4.2700		16.2017	16.8497
Operating income, OI(n) = R(n)-Cfuel(n)-Co&m(n)	36.1	37.1	38.2	39.3	40.4		105.9	108.9
Loan balance at BOY, L(n) (million $)	215.6	213.3	211.0	208.5	206.0		20.5	10.5
Loan payment,q ($)	10.9	10.9	10.9	10.9	10.9		10.9	10.9
Interest payment, I(n) ($)	8.6	8.5	8.4	8.3	8.2		0.8	0.4
Principal repayment, q-I(n) ($)	2.3	2.4	2.5	2.6	2.7		10.1	10.5
Depreciation allowance, D ($)	10.8	10.8	10.8	10.8	10.8		10.8	10.8
Taxable income, TI(n)=OI(n)-I(n)-D	16.7	17.8	19.0	20.2	21.4		94.4	97.8
Taxes, T(n)=0.19 TI(n)	3.2	3.4	3.6	3.8	4.1		17.9	18.6
Net income,NI(n)= OI(n)-q-T(n)	22.0	22.8	23.7	24.6	25.5		77.1	79.5
Outstanding equity E(n)	215.6	222.7	230.0	237.3	244.8		129.5	69.8
Return on equity e(n)	29.1	30.1	31.0	32.0	33.0		17.5	9.4
Free funds available to reduce equity	-7.1	-7.2	-7.4	-7.5	-7.6		59.6	70.0

The levelized cost is a useful tool for estimation of the cost to a consumer of a particular good; however, it does not reflect exactly the true pricing of the good. In the case of levelized cost, a company will prefer to have profit margins on a yearly basis, not until after the final year when all debts are paid off, this will lead to more variable pricing from year to year. However, the levelized cost provides a useful metric for the fuel cycle cost as it represents a more or less time averaged cost of a particular good. Therefore, assuming SWU is sold at cost, using a value of $40.00/SWU to compute the effect on the fuel cycle is a fairly reasonable estimation.

Table 8. Breakdown of the costs that make up the total $ per SWU for FY1

Cost Breakdown ($/SWU) for FY 1			
	Cash Flow	Percentage	$/SWU
Revenue	$39,700,000		
O&M	$650,000	1.64%	$0.65
Capital Repayment	$10,900,000	27.46%	$10.91
Lasers	$3,000,000	7.56%	$3.00
Equity Repayment	$22,000,000	55.42%	$22.01
Taxes	$3,200,000	8.06%	$3.20

It is also of interest to see what the cost composition of the $/SWU looks like. The majority of the levelized cost is from capital and equity repayment (~82%). The costs for replacing the lasers and taxes are each roughly eight percent of the total cost. However, once capital and equity costs have been paid off, the majority of the cost will be due to laser replacement and taxation.

4.1.6. Fuel Cycle Cost Impact

The impact on the fuel cycle from the enrichment process is highlighted in the process diagram shown in Figure 33 below. In light of the numerous processes that nuclear fuel must pass through before being used, it seems that there is little effect from the enrichment stage. This is true in part, but the enrichment stage can be one of the most costly steps within the process. Uranium ore is first mined and milled to remove miscellaneous deposits of other minerals. The pure form of uranium known as yellowcake is then converted from its oxidized form to a fluorinated form, which will be used in the enrichment process. After enrichment the conversion to pure uranium occurs, followed by the expensive fuel fabrication process. The fuel is then ready for insertion into a reactor core.

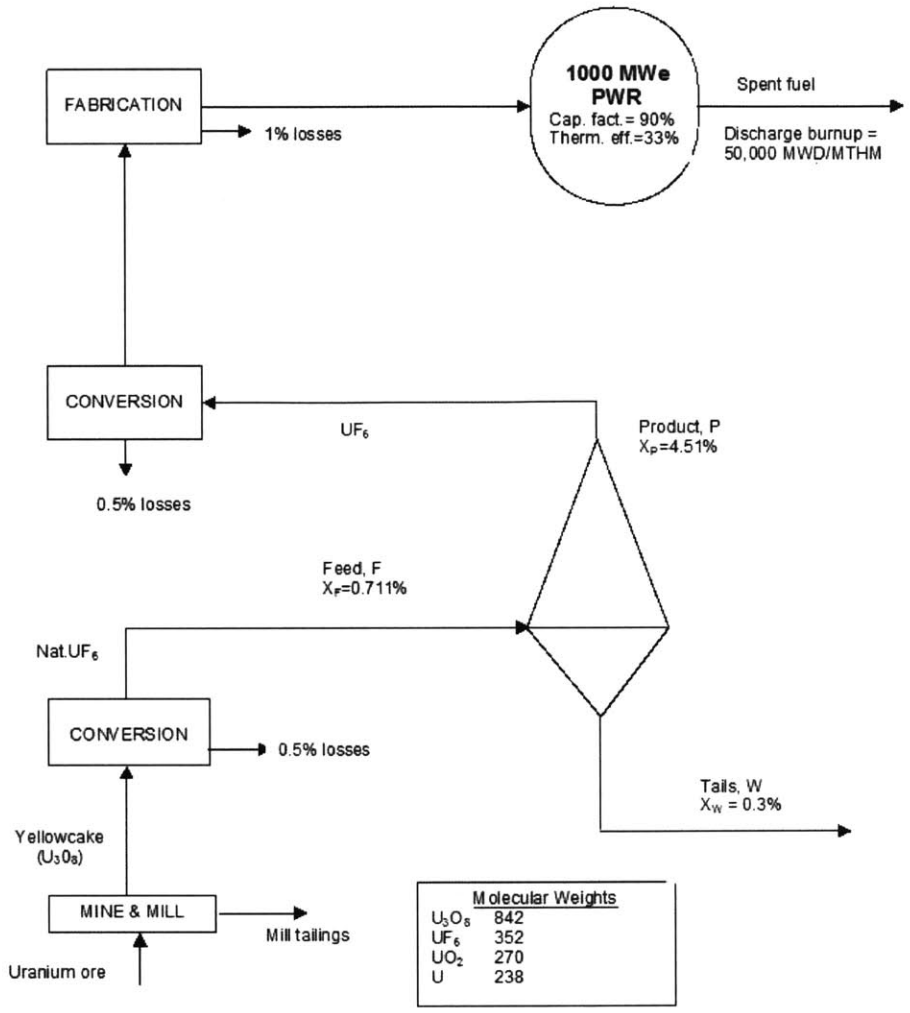

Figure 33. Outline of Nuclear Fuel Cycle [32], this is used for calculations below of SWU and mass flow for 1 kg of fuel through the cycle, which is shown in Table 8.

Table 8 below shows a spreadsheet calculation of the fuel cycle cost, which is part of the operating and maintenance component of the levelized cost of electricity. These costs are based on the amount of uranium needed to provide 1 kg of reactor grade fuel. The values of the masses involved in each step were determined using the model for losses pictured in Figure 33.

Table 9. Fuel cycle cost comparison between SILEX and current average enrichment market price****

PWR BASE CASE Costs*							
Transaction	Unit Cost, Ci ($/kg)	Mass Flow, Mi (kg)	Ti (years)	Direct Cost Mi*Ci ($)	Carrying Charge Mi*Ci*Φ*Ti		Lead Time (yr)
Ore Purchase[1]	88.19	10.45	4.25	921.5855	391.6738375		2
Yellowcake Conversion[2]	11.00	10.45	4.25	114.95	48.85375		2
Enrichment[3]	142.22	6.23	3.25	886.0306	287.959945		1
Fabrication[4]	247.18	1.015	2.75	250.8877	68.9941175		0.5
Interim SF Storage[4]	120.00	1	-2.25	120	-27		Fuel Discharge
Final Disposal[4]	550.00	1	-2.25	550	-123.75		Fuel Discharge
Total				2843.4538	646.73165		
Grand Total					3490.18545		
	Fuel Cycle Cost=		0.0088136	$/kWhr			

PWR w/ LIS Enrichment							
Transaction	Unit Cost, Ci ($/kg)	Mass Flow, Mi (kg)	Ti (years)	Direct Cost Mi*Ci ($)	Carrying Charge Mi*Ci*Φ*Ti		Lead Time (yr)
Ore Purchase[1]	88.19	10.45	4.25	921.5855	391.6738375		2
Yellowcake Conversion[2]	11.00	10.45	4.25	114.95	48.85375		2
Enrichment[5]	40.00	6.23	3.25	249.2	80.99		1
Fabrication[4]	247.18	1.015	2.75	250.8877	68.9941175		0.5
Interim SF Storage[4]	120.00	1	-2.25	120	-27		Fuel Discharge
Final Disposal	550.00	1	-2.25	550	-123.75		Fuel Discharge
Total				2206.6232	439.761705		
Grand Total					2646.384905		
	Fuel Cycle Cost=		0.00668279	$/kWhr **			

[1]-Ore purchase from [42] is \$40/lb-U_3O_8. in 2013, which is within the range [39] gives for contract prices.
[2]-Data taken from UxC/Timera [42] conversion market 2013, spot market price identical to [39] estimate.
[3]-Data taken from 2013 from [17], for average enrichment cost.
[4]-Based on [39] values for PWR in 2007 and inflation adjusted to 2013$.
*All monetary values given in $2013, based on 1kg of enriched fuel, 4.5 years in core, and class notes of 22.812 [32].
**Fuel cycle cost: ($/kg)*(kg/MT)*(MTHM/MWDt)*(days/hr.)*(MW/kW) * (kWh(th)/kWh(e)) where parameters are given in Figure 4 above for a 1000MW PWR.
*** Φ is a carrying charge factor of 0.1/yr.
****The cost of enrichment for different facilities is actually quite variable, ranging from $50-200 [19]. The current price is ~$60/kgSWU, historically averaging at ~$100/kgSWU, but due to data constraints all monetary values are computed using $2013 and values for consistency.

This comparison indicates that a decrease in the enrichment cost from $142.22 to $40.00, corresponds to a cost reduction of 0.2 cents/kWhr, or a reduction of ~25% in the total fuel cycle cost. From this value, and knowing the average yearly electricity use of an American household (10,908 kWh [17]), a rough estimate of the annual cost savings for a typical U.S. family would be $23.24. This amount doesn't seem like a very large reduction; however, considering nuclear power produces 19% of total U.S. electricity [16] and there are roughly 120 million households in the United States, the total cost savings is ~530 million dollars a year to consumers. This seems to be

a large enough market incentive for companies to pursue laser enrichment technologies. However, it is important to note that although there is a projected cost reduction for adopting laser enrichment, there is no hard data to positively claim that there will be a cost reduction relative to centrifuges. In other words there is a partially unsubstantiated underlying assumption of cost that has a large margin for error. Also, as more centrifuge facilities are built, and as the last few diffusion plants are shut down the average cost of enrichment will drop significantly below the 2013 price of $140.00. In fact, as of 2016, with only one diffusion plant remaining open in China, the enrichment spot price has dropped to $60/SWU [42].

Although these types of cost estimates are useful in terms of economic understanding for the industrial decisions regarding particular enrichment technologies, there is little information to be gleaned for the purpose of proliferation analysis. Countries are not necessarily swayed by economic arguments in the development of new nuclear arms capabilities. The data from this section informs the question of whether this is useful for peaceful industrial purposes, but it does not answer the question of the proliferation risk that such a technology poses. Whether SILEX is an economically equivalent investment in comparison to the other techniques does not really approach the heart of the proliferation issue.

Part 5: Proliferation Analysis

Governments are often heavily involved in nuclear development and enrichment, as evidenced by every single enrichment program in the world. These programs most often stem from defense programs, where spending is not usually curtailed or questioned. The factors that control the trajectory of these programs tend to not be only economic, but also based on politics, security considerations, technical feasibility, and scientific expertise. Understanding this framework, and its place in history, is central to our understanding of the way in which a new enrichment technology affects the proliferation landscape. Several pertinent questions direct this analysis: 1) What decisions were made in the past about enrichment technologies that stymied or advanced their prospects? 2) Does the current feasibility of the technology in any way affect the probability that such a technology will be adopted by a particular society? 3) Are there other factors that motivate the choice of a certain technology over another? These questions will be contemplated in the following section in an attempt to understand the proliferation risks associated with nascent enrichment technology, in this case the development of SILEX.

5.1. Proliferation Concerns

The development of SILEX and similar technologies pose an identifiable risk to non-proliferation efforts across the globe. Characterizing the inherent risk and its relative likelihood is central to being prepared to address technologies like SILEX as scientific understanding and technology continues to progress. As was mentioned previously, proliferation of an enrichment technology is governed by two primary forces; politics and technical knowledge. Technological knowledge is the necessary for proliferation, but the course of development is governed by politics. Older technologies will be analyzed historically to understand some of these considerations. SILEX will also be compared to centrifuges in terms of its technical compatibility with proliferation scenarios. Several technical operating parameters have been developed within this thesis that are particularly relevant for proliferation analysis of SILEX. These parameters in some ways incentivize development, and in other ways would deter pursuit of the technology. Through this analysis, and by answering the three questions stated above, a more clear portrayal of the risks that nascent enrichment technologies pose to society will be developed.

Although there seems to be some difficulty with the pulsed laser (see Section 1) currently used for SILEX, this does not detract from the importance of a more general proliferation assessment of SILEX that considers the possibility that laser challenges are overcome in the near future. Innovation in laser technology has continued to progress rapidly and using new discoveries like the Weyl point [73], adjustable lasers in terms of both intensity and wavelength may quickly be on the horizon. A single breakthrough could simplify the process enormously, making SILEX entirely feasible at a large scale.

Technologies that are on the cusp of breakthrough, like SILEX, are excellent candidates for risk assessment because they allow proactive rather than reactive non-proliferation policies. A methodology for addressing any new, generic enrichment technology would be a useful tool for the non-proliferation community; however, this will not be substantially developed in this thesis.

5.1.1. Cascade Considerations

SILEX is capable of a significantly larger enrichment factor than other technologies, including the centrifuge. Proponents of SILEX often quote [15] factors of two or better above centrifuges. While this may be technically achievable, the findings of this thesis suggest lower factors in the range of 1.5-2.2 (Section 1) because the product cut would be much too low for practical cascades at higher enrichment factors. Section 2.1 finds that an enrichment factor around 1.72, with a product cut of 0.21, is more realistic.

These values are still higher than other means of enrichment, suggesting fewer stages. However, with a product cut lower than about 0.4, this rules out the use of a symmetric cascade. An asymmetric cascade, described in Section 3.2, has a larger number of stages than a traditional symmetric cascade; for example, in SILEX LEU production there are 16 vs. 11 stages respectively. A further consideration is that fewer stages may not necessarily be advantageous if each individual stage is large, expensive, or difficult to operate. By comparison to centrifuges, a laser-based separating unit represents a larger and more complex monitoring situation because of the increased size and sets of laser and pumping equipment. SILEX units also have two different output streams, which would also require a separate product handling area.

While a high enrichment factor, fewer stages, and the ability to incorporate many single enrichment units into a larger unit are arguably incentives to pursue SILEX over an alternative technology,

there are also deterrents. The asymmetric cascade is more complex, and the laser system is problematic. Certain sources [20] also indicate that advanced laser technology, requiring specialized knowledge, may deter indigenous proliferation of LIS. Boureston and Ferguson, for example, concluded that a majority of analysts regard LIS technology as too formidable to master for countries that do not have highly advanced technical infrastructures or a specialized knowledge base [20]. An intelligence assessment published in 1982 by the CIA, titled "Uranium Enrichment: Threat of Nuclear Proliferation Increasing," concludes that LIS processes "require very advanced materials and technology, and would be difficult, if not impossible, to [construct]" [6]. However, Ferguson also notes in [20] the view of analyst Stanley Erickson of LLNL, who is confident that as the technology advances LIS will come within the reach of even developing nations. The view that the technology is too advanced to be concerned about proliferation [3, 29] is short sighted and neglects the entire picture; similar statements made about the gaseous centrifuge were proven to be incorrect [27].

Whether or not a certain level of specialized technical knowledge is enough to engender the ability to design enrichment technology is an important point of proliferation analysis. If a country lacks the educated technical personnel, then the likelihood of proliferation diminishes. Identifying the point at which technical understanding is advanced enough is an arbitrary exercise. Nearly every country in the world could probably put together a team of scientists and engineers to learn the fundamentals and propose an enrichment design. Given enough time and resources, they would probably be successful. It is not necessary to start with a specialized knowledge in laser physics, or molecular and quantum dynamics. An undergraduate degree in physics would provide an intelligent scientist with the basis to learn these more advanced topics.

Much of the specialized knowledge needed to develop SILEX is available through open-source literature and textbooks [13, 14, 15, 66], and with the leaps in globalization over the last several decades, knowledge sharing and the transfer of information via the internet has become commonplace. The effects of globalization on knowledge transfer, even in the pre-internet age, have clear implications when viewed in light of proliferation networks like the one run by A.Q. Khan [27]. In the internet age, open-source software, like computational fluid dynamics (CFD) tools, are easily accessible to engineers with an internet connection. Tools like these radically simplify the development of enrichment technology, and eliminate a significant need for laboratory

facilities in the early stages of an enrichment program. These facts suggest that it is antiquated to view limits on precise technical know-how as a barrier to proliferation, and by extension as the means for analyzing proliferation risk. A perfect example of this is the development of a centrifuge in the U.S.; within a year of research and development a team of six scientists at UVA were able to duplicate and run centrifuges successfully with little specialized knowledge in the field of enrichment technology [27]. Therefore, it seems as though the use of technical knowledge as an argument for or against enrichment proliferation has little real bearing on the question of proliferation in the modern era.

5.1.2. Means of Enrichment Detection

Controlling proliferation of laser enrichment technology is another concern that the international community must grapple with. A recent article in *Nature* discussed the newly licensed GLE-SILEX process and argued that the increase in proliferation risks overcome the cost benefits of the new technology. The authors stated that "if laser enrichment is as efficient as has been suggested, then it could occupy a space substantially smaller than a warehouse...and draw no more electricity than a dozen typical houses. This could put such plants well below the detection threshold of existing surveillance technology" [40]. This seems to be a valid argument, but it would be useful to validate it.

Using the information from the MATLAB weapons cascade simulation and a spreadsheet of material balances (the yearly material flow for each given stage) an estimate of the size of such a facility was computed. The estimated area, assuming four square meters of area are needed per unit of 10*10 nozzles[11] (including additional empty space), and 32 stages, the area displaced is equal to approximately 5300 square feet. The spreadsheet table can be seen below in Table 9, with the number of nozzles and enrichment units per stage shown. The calculation was done using the output of one unit of bomb grade material per year (~50 kg of 95% U-235) as the production capability.

[11] This array size is somewhat arbitrary; the underlying assumption is that units in a covert facility would be smaller than in an industrial production facility. Note that this calculation is sensitive to the design and number of nozzles in the separator. Therefore, some uncertainty exists that cannot be completely resolved within this stage of theoretical understanding.

Table 10. Facility area for a clandestine weapons production facility.

Stage #	Output (kg/yr)	Nozzles/Stage	Units/Stage	Area Displaced (m^2)
32	50	2.40	0.02	0.0959
31	110	5.27	0.05	0.2109
30	182	8.71	0.09	0.3486
29	268	12.84	0.13	0.5136
28	371	17.78	0.18	0.7113
27	494	23.70	0.24	0.9482
26	642	30.80	0.31	1.2320
25	819	39.30	0.39	1.5720
24	1032	49.49	0.49	1.9794
23	1286	61.69	0.62	2.4676
22	1591	76.31	0.76	3.0524
21	1956	93.83	0.94	3.7533
20	2394	114.82	1.15	4.5927
19	2918	139.98	1.40	5.5992
18	3546	170.08	1.70	6.8033
17	4300	206.25	2.06	8.2500
16	5199	249.37	2.49	9.9747
15	6286	301.50	3.02	12.0601
14	7566	362.93	3.63	14.5170
13	9148	438.81	4.39	17.5525
12	10939	524.69	5.25	20.9878
11	13315	638.67	6.39	25.5469
10	15654	750.88	7.51	30.0354
9	19573	938.86	9.39	37.5542
8	21816	1046.42	10.46	41.8566
7	29894	1433.92	14.34	57.3567
6	27721	1329.67	13.30	53.1869
5	25222	1209.80	12.10	48.3922
4	21999	1055.21	10.55	42.2084
3	18650	894.57	8.95	35.7828
2	13509	647.98	6.48	25.9190
1	9792	469.69	4.70	18.7874
Totals	256283.71	12292.96	122.93	491.72
			Square Feet	5292.81

Including administrative space the facility would be probably around ten thousand square feet. Such a facility would indeed be as small as the authors contend, the size of a large house or small warehouse with dimensions of roughly 100' by 100'. The power distributed to this facility

is mainly determined by the laser requirements and vacuum pumps, and assuming each laser could be used to irradiate many flows (as was already confirmed in Section 1.5) the total power requirements (by 1kW lasers) for such a facility would be 123 kW (123 separate enrichment units needed using Table 9). The pumping power is another ~125 kW, for a grand total of 250 kW. Using this estimate, under operation twenty-four hours a day, the number of kWh/year in operational power requirements is 438,000 kWh/year, which is about the same yearly average as forty U.S. homes [17]. So, the claim made in [40] seems to be fairly true, if maybe a little overstated; however, it would be additionally useful to compare the size and power estimates here with that of a clandestine centrifuge facility.

The centrifuge facility can just as easily escape detection by technical means [27]. The chances that human or signals intelligence reveal a plant also appears to be low. The historical record suggests, for countries that have developed centrifuge technology indigenously, the "probability of timely detection has been approximately zero" [27]. This is most clearly indicated by the Russian centrifuge program, where research began in 1946. The first Soviet pilot enrichment facility went into operation at Sverdlovsk-44 on October 4th 1957. By 1964 a full-scale commercial facility was built and operating at Sverdlovsk-44. By the middle of the 1970s, centrifuge technology was the primary means of enrichment in the Soviet Union [36]. These facilities went undetected by the United States until 1991 when Russia disclosed that it had four large centrifuge enrichment facilities [36].

It would be useful to estimate the size of a clandestine centrifuge facility for comparison to that of a similar SILEX facility. If they are different in size, there may be an argument to be made in one technology being more difficult to detect. Several thousand centrifuges are sufficient for the creation of a cascade that could produce weapons grade uranium [28]. Using the following equations the separative work needed for a weapon can be calculated, assuming a tails mole fraction of 0.3%, initial fraction of 0.7%, final enrichment of 93%, and a final product amount of 50 kg of ^{235}U.

Given the value function:

$$V(x) = (1 - 2x)\ln\left(\frac{1-x}{x}\right)$$

$$Separative\ Work\ (SW) = Product * V(x_p) + Waste * V(x_w) - Feed * V(x_f)\ \text{, so}$$

$$SW = P(2x_p - 1)\ln\left(\frac{x_p}{1-x_p}\right) + W(2x_w - 1)\ln\left(\frac{x_w}{1-x_w}\right) - F(2x_f - 1)\ln\left(\frac{x_f}{1-x_f}\right)$$

$$\text{where } F = P + W \text{ and } F = P\left[\frac{x_p - x_w}{x_f - x_w}\right]$$

The amount of separative work needed is approximately 10,090 SWU-kg, which given a centrifuge capable of 4 SWU/yr.[12], only ~2500 centrifuges would be needed to produce 50kg of HEU in one year, enough to build a crude gun-type weapon [28]. Then assuming that the footprint of each centrifuge is one square foot, and that a third of the floor space of the facility is occupied by centrifuges, only 7500 square feet of space is needed, the equivalent of a 87' by 87' room. In addition to floor space another five to ten thousand square feet will be needed for storage and administration. The equivalent size of a laser enrichment facility producing the same amount of SWU is projected at around the same value of square feet in the estimate of Table 9. Thus, even though the size of the enrichment section of the facility is slightly smaller, the same difficulty in detection standards come into play as the centrifuge facility.

Therefore, a centrifuge facility using a small number of moderately well performing centrifuges to produce HEU may also be able to escape detection because of its limited observable signature [27]. Another important consideration for the detection of either centrifuge or laser enrichment facilities is whether means other than satellite or energy consumption analysis are more capable of detecting one than the other. In both cases thermal output would be low. Also, in both

[12] This type of centrifuge is on the low end of the spectrum, albeit higher than the IR-1 (the Iranian Centrifuge), it is significantly lower than the American Centrifuge at ~350 SWU/yr. The older Russian centrifuges operated by TENEX tend to be between 4-8 SWU/yr. [1].

cases UF_6 leaks would be negligible. This is because the pressure of the laser irradiation chamber and surrounding components are kept below atmospheric pressure, this inhibits the loss of UF_6 to the atmosphere as the pressure differential ensures flow inward and not out of the devices. The same is true for the centrifuge. Also, electromagnetic signals from centrifuges would cancel out each other; the signals from pumping mechanisms in SILEX may also exhibit similar behavior. Therefore, in terms of size, and leakage of UF_6, it seems that the proliferation of laser enrichment technology can be evaluated in an identical manner to the centrifuge. This collection of similarities suggests that methods of clandestine detection by technical means are going to be similar for the two technologies. However, the means of detection will be somewhat different for discovering a program through procurement activities leading to the construction of such a facility. This is probably a more reliable method of detection because of the difficulty present in technical reconnaissance for laser and centrifugal enrichment.

5.1.3. Technology Detection and Import/Export Control

Although timely detection is important, it is a reactive method of verification. An active solution would be controlling the import of certain technologies, which can be an effective deterrent against uranium enrichment proliferation. By maintaining international safeguards for the shipment of certain items, it is possible to flag a particular set of purchases, or to stop the export of certain technologies all together. The United States is part of several multilateral nonproliferation export agreement groups. One such entity is the Nuclear Suppliers Group (NSG) a coalition of 39 nuclear states that implement guidelines for the transfer of nuclear technology to non-member states. The NSG specifically governs the export of uranium isotope separation equipment and components for "unsafeguarded nuclear fuel-cycle activity"[13]. This would of course prohibit transfer of a laser enrichment laboratory, but not necessarily single components. However, NSG guidelines also list specific equipment that is export controlled (called a trigger list); this list includes several components of the SILEX system. Supersonic expansion nozzles that cool gas mixtures to temperatures below 150 K, and are resistant to UF_6 are controlled as part of this list [70]. Another particularly relevant restriction is on pulsed CO_2 lasers that operation

[13] This expression refers to "research on or development, design, manufacture, construction, operation, or maintenance of any reactor, critical facility, conversion plant, fabrication plant, reprocessing plant, plant for the separation of isotopes of source or special fissionable material, or separate storage installation, where there is no obligation to accept IAEA safeguards at the relevant facility or installation" [71].

between 9-11 μm, have a repetition rate greater than 250 Hz, an average output power greater than 500 W, and a pulse width of less than 200ns. The NSG allows higher power lasers to be exported freely, as long as the pulse width is greater than 200ns. Para-hydrogen Raman shifters operating at 16μm are also controlled. Valves that are lined with nickel alloy greater than 50% in composition are also controlled, which is true of the MONEL valves that would be used in a SILEX facility. Vacuum pumps are also regulated by a maximum pumping speed of $15m^3/s$ and an ultimate vacuum no better than .0133 Pa [71]. However, there are no limits on particular nickel alloy shipments or optics equipment. Manufacture of valves or reconfiguration of an industrial CO_2 laser for SILEX purposes would take time, but would not be extremely difficult, when starting from items not under export control.

The most effective control is likely to be that on the para-hydrogen Raman converter; where the converter is a more difficult technology to develop. Para-hydrogen is not complicated to produce, using a helium refrigeration unit normal hydrogen can be cooled to 20 K, at this point the spin states must flip (initially symmetry is forbidden), which requires a paramagnetic catalyst (activated charcoal is an example). The pure para-hydrogen gas can be brought to room temperature, and will slowly convert back to a normal distribution within several hours [73].

As more advanced tunable lasers are invented, the export control system will have to be adapted to include such items on the trigger lists; but items like para-hydrogen may no longer be required. Export controls and trigger lists can be effective means of retarding the spread of enrichment technology, but technologies can always be developed internally by starting from basic materials and science. This is why it is also important to focus on international politics and nonproliferation regimes like NPT. Such political tactics provide excellent incentives for nation states to refrain from clandestine enrichment activities. Technical difficulties and expertise also can affect the interest in research and development, and are important considerations in proliferation likelihoods, but political concerns (and funding) also determine technical interest.

5.1.4. Historical Research and Development of LIS Technologies

Although it is important to be aware of the technical capabilities and knowledge nations have acquired through proliferation analysis, it is also important to be aware of the way which nation states choose technologies. The history of their past pursuits of laser enrichment helps inform those choices. The next several sections highlight the historical pursuit of LIS in all the

countries that attempted research, in order to better understand the role that LIS has in technology choices.

France (1984-2003):

The French, under the supervision of the Commissariat a l'energie atomique (CEA), began a laser enrichment process in 1984. The focus of their work was on atomic vapor separation in a process similar to the American AVLIS. According to a 1984 CIA report [4], CEA scientists believed that SILVA (the French equivalent of the AVLIS program in the United States) was the most promising LIS technology. The CIA concluded from this report that within three years all research focus would be on SILVA and that research on the chemical process CHEMEX would be abandoned due to economic considerations. The analyst further suggested that a commercial enrichment facility could be in operation by the late 1990s, that this timeline would coincide with increased demand for enrichment services, and that SILVA would be competitive on the world market [4].

In 1990 enrichment levels of five percent in a continuous process were reported in the laboratory. Small scale testing of the SILVA system began in 1996 [45]. In 2000, a feasibility study was begun by CEA to evaluate SILVA in comparison to other options. By the end of 2003 it was clear that centrifuges would be the replacement for the Eurodif gaseous diffusion plant and the SILVA program was discontinued. In summary, the French pursued LIS early because of high cost diffusion plants, and similar research in the U.S., but eventually abandoned the project because of the economic considerations of competing technologies.

USSR (1970s-1990s):

In the late 1960s, basic research was conducted by V.S. Letokhov for LIS techniques, both for AVLIS and MLIS. After becoming director of the Institute of Spectroscopy (IOS) he became a staunch advocate in the 1970s for active investigation of atomic excitation, which could be used in subsequent isotope separation experiments [8]. Apparently, the application to receive financial support for the research was partly successful due to its potential use in uranium enrichment. Letokhov believed that MLIS would be easier to obtain, and is probably responsible for its research dominance over AVLIS in the USSR. (A few AVLIS experiments were conducted at IOS between 1976 and 1978, but mainly for non-LIS applications and enrichment of rare earth elements [8].)

During the late 1970s techniques using supercooled UF_6 molecules were the main subject of research [8].

In 1986 a Science and Weapons report on Soviet research into LIS stated that little of the laser isotope research done by the Soviets was with uranium, and only then using MLIS techniques, and that they were still in the early stages of development. The report concludes that the Soviet MLIS programs were only of an "academic or basic physics nature," and still were in the laser spectroscopy phase [8]. The report goes on to describe the extensive enrichment research done by the United States and paints a picture of a competitive lead. It is important to note that this report also incorrectly suggests that the Soviets would have to choose between pursuing the gas centrifuge or LIS to maintain current levels of enrichment capacity. At this point the Soviets had been operating centrifuge plants for over twenty years apparently unbeknownst to the U.S. intelligence services [27, 36]. Other CIA reports contend that the Soviets had a strong economic incentive to pursue LIS in order to increase profits from enrichment contracts [7]. This contention was completely incorrect, the massive, cheap Soviet centrifuge system made any other technique pale in economic comparison. The existence of large centrifuge facilities, like Sverdlosk-44 (Свердло́вск-44), likely made an impact on the level of interest in new laser enrichment technology.

In the mid-1990s Russia began negotiations to sell a laser enrichment laboratory to Iran. Under pressure from the United States, plans to sell LIS technology were discontinued in 2000 [46]. In 2013 the director of the Russian Power Engineering and Safety Center, Anton Okhlopkov, stated that:

> "The Soviet Union and then Russia pursued research [on laser enrichment] in the past, only to conclude that the technology can be effectively used in a laboratory environment, but is no good for use on industrial scale. Whatever cost value gains have been made in a lab will be lost in switching over to industrial production" [47].

There is no evidence of renewed interest in LIS research in Russia, and publically all new enrichment developments seem to center around the tenth generation of Russian centrifuges. This makes great economic sense because Russian centrifuges are the cheapest (32-45$/SWU [88]) in the world, and there is no incentive to invest time and resources into a possibly economically equivalent, high risk technology.

Japan (1982-2001):

In 1984 Japan began an assessment program for LIS technology, specifically researching and developing AVLIS technology. This work began after preliminary analysis of LIS beginning in 1982. Research was conducted at the Japan Atomic Energy Research Institute (JAERI) as well as other organizations. At the beginning of 1987 nine electric companies established the Laser Enrichment Technology Research Organization to further the development of LIS techniques in Japan [49]. The first prototype system was constructed in 1988 and completed tests that same year, achieving laser target intensities. All the major components of the enrichment system were well understood by Japanese research laboratories, based on scientific publications produced by JAERI in the early 1990s [48].

By the 1990s the theoretical and scientific work for a production system of five percent enrichment had been completed, and the Japanese corporation LASER-J was selected to develop hardware while JAERI continued with separation process development. However, MLIS was not entirely ignored in Japan; the Institute of Physical and Chemical Research worked in parallel with AVLIS development on molecular techniques. There was some success using Raman scattering through para-hydrogen to achieve enrichment levels of 3.3% $^{235}UF_6$ [49]. This process was called RIMLIS (RIKEN's Molecular Laser Isotope Separation). This process used a super-cooled, supersonic UF_6 flow and a 16μm laser to produce $^{235}UF_5$ particles [45]. However, on October 2, 2001 the Japanese Ministry of Economy, Trade, and Industry decided to cease research and development on LIS technology in favor of improved centrifuge methods. In summary, Japan pursued LIS early because of an interest in developing indigenous (non-diffusion) enrichment capability, but eventually abandoned the project because of the economic considerations of competing technologies.

Brazil (1975-1990):

Brazilian investment in enrichment technology began with the purchase of Becker nozzle technology from West Germany. A small pilot plant was built with 24 nozzle separation stages, and was operational by 1984 [50]. This would have provided Brazilian nuclear services with knowledge of nozzle separation processes, an important stage of the MLIS process. In terms of laser enrichment both the Army and Air Force explored laser applications, but in 1975 the Brazilian

Air Force adopted sole responsibility for research on laser enrichment while the Army pursued centrifuge technology [51].

In a seminar on Argentine-Brazilian Nuclear Rapprochement, Dr. Marco Marzo (an ABACC senior officer), stated that the Air Force's work on laser enrichment had practically ceased in 1988-1989. He also stated that in an earlier visit to the facility, in 1985-1986, the project was still underway [52]. Publically, in 1990, the Air Force's laser enrichment program was cut and soon after terminated as spending priorities changed [53]. The successful development of a Brazilian centrifuge (if indeed independently developed) by the Brazilian Navy led to its establishment as the enrichment method of choice in the late 1990s [54]. In summary, Brazil co-pursued LIS early because of similar research programs globally, but eventually abandoned the project as successes in centrifuge development directed future investment.

Iran (1975-1978, 1983-2003?):

Iran began its development of a nuclear energy program at the beginning of 1974. Soon after the inception of this program the Laser Technology Division (LTD) within the Tehran Nuclear Research Center (TNRC) was born. In the beginning of 1975 the LTD began research work exploring both AVLIS and MLIS enrichment techniques [30]. Spectroscopic work quickly followed, and many laser specialists were brought onto the project (both foreign and domestic). One of these specialists was Dr. Jozef Eerkens, who had contacted Shah Pahlavi, the ruler of Iran, about his work in laser enrichment and received word from the TNRC of their interest in bringing him on board. Eerkens, together with several investors, formed a company called Lischem to work on developing the laser systems needed for the Iranians' enrichment laboratory. The work was conducted in the United States, and the equipment would be accompanied by Eerkens to Iran once completed. Agreements between Lischem and the TNRC were finalized in 1977 [30]. Eerkens would be a consultant for the project for a period of two years, and the equipment would be provided in two separate shipments.

By 1977, the Iranians had also placed orders with South Africa for conversion apparatus to begin producing uranium hexafluoride, which is the feed material for MLIS processes. In 1978, after an extensive review of the export application, the shipment of equipment to Iran was approved. During this time the U.S. was also in negotiation of a peaceful nuclear energy cooperation agreement (termed the 123 agreement) [30], to begin exporting reactors to Iran.

Interestingly enough, comprehensive reviews of technology to be exported, and associated proliferation risks were policies just beginning to be considered by the DOE. In late 1978, political unrest and economic crisis led to the cancellation of many nuclear projects. The shipments of lasers and irradiation chambers were still sent to Iran in November of 1978 to fulfil the contracts. However, the optical equipment never reached Tehran, it was stopped in the Netherlands with Eerkens by the State Department, due to the political unrest in Iran. The new government had little interest in the technology, and the previously involved members of leadership in the TNRC fled the country.

The equipment was unused until 1983 [30], when the government decided to begin enrichment research anew. The enrichment unit was incomplete, due to the missing optics, and apparently attempts failed to re-engineer the full design [30]. Iran resumed research in the 1990s into AVLIS, with significant resources, using German and Chinese equipment [30]. In May of 2004, Tehran informed the International Atomic Energy Agency (IAEA) that as of May 2003 all laser enrichment equipment had been dismantled and research had ceased. However, in 2010, then President Ahmandinejad stated that Iran had significant laser enrichment technology capabilities [30]. Iranian government officials later clarified this statement in 2014 to the IAEA, saying that no new research had been conducted since 2003 at the Lashkar Ab'ad Laser Center [55]. However, without renewed inspection of the facility the current status of laser enrichment in Iran is unknown. In summary, Iran pursued LIS early because of an interest in developing new technology, but due to political unrest and success in centrifuge development, there has been no further need to continue LIS research.

Germany:

West Germany, or the Federal Republic of Germany (FRG) concentrated mostly in the 1980s on MLIS technology, finding it more competitive than AVLIS. The company that led research in the FRG was known as Uranit (a shareholder in URENCO). In 1988 a separation factor of 15 was reportedly achieved on a laboratory scale. At this time Uranit planned to build a 1:100 scale pilot plant to be operation by 1996, and a 1:10 scale plant by the beginning of the 21st century [56]. In summary, the FRG developed LIS early in an attempt to design a competitor for high cost diffusion plants, but eventually abandoned the project because of the economic considerations of competing technologies.

India (1980-present):

Research in laser enrichment in India took place at the Bhabha Atomic Research Center, the same location as the CIRUS-Dhruva nuclear reactors. The same location also hosted research on centrifuge development. By 1984, the director of the center, Dr. P.K. Iyengar, suggested that enrichment had been successful, whether or not this was in reference to experiments dealing with the centrifuge or a laser process is unclear [57]. The Center for Advanced Technology (CAT) in Indore was also involved in developing laser enrichment technology by 1993.

A second facility, called the Laser Enrichment Plant, also began research work in 1993 [58]. The focus of research at CAT was on laser development for multiple projects including high power carbon dioxide and copper vapor lasers, which are key to LIS uranium enrichment. Research was still ongoing in 2004, according to M.V. Ramana a researcher at ISEC in Bangalore [59]. According to an interview in 2013 with Dr. R.K. Sinha, Chairman of India's Atomic Energy Commission and Secretary of Atomic Energy, there still exists an active research program on laser enrichment [60].

Israel (1974-?):

In 1974 a physicist within Israel's Ministry of Defense claimed that Israel had already demonstrated success with laser enrichment. In 1986 Mordechai Vanunu, a nuclear technician who later become an activist, described the existence of an Israeli laser enrichment facility, at Dimona Center (a location which was used for the sole purpose of enriching uranium and purifying plutonium), specifically in the building known as Machon 9 [61]. Vanunu stated that in 1981 Israeli scientists began to use lasers to separate uranium isotopes, and were able to expand the design to production scale by the time he left in 1985. The U.S. rebuffed his claim, stating that at that time there was no known Israeli capability for full-scale enrichment, but that all laser isotope separation had occurred in a laboratory setting. In the late 1980s a LLNL source also reported that Israel was seriously investigating the AVLIS process as well [56]. Given that most countries have stopped, it seems unlikely research in AVLIS is still ongoing, but impossible to know due to Israeli secrecy and their non-membership in the NPT.

China (1975-1993):

CIA declassified reports on the PRC concluded, in 1986, that the Chinese began studying LIS in 1975 [5], but were decades away from building and operating a commercial LIS uranium enrichment facility at that time [9]. China has initiated research and development of both MLIS and AVLIS processes. The Chinese conducted experiments at the Physicochemical Engineering Research Institute of the Nuclear Industry Ministry and within the Chinese Academy of Science. Due to early Soviet interest in MLIS, the Chinese concentrated their efforts on such techniques and processes. Some results using MLIS were achieved by 1979.

However, in 1985 research became focused on the development of AVLIS, with the possibility of a pilot plant being built by 1990. At Fudan University a replication of the CRISLA process (another result of Jozef Eerkens' work with Isotope Technologies) was constructed using published and open-source data [56]. Notably, in 1993 China decided to purchase centrifuge technology from Russia and develop more advanced technology in cooperation [46]. Since that point several industrial enrichment plants using centrifuge technology have been completed. The current status of research in China on LIS is unknown, but laboratory scale research could possibly still continue.

Canada (1990-1993):

In 1990 CAMECO, the Canadian uranium producer, invested heavily in Isotopes Technology Inc., another company founded by Eerkens, to pursue a new enrichment methodology known as CRISLA. The company relocated to Saskatoon, Saskatchewan, Canada. Research and development continued under CAMECO leadership until 1993 when the Board of Directors voted to cease funding in the development of CRISLA in favor of buying Russian LEU [30] (the vote was 5-4). The Canadian interest in indigenous laser enrichment was likely the shortest lived of all of the LIS programs. It is important to note that CAMECO invested in a 24% stake in GLE; the current LIS scheme being tested in the United States.

United Kingdom (1982-1994):

The United Kingdom Atomic Energy Authority (UKAEA) began LIS work in 1983 by studying molecular laser separation; however, in 1984 decided to pursue the atomic separation process AVLIS instead. British Nuclear Fuels had begun a laser isotope separation program in

1982 and by 1986 was of the opinion that by the late 1990s a commercial facility could be built. Development of an AVLIS facility involved cooperation between UKAEA and BNF, and a small-scale demonstration plant was planned for completion in the mid-1990s [56]. It was projected that by 1992 an evaluation of AVLIS' competitiveness with the centrifuge would be completed. However, comparison with centrifuge technology made it clear that it was cheaper and by 1994 research and development on AVLIS was for all practical purposes defunct.

Australia (1988-2007):

Development of SILEX began within Silex Systems Ltd., a corporation run by Michael Goldsworthy in 1988. Michael Goldsworthy and Horst Struve, both South African scientists, reportedly discovered the SILEX process. SSL sold a license to use the technology in 1996 to the United States Enrichment Corporation (USEC). However, due to political factors USEC never implemented the technology in the US. At this time, USEC was in the process of being privatized and had little options after the failure of AVLIS to be commercially viable. Research and development continued in Australia at the company's facility in Lucas Heights near Sydney. A joint classification agreement of the technology between the United States and Australia was reached in 2001 [10]. Secondary testing was completed in 2005 and an enrichment test loop program was developed by 2007, this program was exported to the Wilmington, NC as a result of an agreement with GE-Hitachi Nuclear Energy under the auspices of GLE.

South Africa (1980-1997):

Research on AVLIS began in the early 1980s at the National Physical Research Laboratory in Pretoria. By 1986 research on dye lasers, for the purpose of implementation in an AVLIS separation process, was concluded. Apparently MLIS research was also ongoing during this time as well. According to a paper presented at the 1992 International Symposium on Isotope Separation and Chemical Exchange Uranium Enrichment, South Africa's MLIS project was in the pilot plant stage, and work continued on "eliminating part of the laser energy by using chemical energy or reactions (CRISLA process)." This MLIS laser enrichment R&D facility [62] was inspected by the IAEA in 1991.

Most work on uranium enrichment during the earlier decade seemed to be focused on the Helikon vortex separation process, an aerodynamic technique that requires large amounts of

power. After the Helikon system was shut down, South Africa planned to use the old facility as the location of a new demonstration plant for their MLIS laser enrichment process, to be built in 1993-1994. MLIS became the focus of the enrichment effort in South Africa, where the end goal was to export LEU to other countries. In 1994, SA announced that it had decided to construct a MLIS plant; however, international partners were needed to help develop the technology. At the end of 1997, the Atomic Energy Commission of South Africa announced that MLIS research and development would cease; this following the withdrawal of Cogema (now AREVA). This decision, and the ensuing budget cuts to the AEC, effectively ended laser enrichment development in South Africa [63].

South Korea (1975-2004):

Research into lasers for the purpose of isotope selectivity began in the late 1970s. Early work focused on the development of high power CO_2 lasers and polarization spectroscopy. The Korea Atomic Energy Research Institute (KAERI) was responsible for research efforts. From 1975 to 1985 MLIS work focused on multi-photon dissociation of light elements, this focused on deuterium and tritium. It is unlikely that any MLIS research was attempted to enrich heavier elements like uranium. Both the United States and Russia provided technical knowledge to South Korean scientists; the former on laser technology, the latter on particulars of AVLIS technology. Although uranium separation may have been a laboratory interest, it seems as though most of the AVLIS work involved separation of rare earth metals for burnable poisons to be added to nuclear fuel. Ytterbium may have been the main target of experimental analysis [64]. Using knowledge of ytterbium separation it is relatively straightforward (through laser wavelength adjustment) to apply the same AVLIS process to uranium. In 2004 it was discovered that KAERI had in fact been using AVLIS techniques to enrich uranium isotopes. In 2000 roughly two-hundred milligrams of enriched uranium (ranging from 10-80% in isotopic abundance) was produced from a feed of 3.5 kg. The enrichment experiments appear to have been only at a laboratory scale, and seems that no effort to develop pilot facilities was attempted [65]. In summary, the South Korea pursued LIS in a similar way to Japan, for the purpose of building indigenous enrichment capability; however, with fuel agreements and political agreements with the U.S. it has been unnecessary (under U.S. encouragement) for SK to develop enrichment technology.

5.1.5. Discussion of Nation State Histories

These histories provide several interesting points of note. First, in all countries where laser enrichment was pursued, it was one of several competing technologies. Nations approached the issue of enrichment by hedging technologies, and opting for a multi-tiered plan of research. This may be applicable to the future, in the sense that nations interested in pursuing enrichment will adopt laser programs as well. If, as is predicted in this thesis, the centrifuge and laser are roughly economically equivalent, there is likely to be less interest in laser development in countries where enrichment facilities already exist (that is assuming the technical feasibility of SILEX in the future). The locations where laser facilities may thrive will likely be nation states new to enrichment technology, where technical understanding and faster engineering delivery will determine enrichment choices. Nations experienced in the enrichment hierarchy may be less likely to pursue laser enrichment due to locked-in investments and economic considerations, and possibly disaffection with past LIS failures. A more general example of this is in China, where many different types of nuclear reactors are being co-developed and one or more designs (possibly not LWRs) will become prevalent. Therefore, new entrants into enrichment development may be more likely to pursue research and development into alternative enrichment technologies, like laser separation (and may be more successful at LIS than established enrichment nations).

5.2. Proliferation Conclusions

Even though nearly all LIS projects have been abandoned by many of the countries that explored them because of technical difficulties and economic concerns, this does not mean the future will not make the technology viable. As social factors and technical understanding change, and the demand for enrichment services increase, scientific exploration into isotope separation techniques will likely continue [38]. Proliferation of the technology is only one issue, but also the ability of LIS to produce HEU is another important consideration. John Lyman in his report on the status of SILEX technology concluded that the process was not "currently" able to produce significant amount of HEU [34]. If SILEX was only capable of producing enrichment of less than 30%, there would be less concern about weapons production.[14] There seems to be little consideration of these issues in the current literature, and even among decision makers when

[14] It is unlikely that SILEX is limited to such constraints. Lyman's reference refers to the laboratory setup of SILEX, and the current experiment, not necessarily a lack of capability by the process physics.

discussing the development of laser enrichment facilities. The potential for proliferation of the technology has been seen as a relatively minor concern in history, although LIS is theoretically as prone to proliferation as the centrifuge. There must be a recognition that SILEX is one step away from being both an economically competitive option as well as a proliferation risk. The game changer for SILEX is an advanced, cheaper laser, which is likely inevitable with the current progress in laser technology. Other uses for SILEX must also be considered in a non-proliferation regime, like whether or not it is viable for use in plutonium isotope purification. In conclusion, policy makers must be aware that technical vigilance both in terms of monitoring exports and R&D in developing countries, as well as continuing to strengthen political agreements is still the best way to minimize proliferation risk from technologies like the gaseous centrifuge or SILEX.

Conclusion

The purpose of the research undertaken and described in this thesis was to evaluate the LIS process SILEX in terms of both its technical parameters and its proliferation potential. In terms of technical analysis the physical behavior governing the isotope separation process was discussed. Using this physical framework it was possible to develop simulations to optimize the operating conditions of such a facility. The simulation suggests that enrichment factors between 1.5 and 2 are reasonable estimates for this technology. It seems likely that the enrichment factor within this environment is higher than modern centrifuges; however, a lower product cut (~0.25) requires a larger and asymmetric cascade design. As a result, the advantages of a higher enrichment often cited—fewer stages to go to weapon-grade, for example—may be offset by the complexity of the asymmetric cascade. Using fluid dynamics software, initiated by the optimal physics results, a region of probable irradiation within the supersonic flow was determined. This region, and the flow behavior provide a useful prediction for the development of a test unit. The laser irradiation region is close to the output of the nozzle, and occupies a fairly large area, which suggests that laser placement may not have to be incredibly precise. The development of a theoretical SILEX facility was also considered, a cascade model for two levels of product enrichment (reactor and weapons grade) was computed. This provided evidence that although there is added complexity, the number of stages in a SILEX cascade is still lower than that of a centrifuge. It was determined that the cascade of choice would be a two-up one-down design, which is optimal for cuts ranging from 0.2-0.3. The next step was an engineering design of a SILEX unit. Maximizing throughput,

by utilizing many supersonic streams in a single unit, may be the most effective way to cut costs. In order to do this, it was verified that a single laser would be able to penetrate multiple parallel streams of gas. Under this assumption a preliminary engineering unit design using materials like Monel, nickel alloys, steel, aluminum, and Teflon was considered.

Based on this engineering model, and using the cascade model that was developed it was possible to determine several useful economic metrics for the technology. First, a calculation of the capital costs determined that a 1 MSWU facility would cost a producer roughly 0.5 B ($US), based on the cost for materials to construct and design such a facility. This estimate enabled the levelized cost for SWU to be computed, at $39.72; a value approximately equal to the cheapest centrifuge enrichment plants. The impact on the total cost of the nuclear fuel cycle was also considered, using this levelized $/SWU value. The impact was minimal, and resulted in roughly a one cent decrease in cost per kW/hr. It is important to note that these economic models assume that the development of continuous laser has already occurred, without the added complexity of a Raman cell. This will likely be necessary before SILEX is economically viable. As soon as a new 16 μm, high-powered, continuous laser enters the mix, there will be a significant economic incentive for pursuing SILEX. Thus, because of high probability of future laser innovation, it is necessary to discuss methods of minimizing proliferation of enrichment technology. Several important analyses of the proliferation potential of SILEX were undertaken. These analyses included determining the size and characteristics of a small weapons grade production plant (in comparison to one using centrifuges) and possible methods of detection. There was little difference in these points of analysis between SILEX and the centrifuge. The physical space required by both technologies in a clandestine facility is nearly identical, both could fit inside a small warehouse. Similar operating characteristics make such facilities nearly impossible to detect by tracing effluent streams or by power consumption. Another option is to monitor technical knowledge and capabilities in proliferation assessments; however, it is likely that indigenous capabilities and minimal technical know-how may be sufficient to develop research and development programs. Finally, a historical analysis provided some evidence that the most likely entrants into SILEX R&D will be countries pursuing enrichment for the first time; unless the cost of SWU in SILEX ends up being lower than the centrifuge. Nonetheless, it seems likely that the most effective means for the United States to ensure non-proliferation of SILEX technology is to continue adopting proactive technical standards and to maintain strong international agreements.

Appendices

Appendix 1: SILEX Physics & Enrichment Factor Calculation Code

```
%% Extraneous variables (User Input Stage)
%{
prompt='Desired Gas Expansion Temperature (K):';
T=input(prompt);

prompt2='Pressure of carrier gas (torr):';
Pm=input(prompt2);

prompt3='Mole fraction of UF6 required:';
yq=input(prompt3);
ym=1-yq;

prompt4='Required Radius of Supersonic Jet (cm):';
R=input(prompt4);

prompt5='Required Length of Supersonic Jet (cm):';
L=input(prompt5);

choice=menu('Carrier Gas','H2','He','N2','Ar','Xe','SF6');
switch choice
    case 0
        carrier='Xe';
    case 1
        carrier='H2';
    case 2
        carrier='He';
    case 3
        carrier='N2';
    case 4
        carrier='Ar';
    case 5
        carrier='Xe';
    case 6
        carrier='SF6';
end

%}
%-------------------------------------------------------------------------
T=0;
cut=zeros(100,1);
factor=zeros(100,1);
count=0;
thetaom=0;
while (thetaom<1 && count<100)
carrier='Xe';
h=1;                              %Planck's constant
count=count+1;
T=T+1;                           %gas expansion temperature in K
T0=300;                           %gas reservoir temperature in K
Pm = .0035;                       %pressure in torr of carrier gas
```

```
yq= .02;                          %mole fraction of UF6
ym=.98;                           %mole fraction of carrier gas
xi=.0072;                        %isotopic abundance of U-235 hexafluoride
R=1;                              %radius of the skimmer at the exit of the
free jet (cm)
L=20;                             %length of the jet from nozzle output to
skimmer(cm)
%-------------------------------------------------------------------------
%ONLY EDIT VARIABLES ABOVE THIS LINE
%-------------------------------------------------------------------------
Mq = 352.019;                     %mass of QF6 in amu
Mm = 146.055;                     %mass of carrier gas in amu (SF6)
sigmacQQ=370.3;                   %collision cross section for UF6/UF6 (A^2)
Pq=2*10^-4;                       %partial pressure of UF6 (torr)
rhoq=5.09;                        %density of UF6 condensate (g/cm^3)

roQ= 6;                           %collision radii of UF6

if strcmp(carrier,'H2')
    Lr=.107;                      %repulsive range (A)
    Mm=2.016;                     %molar mass of H2 (amu)
    Mqm=1.99;                     %reduced mass of carrier gas, QF6 system
    sigmacQM=221.0;               %collision cross section for G and QF6
    roG=2.959;                    %collision radii of carrier gas
    Uso=1321;                     %reservoir sonic velocity at T=300K (m/s)
    gamma_aero=1.4;               %gamma_aero=cp/cv
elseif strcmp(carrier,'He')
    Lr=.117;
    Mm=4.0026;
    Mqm=3.96;
    sigmacQM=201.0;
    roG=2.57;
    Uso=1019.3;
    gamma_aero=1.667;
elseif strcmp(carrier,'N2')
    Lr=.117;
    Mm=28.014;
    Mqm=25.9;
    sigmacQM=260.6;
    roG=3.68;
    Uso=353;
    gamma_aero=1.4;
elseif strcmp(carrier,'Ar')
    Lr=.135;
    Mm=39.948;
    Mqm=35.9;
    sigmacQM=245.9;
    roG=3.42;
    Uso=322;
    gamma_aero=1.667;
elseif strcmp(carrier,'Xe')
    Lr=.146;
    Mm=131.293;
    Mqm=95.9;
    sigmacQM=282.8;
    roG=4.055;
    Uso=178;
```

```
    gamma_aero=1.667;
elseif strcmp(carrier,'SF6')
    Lr=.096;                    %repulsive range parameter in angstroms
    Mm=146.055;
    Mqm=103.2259;               %reduced mass in amu
    sigmacQM=342.2;             %cross section for collision (Angstrom^2)
    roG=5.01;
    Uso=150.7;
    gamma_aero=1.33;
end

% Aerodynamics Calculations

Ust=((2/(gamma_aero+1))^(1/2))*Uso;
U=Uso*(((2/(gamma_aero-1))*(1-T/T0))^(1/2));
t_tr=(2*L/(U+Ust))/100;         %travel time of gas from nozzle to skimmer

%% Laser Excitation of UF6

IL=2000;                        %W/cm^2 intensity of laser
sigmaA = 10^-18;                %typical laser photon absorption cross
section for v3 @ T<150K (cm^2)
eL = 628;                       %cm-1 laser photon energy or h*vL for v3
vibration of U235 e3 = 628.3
phiL = (5.055*10^22)*IL/eL;     %photons/cm^2-s called laser flux
Ka = phiL*sigmaA;               %units: molecules/sec called laser excitation
rate

%% Spontaneous Emission of UF6  v3=1--->0

lambda3=15.9*10^-4;             %15.9um for UF6
AEse = 12.0;                    %measured value for UF6 (v3) spontaneous
emission rate per sec
Tse = .083;                     %measured value for time before spontaneous
emission of photon
M3 = 119.88;                    %vibrational mass of UF6(v3) from measured
value (calculated from AEse or "Einstien rate")
Z3 = 5.46;                      %derivative depole change
x3= .0017;

%Unlikely that UF6 will lose vibrational energy in supersonic free jet

%If v3 vibration is excited in UF6:G or UF6:UF6 dimers, predissociations
%prevail over relaxation due to photon spontaneous emission-few photons are
%released.

%%  Collision Induced Reaction of UF6 (Process 1)

nm=(.97*10^19)*Pm/T;                %cm^-3
%Mqm = Mq*Mm/(Mq+Mm);               %reduced mass for UF6/SF6 from table 1A
%sigmacQM = 342.2*10^-16;           cross section from table 1A in EERKENS
2004 (cm^2)
uQM = (1.457*10^4)*(T/Mqm)^(1/2);   %relative molecular velocity (cm/s)
Kc = nm*sigmacQM*uQM*(10^-16);          %collision rate with all particles
(G & QF6), collisions per second
%Kc=(1.41*10^7)*sigmacQM*Pm/((T*Mqm)^(1/2));
```

```
sigmacQG = sigmacQM;            %M can simply be replaced by G with high
percentage of carrier gas, neglect elastic QF6 collisions
lc = (1.04*10^-3)*T/(sigmacQG*Pm);   %might be Pg if Pg is different than Pm
(cm), mean free collision path

%vast majority of QF6 + M(G) result in elastic collsions
%some result in the formation of QF6:M dimers
%for excited QF6*, encounters can cause VT or VV transfer
%to minimize losses due to VV transfer high carrier gas dilution is needed
%VV transfers cause isotope scrambling which mixes the excited QF6 isotope

%% Direct Specular VT Relaxation (Process 2)

%REACTION:  QF6*+G-->QF6*:G-->QF6 + G + K.E.

k=.695;                                 %cm-1/K
v3=627.7;                               %vibrational state v3 for UF6 cm-1
e3= v3*h;                               %energy quantum in cm-1 for VT

X3=.21*Mqm*(Lr^2)*(e3^2/T);
if X3 < 20
    Fc=(1+.4548*X3^(5/6))*((1.5*X3^(1/3))^2)*(csch(1.5*X3^.5)); %in
nonsimplified
%case where X<20, also known as collision function
else
    Fc=4*((pi/3)^.5)*(X3^(3/2))*exp(-3*X3^(1/3)); %where X>20
end

squigglevt3=(2*k*T/e3)*(M3/Mqm)*Fc*exp(-.5*e3/(k*T));

if T==100 && strcmp(carrier,'H2')
        X3= 18.9;
        Fc=.1357;
        squigglevt3=4.09*10^-2;
elseif T==100 && strcmp(carrier,'He')
        X3=44.9;
        Fc=3.15*10^-2;
        squigglevt3=4.76*10^-3;
elseif T==100 && strcmp(carrier,'N2')
        X3=296.5;
        Fc=4.4*10^-5;
        squigglevt3=1.01*10^-6;
elseif T==100 && strcmp(carrier,'Ar')
        X3=540.6;
        Fc=1.3*10^-6;
        squigglevt3=2.11*10^-8;
elseif T==100 && strcmp(carrier,'Xe')
        X3=1696;
        Fc=8.3*10^-11;
        squigglevt3=5.23*10^-13;
elseif T==100 && strcmp(carrier,'SF6')
        X3=796.1;
        Fc=4.4*10^-5;
        squigglevt3=1.01*10^-6;
elseif T==30 && strcmp(carrier,'H2')
        X3=63.0;
        Fc=1.34*10^-2;
```

```
        squigglevt3=1.55*10^-8;
elseif T==30 && strcmp(carrier,'He')
        X3=150.0;
        Fc=8.99*10^-4;
        squigglevt3=5.24*10^-10;
elseif T==30 && strcmp(carrier,'N2')
        X3=988.3;
        Fc=1.34*10^-8;
        squigglevt3=1.19*10^-15;
elseif T==30 && strcmp(carrier,'Ar')
        X3=1802;
        Fc=4.4*10^-11;
        squigglevt3=2.81*10^-18;
elseif T==30 && strcmp(carrier,'Xe')
        X3=5653;
        Fc=1.1*10^-17;
        squigglevt3=2.59*10^-25;
elseif T==30 && strcmp(carrier,'SF6')
        X3=2154;
        Fc=5.1*10^-13;
        squigglevt3=1.14*10^-20;
else
end

Kvt=Kc*squigglevt3;              %VT relaxation rate

%probabilities for comparison and values are found in Eerkens2004 Table 1B
%There is a probability for VT de-excitation with QF6 and QF6*, however the
%probability is extremely low, much more likely to experience resonant VV.

%% Direct Specular Resonant VV Transfers (Process 3)

Mqq=.5*Mq;                                    %reduced mass of identical dimer
system

cqq1=(sigmacQQ/sigmacQM)*((Mqm/Mqq)^(1/2)); %correction factor for cross
section and masses
cqq=((2*roQ/(roQ+roG))^2)*((2*Mm/(Mm+Mq))^.5);
squigglevv3=(M3/Mqq)*(k*T/e3)*x3;             %probability of vv collision

Kvv=squigglevv3*yq*cqq*Kc;                    %VV transfer rate (VALUE SEEMS
TOO LOW, DOESN'T MATCH EERKENS)

%% Dimer Formation Rates (Process 4)

%epsilona= h*va;                  fundamental energy (frequency) quantum of
dimer bond
switch carrier
    case 'H2'
        Da=88.19;                %well depth of the dimer band, Table 4,
Eerkens 2001a
        epsilona=62.8;
        epsilonq=5.103;
        zeta=.0113;
    case 'He'
        Da=47.83;
        epsilona=34.4;
```

```
        epsilonq=10.15;
        zeta=.0226;
    case 'N2'
        Da=139.3;
        epsilona=20.1;
        epsilonq=66.56;
        zeta=.1510;
    case 'Ar'
        Da=162.2;
        epsilona=19.0;
        epsilonq=92.17;
        zeta=.2110;
    case 'Xe'
        Da=220.2;
        epsilona=12.7;
        epsilonq=245.4;
        zeta=.5870;
    case 'SF6'
        Da=234.3;
        epsilona=11.4;
        epsilonq=264.8;
        zeta=.6356;
    otherwise
        Da=0;
end

vd=2*(Da/epsilona)-.5;          %highest dissociation vibrational quantum
level in dimer potential well
etax=.25*(epsilona^2)/(Da*k*T);
fqm = (yq*Mq+ym*Mm)*(yq*Mm/Mq + ym*Mq/Mm)/(Mq+Mm+yq*Mq+ym*Mm);
pqm=Mm*(2*Mq+Mm)/((Mq+Mm)^2);
squiggle1=2*pqm*(k*T/epsilona)*exp(-.5*etax);
squiggle0=squiggle1*exp(-squiggle1);
squiggledf=fqm*vd*squiggle0*(1-(1+etax)*exp(-etax));

Kdf=Kc*squiggledf;              %dimer formation rate for QF6:G

%% Collisional Dissociation Rates of Dimers (Process 5)

%probability that dimer UF6:G dissociates to UF6 + G in collision with
%molecule G.

squiggledd=.5*(exp(-Da/(k*T)))*(1-exp(-epsilona/(k*T)));
ad=(((roQ+2*roG)/(roQ+roG))^2)/((1+(Mm^2)/(Mq^2 +2*Mq*Mm))^(1/2));

Kdd=Kc*ad*squiggledd;   %dissociation rate of dimers (s^-1)

%% Molecular Migrations and Thermalization of Epithermals (pg. 234-235)

Pg= Pm;                             %carrier gas pressure is the same as
pressure m
epsilont=k*T;                       %thermal kinetic energy, final energy
state

%Kw=(29.3*T^(3/2))/(Pg*R^2*sigmacQG*(Mqm^.5)); %alternative Kw calculation
scheme
```

```
Kw=1.928*Kc*(lc/R)^2;                %rate of non-excited and vibrationally
excited monomers that strike wall of jet/escape (100% absorbent)

eta_qg=Mm/(Mm+Mq);
a=epsilonq/epsilont;
mu1=(a/log(1+a))^(1/2);

Kw1=mu1*Kw;                          %epithermal wall escape rate
theta1=1-exp(-1*mu1*Kw*t_tr);        %epithermal escape fraction, depends on
travel time t_tr

phid=(((roQ+roG)/(roQ+2*roG))^2)/((1+(Mm^2)/(Mq^2 +2*Mm*Mq))^(1/2));
%migration rate correction factor (<1)
Kwd=phid*Kw;                         %escape rate for dimers from the free jet
thetad=1-exp(-1*phid*Kw*t_tr);

alpha=((Mq-Mm)/(Mq+Mm))^2;
zeta=1+(alpha/(1-alpha))*log(alpha); %average logarithmic energy  decrement
Nt=(zeta^-1)*log(1+a);               %average number of collisions to
thermalize a epithermal molecule

omegabar=1-(alpha+1)/2;              %average fractional energy loss for each
epithermal momentum transfer collision
Sth=1.41*(Nt^(1/2))*lc;              %slowing down length, or migration
distance of the epithermal

vT=(1/3)*(lc^2)*Nt;                  %thermalization age of epithermal
molecule

Kth=mu1*Kc/Nt;                       %thermalization rate of epithermals in a
gas, feed term for the thermal group

%% Populations of Dimers, Laser-excited Molecules, and Epithermals

%Monomer Excitation Scheme(Excitation-->Dimerization-->Dissociation--
>Thermalization)

estar=exp(-.519*((lc/R)^2)*(squiggledf+squigglevt3+squigglevv3+AEse/Kc));
%To-the-wall survivial probability for QF6*,~0
e1=exp(-.519*((R/lc)^2)/Nt);         %to-the-wall survival probability for
epithermals
kappa1=(1-estar)*(Kdf+Kvt)/((1-e1)*Kth+e1*Kw1);
omegad=Kdf/(Kdf+Kdd);
fistar=((1-omegad)*Ka)/((kappa1+1)*(1-omegad)*Ka+(1-
estar)*(Kdf+Kvv+Kvt+AEse)+estar*Kw);
fid=(1-(kappa1+1)*fistar)*omegad;    %fraction of non-excited dimers
fiexc=kappa1*fistar;                 %the higher this value the higher the
isotope separation is, fraction of epithermal iQF6 molecules
fim=1-fistar-fid-fiexc;              %fraction of non-excited monomers, iUF6

%Dimer Excitation Scheme(Dimerization-->Excitation-->Dissociation--
>Thermalization)

fiexc_d=(1+(Kth/Kdf)+(Kth/Ka)*(1+Kdd/Kdf))^-1;
fid_d=(1+(Ka/Kth)+(Ka/Kdf)+(Kdd/Kdf))^-1;
fim_d=1-fid_d-fiexc_d;
```

```
%% Enrichment factor Bm for Monomer Laser Excitations

phi_1=(1-exp(-1*Kw1*t_tr))/(1-exp(-1*Kw*t_tr));
phi_d=(1-exp(-1*Kwd*t_tr))/(1-exp(-Kw*t_tr));
Beta_m=(1+fiexc*(phi_1-1)-fid*(1-phi_d))/(1-omegad*(1-phi_d)+xi*(omegad*(1-
phi_d)+fiexc*(phi_1-1)-fid*(1-phi_d)));  %Enrichment factor

cd=omegad*(1-phi_d);

%% Enrichment factor Bm for Dimer Laser Excitations

%lambda1=Ka/Kth;
%Beta_d=(1+((phi_1-1)*lambda1-1+phi_d)*fid_d)/(1-cd);        %Enrichment
factor, true for xi<<1

%% Product cuts for Laser Excitations

theta=1-exp(-1*Kw*t_tr);
thetaom=theta*(1-cd+xi*fistar*((phi_1-1)*kappa1+cd*(kappa1+1)));    %product
cut of UF6-235
gamma=(1-Beta_m*thetaom)/(1-thetaom);

%thetaod=theta*(1-cd+xi*((phi_1-1)*lambda1*fid_d-(1-phi_d)*fid_d+cd));  %if
dimer product cut is of interest

%% Nucleation and Growth

Nstar=2;
yc=.20;                              %condensation fraction (i.e. 20%)
ZNstar=(2^(7/2))*(((Nstar-1)^(1/2))/((Nstar^(10/3))*(Nstar+1)));
squigglec=exp(-1*Da/(k*T))*(1-exp(-1*epsilona/(k*T)));
g=(1-(1+(.25*epsilona^2)/(Da*k*T))*(exp((-
.25*epsilona^2)/(Da*k*T))))/squigglec;
lambdastar=squigglec*ZNstar*(g^-2)*((log(1+g))^Nstar);
nQ=.97*10^19*Pq/T;
omegaQ=1.66*Mq/rhoq;
tau4=((1.65*10^-49)*(nQ^4)*((T/Mq)^2)*(omegaQ^(8/3))*lambdastar)^(-1/4);
tc=tau4*(((yc^-1)-1)^(1/4));        %amount of seconds before condensation

cut(count)=thetaom;
factor(count)=Beta_m*(1-xi)/(1-(Beta_m*xi));
end
```

Appendix 2: Ideal Symmetric Cascade Design Program

```
%% Separative Work Calculations

xp=.85;                                 %molar fraction of U-235 in product
xw=.00221;                              %molar fraction of U-235 in tails/waste
xf=.0072;                               %molar fraction of U-235 in feed

P=10;                                   %required amount of product in kg
F=P*((xp-xw)/(xf-xw));                  %feed amount based on product required
W=F-P;                                  %waste from process in kg
S=P*(2*xp-1)*log(xp/(1-xp))+W*(2*xw-1)*log(xw/(1-xw))-F*(2*xf-1)*log(xf/(1-
xf));        %separative work (kgSWU)

cs=40;                                  %cost per separative work unit
Cost=S*cs;                              %cost to acheive a certain product mass

alpha=1.20;                             %stage enrichment factor, alpha
beta=sqrt(alpha);                       %heads separation factor, beta
gamma=0.8169;                           %tails depletion factor, gamma
thetaom=.45;                            %product cut

%% Separative Work per Stage

delta_z=(thetaom*(1-thetaom)*(alpha-1)^2)/2;
z=.042;                                 %stage feed composition
delta_z2=(1/(gamma-1))*(gamma*(beta-1)*log(gamma)-(gamma-
1)*log(beta)+z*((beta+1)*(gamma-1)*log(beta)-(gamma+1)*(beta-1)*log(gamma)));

%% Ideal Cascade Construction
n=(2*log((xp*(1-xw))/((1-xp)*xw))/log(alpha))-1;
n_s=(log(xf*(1-xw)/((1-xf)*xw))/log(beta))-1;

n_s=ceil(n_s);
n=ceil(n);
n_e=n-n_s;

i=n_s:1:n;
j=0:1:n_s;

Mj_s=(W./(beta-1)).*(xw.*beta.*((beta.^j)-1)+(1-xw).*(1-(beta.^-j)));
Mj_e=1+(P./(beta-1)).*(xp.*(1-(beta.^(i-n)))+(1-xp).*beta.*((beta.^(n-i))-
1));

Mj_s=.5*Mj_s;
Mj_e=.5*Mj_e;

Mj=[Mj_s Mj_e(2:length(Mj_e))];

plot(Mj_s,j,Mj_e,i,-1*Mj_s,j,-1*Mj_e,i)
xlabel('Heads flow rate')
ylabel('Stage Number')
```

Appendix 3: Two-Up One-Down Asymmetric Reactor Cascade

```
%% Ideal, Two-up, One-down Cascade with Constant Cut (from Olander & BPL)

%could include derivation for number of stages and mole fractions

nS=6;
n=16;

xf=.0072;
xp=.0513;
xw=.00204;
xq=.0431;

alpha=1.71;
beta=alpha^(2/3);
gamma=alpha^(1/3);

r=((1/(gamma*(gamma+1)))+(1/(gamma*(gamma-1)*(2*gamma+1)))-(1/((gamma-
1)*(gamma+2))))*((-1/(gamma+1))^(nS-1))-((1/((gamma-
1)*(2*gamma+1)))*((1/gamma)^nS))+(1/((gamma-1)*(gamma+2)));
s=((1-(gamma^2/((gamma-1)*(2*gamma+1)))+(1/((gamma-1)*(gamma+2))))*((-
(gamma+1))^(n-nS)))+(gamma^(n-nS+2)/((gamma-1)*(2*gamma+1)))-(1/((gamma-
1)*(gamma+2)));
t=(((-gamma/((gamma-1)*(2*gamma+1)))+(1/((gamma-1)*(gamma+2))))*((-
(gamma+1))^(n-nS)))+(gamma^(n-nS+1)/((gamma-1)*(2*gamma+1)))-(1/((gamma-
1)*(gamma+2)));

Q_P=(r*((gamma^(n+2))-(gamma^(nS+1)))-s*(gamma^(nS+1)-1))/(t*(gamma^(nS+1)-
1)-r*(gamma^(n+1)-gamma^(nS+1)));
W_P=(t*(gamma^(n+2)-gamma^(nS+1))-s*(gamma^(n+1)-
gamma^(nS+1)))/(t*(gamma^(nS+1)-1)-r*(gamma^(n+1)-gamma^(nS+1)));

j=1:1:nS;
i=nS:1:n;

Mi_P=((-(gamma+1)).^(n-i))-(((gamma.*(gamma+Q_P))./((gamma-
1).*(2.*gamma+1))).*(((-(gamma+1)).^(n-i))-(gamma.^(n-
i))))+(((1+Q_P)/((gamma-1).*(gamma+2))).*(((-(gamma+1)).^(n-i))-1));

k=(1/(gamma*(gamma+1)))+(1/(gamma*(gamma-1)*(2*gamma+1)))-(1/((gamma-
1)*(gamma+2)));
Mj_W=(k*((-1/(gamma+1)).^(j-1)))-((gamma.^(-j))/((gamma-
1)*(2*gamma+1)))+(1/((gamma-1)*(gamma+2)));

P=31867;
W=(Mi_P(1)/Mj_W(6))*P;
F=W+P+Q_P*P;

Mj=Mj_W*W;
Mi=Mi_P*P;

M=[0 Mj Mi(2:11)];
```

```
yaxis=0:1:n;
M=M'*.5;
plot(M,yaxis,-M,yaxis)
xlabel('Material Flow');
ylabel('Stage Number')
%% Separative Work

Q=Q_P*P;

F=(P*xp+W*xw+Q*xq)/xf;

SWU=P*(2*xp-1)*log(xp/(1-xp))+Q*(2*xq-1)*log(xw/(1-xw))+W*(2*xw-1)*log(xw/(1-
xw))-F*(2*xf-1)*log(xf/(1-xf));
```

Appendix 4: 2-Up 1-Down Asymmetric Weapons Cascade Design

```
%% Ideal, Two-up, One-down Weapons Cascade with Constant Cut (from Olander &
BPL)

xf=.0072;
xp=.948;
xw=.002031;

alpha=1.72;
beta=alpha^(2/3);
gamma=alpha^(1/3);

xq=xp/gamma;

nS=(log(xf/xw)/log(gamma))-1;
n=(log(xp/xw)/log(gamma))-2;
%%
nS=round(nS);
n=round(n);
%%

r=((1/(gamma*(gamma+1)))+(1/(gamma*(gamma-1)*(2*gamma+1)))-(1/((gamma-
1)*(gamma+2))))*((-1/(gamma+1))^(nS-1))-((1/((gamma-
1)*(2*gamma+1)))*((1/gamma)^nS))+(1/((gamma-1)*(gamma+2)));
s=((1-(gamma^2/((gamma-1)*(2*gamma+1)))+(1/((gamma-1)*(gamma+2))))*((-
(gamma+1))^(n-nS)))+(gamma^(n-nS+2)/((gamma-1)*(2*gamma+1)))-(1/((gamma-
1)*(gamma+2)));
t=(((-gamma/((gamma-1)*(2*gamma+1)))+(1/((gamma-1)*(gamma+2))))*((-
(gamma+1))^(n-nS)))+(gamma^(n-nS+1)/((gamma-1)*(2*gamma+1)))-(1/((gamma-
1)*(gamma+2)));

Q_P=(r*((gamma^(n+2))-(gamma^(nS+1)))-s*(gamma^(nS+1)-1))/(t*(gamma^(nS+1)-
1)-r*(gamma^(n+1)-gamma^(nS+1)));
W_P=(t*(gamma^(n+2)-gamma^(nS+1))-s*(gamma^(n+1)-
gamma^(nS+1)))/(t*(gamma^(nS+1)-1)-r*(gamma^(n+1)-gamma^(nS+1)));

j=1:1:nS;
i=nS:1:n;

Mi_P=((-(gamma+1)).^(n-i))-(((gamma.*(gamma+Q_P))./((gamma-
1).*(2.*gamma+1))).*(((-(gamma+1)).^(n-i))-(gamma.^(n-
i))))+(((1+Q_P)/((gamma-1).*(gamma+2))).*(((-(gamma+1)).^(n-i))-1));

k=(1/(gamma*(gamma+1)))+(1/(gamma*(gamma-1)*(2*gamma+1)))-(1/((gamma-
1)*(gamma+2)));
Mj_W=(k*((-1/(gamma+1)).^(j-1)))-((gamma.^(-j))/((gamma-
1)*(2*gamma+1)))+(1/((gamma-1)*(gamma+2)));

P=50;
W=(Mi_P(1)/Mj_W(6))*P;
F=W+P+Q_P*P;

Mj=Mj_W*W;
```

```
Mi=Mi_P*P;

M=[0 Mj Mi(2:(n-nS+1))];
yaxis=0:1:n;
M=M'*.5;
plot(M,yaxis,-M,yaxis)
xlabel('Material Flow');
ylabel('Stage Number');
title('Weapons Production SILEX Cascade');

%% Separative Work

Q=Q_P*P;

F=(P*xp+W*xw+Q*xq)/xf;

SWU=P*(2*xp-1)*log(xp/(1-xp))+Q*(2*xq-1)*log(xw/(1-xw))+W*(2*xw-1)*log(xw/(1-
xw))-F*(2*xf-1)*log(xf/(1-xf));
```

Appendix 5: SILEX Molecular Physics Derivation

The physics and relations described in this section are summarizations and direct transfer of mathematical equations developed in [13] and [75]. For the sake of brevity, the information is not constantly cited, but important contributors are noted where appropriate. The descriptions are summaries of explanations given in [13] and should not be considered original work.

1. Laser Excitation of QF_6

The rate of excitation in the supersonic flow by absorption of a photon is represented by K_A

$$K_A = \Phi_L \sigma_A \ \ s^{-1} \text{ per } {}^{i}QF_6 \text{ molecule}$$

where σ_A represents the laser photon absorption cross-section (cm^2). As the temperature decreases the cross section has sharper and higher peaks. Typical values for temperatures at 150 K and ν_1 or ν_3 are 10^{-18} cm^2 and 10^{-22} cm^2 respectfully.

$$\Phi_L = \frac{5.055*10^{22} I_L(\frac{W}{cm^2})}{\varepsilon_L}$$

Φ_L represents the laser flux, the photons per cm^2 per second emitted by the laser apparatus. The variable ε_L is the vibrational excitation quantum number, where $\varepsilon_L = h\nu_L$ and represents the laser photon energy in cm^{-1}. For example, for the ν_3 vibrational level of $^{235}UF_6$, $\varepsilon_L = \varepsilon_3 = 628.3 cm^{-1}$. Lastly, I_L represents the intensity of the laser, which of course is dependent on the power and type of laser selected. For the sake of example, in the case of $^{235}UF_6$, with an intensity of 1000 $\frac{W}{cm^2}$, the excitation rate K_A is equal to $8.02*10^4$ moleculelar excitations per second.

2. De-excitation by Spontaneous Emission (Process 1)

Spontaneous emission occurs when a photon of energy equal to the quanta of energy absorbed by a molecule is re-emitted as the molecule, in this case $^{235}UF_6$, returns to its ground state. The rate at which this process occurs is known as the "Einstein rate" for spontaneous emission.

$$AE_{SE} = \frac{32\pi^3}{3}[\frac{e^2}{\hbar c}][\frac{c\Re_{01}^2}{\lambda_3^3}]$$

$$= [\frac{8\pi^2}{3}][\frac{e^2}{c}][\frac{Z_3}{\lambda_3}]^2[\frac{1}{M_3}]$$

where Z is the derivative dipole change determined by measurements and where

$$\Re_{01}^2 = (\frac{\hbar}{4\pi c})\frac{\lambda_3 Z_3^2}{M_3} \ cm^2$$

so that

$$AE_{SE} = 1.220 * 10^4 [\frac{Z_3^2}{\lambda_3}](\frac{1}{M_3}) \ s^{-1}$$

M_3 is vibrational mass, given by Krauss 1967, also for UF_6 the excitation wavelength is $\lambda_3 = 15.9 \mu m$.

Experimental measurements for UF_6 give an Einstein rate of 12 s^{-1} or a single spontaneous emission every .083 seconds. Thus for transit times within the supersonic free jet that are less than several milliseconds (2-3) any losses of excitation by spontaneous emission are unlikely to occur within the system. Similarly, if dimer excitation is the primary means of excitation, rather than monomer excitation, then when QF_6:G or QF_6:QF_6 dimers are excited by laser absorption the process of predissociation prevails over relaxation. In other words spontaneous emission is once more held to a minimum and few (if any) photons are emitted.

3. Collision Induced Reactions

Although several modes of collisions are possible within the gas mixture, the vast majority occur between carrier gas molecules. These inert gas interactions are able to produce dimers or undergo elastic collisions, but these modes of interaction are not especially relevant to enrichment rates. The most significant interaction, that affects the outcome of enrichment, is the collision induced reactions between UF_6 and the carrier gas molecules. It is also possible to have collisions that occur between UF_6 molecules. These types of interactions can lead to the formation of homodimers, the formation of homodimers causes isotope scrambling, a phenomenon which must be minimized at all cost. In order to minimize such interactions the ratio of carrier gas to UF_6 must be quite large, approximately 20:1, to minimize the effects of isotope scrambling. The collision rate for interactions between a UF_6 molecule and a molecule M (M=G or UF_6) is defined as K_c, where:

$$K_c = n_m \sigma_{CQ/M} \bar{u}_{Q/M}$$

$$K_c = \frac{1.41 * 10^7 \sigma_{CQ/M} p_M}{\sqrt{T M_{Q/M}}}$$

n_m is the molecular density (cm^{-3}) of M.

$\sigma_{CQ/M} = \pi (r_{OQ} + r_{OM})^2$ is the collision cross section ($Å^2$) for QF_6 + M

$\bar{u}_{Q/M}$ is the relative molecular velocity (cm/s)

$$\bar{u}_{Q/M} = \sqrt{\frac{8}{\pi} \frac{kT}{M_{Q/M}}}$$

p_m is the partial pressure of the gas M (torr)

$M_{Q/M}$ is the reduced mass of the two particles that collide

r_{OQ}, r_{OM} are molecular contact radii of UF_6 and G

For UF_6 diluted at .01 torr Argon at T=50 K, $K_c(\frac{UF_6}{Ar}) = 9.88*10^5$ collisions per seconds. (Additional K_c rates are found in Table 1A of [13]). The mean free path, or average distance between collisions, ℓ_c, for UF_6 diluted in G at temperature T is:

$$\ell_c = (n_g \sigma_{CQ/G})^{-1} = \frac{1.04*10^{-3} T}{\sigma_{CQ/G} p_G}$$

Functionally the value for $\sigma_{CQ/G}$ is equivalent to $\sigma_{CQ/M}$ or M=G, as long as interactions being considered are solely between the carrier gas and UF_6. This is a valid assumption if the ratio of carrier gas to uranium hexafluoride is large. The variable p_G represents the the carrier gas partial pressure. There are several important observations to make about these collisions. The vast majority of UF_6+M interactions result in elastic collisions, these do not involve the formation of polymers (dimers, trimers, etc.). Some interactions do cause the formation of UF_6 dimers, the majority of which are UF_6:G dimers. For excited molecules, UF_6^*, that interact with the carrier gas, dimers can be formed and decay using vibrational to translational conversions (VT) or vibrational to vibrational (VV) transfers of energy. Each of these processes have a defined probability of occurrence, once again minimizing VV conversions is important to inhibit isotope scrambling. The net energy distribution of the gas is not changed but VV isotopic exchanges can scramble excitation, as seen in the following equation:

$$^{235}UF_6^* + {}^{238}UF_6 \rightarrow {}^{235}UF_6 + {}^{238}UF_6^*$$

It is important to minimize "isotope scrambling" so high dilution of the gas undergoing separation with the carrier gas is necessary.

4. Direct Specular VT Relaxation (Process 2)

The process of VT relaxation for an excited molecule of UF_6 is:

$$^{i}UF_6^* + G \rightarrow {}^{i}UF_6^* : G \rightarrow {}^{i}UF_6 + G + \text{K.E.}$$

The amount of kinetic energy transferred to the $^{i}UF_6$ is dependent on the mass of the carrier gas. For example, the mass of SF_6 is much larger than the mass of Ar or Xe, which if used would ensure that more kinetic energy would be passed to the U-235 molecule. The rate at which this process occurs can be determined by the following relation:

$$K_{VT} = K_c \wp \text{ collisions per second}$$

where $\wp VT3$ (the probability of VT relaxation for the ν_3 energy level) is equal to:

$$\wp_{VT3} = \frac{8kT}{\varepsilon_3} \frac{M_3}{M_{Q/G}} \zeta_3^2 F_A F_C e^{\frac{\varepsilon_3}{2kT}}$$

therefore, because $\varepsilon_3 = \hbar\nu_3$, assume that $\zeta_3^2 F_A : .25$, which simplifies $\wp_{VT3}$ to:

$$\wp_{VT3} = \frac{2kT}{\varepsilon_3}\frac{M_3}{M_{Q/G}} F_C e^{\frac{\varepsilon_3}{2kT}}$$

where the collision function F_c is:

$$F_c(X) = (1 + .4548X^{\frac{5}{6}})(1.5X^{\frac{1}{3}})^2 \operatorname{csch}^2(1.5X^{\frac{1}{2}})$$

$$\text{and } X = X_{Q/G} = \frac{.21 M_{Q/G} L_R^2 \Delta\varepsilon^2}{\Delta T}$$

where L_R is repulsive range parameter in Å

$\Delta\varepsilon = \varepsilon_3$ equals the energy quantum that is V – T converted (cm^{-1})

For values of X greater than 20, $F_c(X)$ reduces to:

$$F_c(X) = 4(\frac{\pi}{3})^{\frac{1}{2}} X^{\frac{3}{2}} e^{-3X^{\frac{1}{3}}}$$

These types of VT de-excitations can also occur when ${}^{i}UF_6^*$ and ${}^{j}UF_6$ collide (the superscripts of i and j connotate U-235 and U-238 respectively). However, there is a much lower probability for such interactions between different isotopes of UF_6, they are more likely to experience resonant VV interactions that will induce isotope scrambling. A further resource for $\wp_V T$ probabilities can be found for a variety of gases in Table 1B of [13].

5. Direct Specular Resonant VV Transfers

This specific type of interaction does not involve the carrier gas, and as mentioned previously occur when ${}^{i}UF_6^*$ and ${}^{j}UF_6$ interact. This type of energy transfer can be minimized by increasing the ratio of carrier gas to UF_6. The process involved in a resonant VV transfer is the following:

$${}^{i}UF_6^* + {}^{j}UF_6 \rightarrow {}^{i}UF_6^* : {}^{j}UF_6 \rightarrow {}^{i}UF_6 + {}^{j}UF_6^*$$

The contact probability for this process of energy transfer is:

$$\wp_{VV3} = \mathsf{T}_3 \Re_3 = (\frac{M_3}{M_{Q/Q}})(\frac{kT}{\varepsilon_3}) X_3$$

where $\mathsf{T}_3 \equiv \mathsf{T}(QF_6(\nu_3)/QF_6)$

$$= 16kT(\frac{\zeta_3^2}{\hbar^2})(\frac{M_3^2}{M_{Q/Q}})F_A F_C e^{\frac{-|\Delta\varepsilon|}{2kT}}$$

$$\cong 4(\frac{kT}{\hbar^2})(\frac{M_3^2}{M_{Q/Q}})$$

$$\text{where } \Re_3 \equiv \Re(QF_6(\nu_3)/QF_6)$$

$$= \frac{1}{2}[\frac{\hbar^2}{M_3\varepsilon_3}]\Omega_{anh} = \frac{\hbar^2 X_3}{4M_3\varepsilon_3}$$

The fundamental frequency, ν_b, is in this case ν_3; the anharmonic constant, X_b, is X_3; the mass constant, M_b, is M_3; and the steric collision factor, ζ_b^2, is ζ_3^2. The steric collision factor can be assumed to be 0.25 and F_c=1. Also, the reduced mass in this case will be $\frac{1}{2}M_Q$, this is a slight simplification due to the fact that the isotopic masses of U-235 and U-238 will be almost identical.

The rate of resonant VV transfer, K_c, can be shown to be:

$$K_c = \tau_{VV}^{-1} = \wp_{VV3} Y_Q C_{Q/Q} K_c \quad s^{-1}$$

where Y_Q is the mole fraction of QF_6 in gas mixture

and $C_{Q/Q}$ is a correction factor for cross-section and mass difference between ${}^{i}UF_6^*$ and ${}^{j}UF_6$

For example, using Table 1 values at 50 K, $\wp({}^{i}UF_6^*/{}^{j}UF_6) = 6.40*10^{-5}$ for two percent UF_6 in 10^{-2} torr Argon, which will have a rate for VV transfer of $4.237*10^2$ molecules per second. In terms of time, τ_{VV}, the time between such interactions would be $2.36*10^{-3}$ seconds per collision.

6. Dimer Formation Rates

The formation of dimers within the flow can be expressed by the following probability (derived in [75]):

$$\wp_{df} = f_{2Q/M}\nu_d\wp_0(1-(1+\eta_*)exp(-\eta_*))$$

where:

$$\eta_* = \varepsilon_*/kT = .25(\varepsilon_\alpha)^2/(D_\alpha kT)$$

$$i_* = 1-(1+\eta_*)exp(-\eta_*)$$

$$f_{2Q/M} = (y_Q M_Q + y_M M_m)(y_Q M_M/M_Q + y_M M_Q/M_M)/(M_Q + M_M + y_Q M_Q + y_M M_M)$$

$$\nu_d = 2D_\alpha/\varepsilon_\alpha - .5$$

$$\wp_0 = \wp_1 exp(-\wp_1)$$

$$\wp_1 = 2\rho_{Q/M}(kT/\varepsilon_\alpha)exp(-.5\eta_*)$$

$$\rho_{Q/M} = M_M(2M_Q + M_M)/(M_Q + M_M)^2$$

Theses variables represent molecular masses and mole fractions, where M=G and Q=UF_6. The variable ν_d represents the highest dissociation vibrational quantum level in the potential well of the dimer that is formed. Here ε_a is the fundamental energy quantum and D_α is the depth of the dimer bond. All of these values are available for different combinations of gases in open literature (Eerkens 2001a). The formation rate for dimers can be expressed as:

$$k_{df} = k_c \wp_{df} \quad s^{-1}$$

7. Collisional Dissociation Rates of Dimers

The following process describes the dissociation of dimers a a result of collisions between molecules. This on the fact that the partial pressure of UF_6 is less than the nucleation pressure for homogeneous clusters. This simply requires that the molar fraction of UF_6 within the gas is less than 5 percent. The dimer dissociation rate is described as follows:

$$k_{dd} = k_{cd}\wp_{dd} = k_c a_d \wp_{dd}$$

where:

$$\wp_{dd} = .5(exp(-D_\alpha/kT))(1-exp(-\varepsilon_\alpha/kT)$$

$$a_d = ((r_{oQ} + 2r_{oG})/(r_{oQ} + r_{oG}))^2/(1 + M_G^2/(M_Q^2 + 2M_Q M_G))^{.5}$$

These variables have been all used previously with the exception of the contact radii r_{xx}, these are available in Eerkens 2005.

8. Radial Molecular Migrations and Jet Escapes

Within the supersonic jet molecules migrate from position to position. The molecules of interest are those $^{235}UF_6$ that are able to escape the jet and be collected in flow that bypasses the skimmer. The jet can be modeled as a cylindrical flow with some rate constant of jet escapes per second. These rates are derived in [75] and are listed below, beginning with the escape rate for non-excited and vibrationally excited monomer molecules:

$$k_w = 29.3T^{3/2}/(p_G R^2 \sigma_{cQ/G} M_{Q/G}^{1/2}), s^{-1}/\text{molecule}$$

where R is the radius of the cylindrical flow, and $\sigma_{cQ/G}$ is collision cross-section of the carrier gas

and the UF_6.

The next equation represents the epithermal migration rate of molecules outside of the cylindrical flow.

$$k_{w1} = \mu_1 k_w$$

where:

$$\mu_1 = (a/ln(1+a))^{1/2}$$

and

$$a = \varepsilon_Q/\varepsilon_T = \eta_{Q/G}\varepsilon_a/\varepsilon_T$$

with:

$$\varepsilon_T = kT \text{ and } \varepsilon_Q + \varepsilon_T = (1+a)\varepsilon_T \text{ and } \varepsilon_a = \varepsilon_3$$

Furthermore k_{w1} can be written as:

$$k_{w1} = 1.928\mu_1(\ell_c/R)^2 k_c$$

The thermal escape fraction, given by θ_1 is:

$$\theta_1 = 1 - exp(-\mu_1 k_w t_{tr})$$

Then for a rate to describe the population of dimers that move at thermal energies, where the collision cross-section is higher as is the reduced mass, a new expression must be given to describe the population that escapes the flow, called k_{wd}.

$$k_{wd} = \phi_d k_w = 1.928(\ell_c/R)^2 \psi_d k_c$$

$$\psi_d = ((r_{oQ} + r_{oG})/(r_{oQ} + 2r_{oG}))^2/(1 + M_G^2/(M_Q^2 + 2M_Q M_G))^{1/2}$$

with dimer escape fraction of:

$$\theta_d = 1 - exp(-\psi_d k_w t_{tr})$$

9. Slowing Down for Epithermal Molecules

Then using "Fermi Age Theory" it is possible to obtain a rate of thermalization for the epithermal population. This theory was developed in 1952 by Glasstone and Edlund. The average number of collisions necessary to bring an epithermal back to thermal energies is described by the following:

$$N_T = \zeta_{-1} ln(1 + \varepsilon_Q/\varepsilon_T) = \zeta_{-1} ln(1+a)$$

where

$$\zeta = 1 + (\alpha/(1-\alpha))ln(\alpha)$$

and

$$\alpha = ((M_Q - M_G)/(M_Q + M_G))^2$$

The thermalization rate for epithermals becomes:

$$k_{th} = \mu_1 k_c/N_T$$

This rate is fairly large which means that epithermals are forced to cycle between existing as thermal monomers and excited monomers. This process as discussed in the introduction to this section is part of the rapid cycling between monomers as they move from excitation to dissociation to epithermalization to re-thermalization. In order to determine the fraction of migration of the UF_6 it is necessary to consider the population fractions, which in turn will allow the enrichment factor

associated with the process to be determined.

10. Population of Dimers, Excited, and Epithermal Molecules Under Monomer Excitation

There are four distinct groups of particles in the flow, the excited monomer (*), the unexcited monomer (m), the epithermal (!), and the non-excited dimer (d). The fraction of these particles must add up to one as is expected:

$$f_{i*} + f_{i!} + f_{im} + f_{id} = 1$$

Skipping the derivation of intermediate properties it can be determined that the to the wall survival probability for an excited monomer is:

$$e_* = exp(-.519(R/\ell_c)^2) \ \ s^{-1}$$

and the wall survival probability for an epithermals is:

$$e_1 = exp(-.519(R/\ell_c)^2/N_T)$$

and the fractions for each of the populations can be shown to equal the following expressions:

$$f_{i*} = (1 + \kappa_1 + k_{df}/((1-\omega_d)k_A)^{-1}$$

$$f_{i!} = \kappa_1 f_{i*}$$

$$f_{id} = (1-(\kappa_1 + 1)f_{i*})\omega_d$$

$$f_{im} = 1 = f_{id} - f_{i!} - f_{i*}$$

where:

$$\kappa_1 = (1-e_*)(k_{df} + k_{VT})/((1-e_1)k_{th} + e_1 k_{w1})$$

and

$$\omega_d = k_{df}/(k_{df} + k_{dd})$$

This process neglects to include the laser excitation of epithermals of further excitations of monomers, due to the low probability for such interactions to occur during the process. These equations describe the populations of molecules for a system that uses monomer as its laser induced excitation particle of choice. For dimer laser excitation other expressions must be derived.

11. Expressions for the Populations of Molecules Under Dimer Excitation

The following expressions describe the four group populations under a dimer excitation scheme (likely the scheme used by GLE in their SILEX facility):

$$f_{id} = k_d f/((1 + \lambda_1)k_{df} + k_A)$$

$$f_{i!} = \lambda_1 f_i d$$

with

$$\lambda_1 = k_A.((1-e_1)k_{th} + e_1 k_{w1}$$

$$f_{i!d} = (f_{i!})d = [1 + k_{th}/k_{df} + (k_{th}/k_A)(1 + k_{dd}/k_{df})]^{-1}$$

$$f_{idd} = (f_{id})d = [1 + k_A/k_{th} + k_A/k_{df} + k_{dd}/k_{df}]^{-1}$$

Although dimer excitation is possible, it is likely that monomer excitation is more favorable for production capability. This is due to the fact that the higher and larger cross-sections add an order of magnitude higher to the cross-section of the $^{235}UF_6$ monomer molecules. The following section will define the enrichment factor for the entire process.

12. Enrichment Factor for Monomer Excitation

The enrichment factor β_m is defined as the ratio of the isotopic abundance of the product material over the isotopic fraction of feed material ($x_i^{'}/x_i$). Therefore, since we are given the initial isotopic fraction, x_i =.0072, the only variable that needs to be defined is $x_i^{'}$.

$$x_i^{'} = [Escaped\,^{'}UF_6]/[EscapedUF_6]$$

which leads to an expression for β_m of:

$$\beta_m = (1-\omega_d(1-\theta_d)(1-(\kappa_1+1)f_{i*}) + \kappa_1 f_{i*}(\phi_1 - 1))/(1-\omega_d(1-\phi_d) + x_i f_{i*}((phi_1 - 1)\kappa_1 + \omega_d(1-\phi_d(\kappa 1+1)))$$

where

$$\phi_1 = (1-exp(-\mu_1 k_W t_{tr}))/(1-exp(-k_w t_{tr}))$$

$$\phi_d = (1-exp(-\psi_d k_w t_{tr}))/(1-exp(-k_w t_{tr}))$$

13. Enrichment Factor for Dimer Excitation

In a similar context to monomer excitation the enrichment factor for dimer excitation is represented by the following expression:

$$\beta_d = (1+((\theta_1 - 1)\lambda_1 - 1 + \theta_d)f_{idd})/(1-c_d(1-x_i) + x_i f_{idd}((\theta_1 - 1)\lambda_1 - 1 + \theta_d))$$

where

$$c_d = \omega_d(1-\theta_d)$$

14. Product Cuts for Excitation

The product output cut of a separation process refers to the fractional loss of the target particle in the feed stream in comparison to the product stream. The product cut for the monomer excitation process is:

$$\sigma_{om} = \sigma[1 - c_d + x_i f_{i^*}((\phi_1 - 1)\kappa_1 + c_d(\kappa_1 + 1))]$$

and for the dimer excitation process is:

$$\sigma_{od} = \sigma[1 - c_d + x_i((\phi_1 - 1)\lambda_1 f_{idd} - (1 - \phi_d) f_{idd} + c_d))$$

To understand the derivations of all equations and full theoretical basis for this laser isotope separation process please review the papers from which the equations shown in this thesis are taken. The two most useful are Dr. J.W. Eerkens' [75] and [13]. The previous appendices described how the physics equations shown here were translated into a MATLAB program (Appendix 1, 2) and an optimal set of conditions for SILEX operation was determined.

Bibliography

[1] "American Centrifuge Overview." *United States Enrichment Corporation (USEC)*. American Centrifuge Project Presentation at Governor's Energy Summit (December 2011): 1-12.

[2] Beyer, Clark; Combs, Jeff. "A distorted market." *Nuclear Engineering International*. (September 2002): 1-5. <http://www.neimagazine.com/features/featurea-distorted-market/>

[3] Casper, Barry M. "Laser Enrichment: a new to proliferation?" *Bulletin of the Atomic Scientists* 33, Issue 1/2 (January 1977): 28-41.

[4] Central Intelligence Agency: Directorate of Intelligence. "Declassified Report on French Development of LIS". *Science and Weapons Daily Review* (August 1984): 8-10.

[5] Central Intelligence Agency: Directorate of Intelligence. "Weekly Surveyor: PRC Laser Isotope Technology Research May Be Under Way." (January 1975): 1-3.

[6] Central Intelligence Agency: Directorate of Intelligence. "Uranium Enrichment: Threat of Nuclear Proliferation Increasing." (April 1982): 9.

[7] Central Intelligence Agency: Directorate of Intelligence. "Soviet Research on Uranium Laser Isotope Separation." *Supplement to Scientific Intelligence Digest* (September 1976): 1-6.

[8] Central Intelligence Agency: Directorate of Intelligence. "Soviet Research on Laser Isotope Separation for Uranium Enrichment." (September 1985): 3-14.

[9] Central Intelligence Agency: Directorate of Intelligence. "China: Shift in Laser Isotope Separation Program." *Science and Weapons Daily Review* (February 1986): 2-3.

[10] Clinton, William J. "Agreement for Cooperation between the United States of America and Australia Concerning Technology for the Separation of Isotopes of Uranium by Laser Excitation—Message from the President," *Congressional Record—Senate, S13793* (November 3, 1999).

[11] Crawford, Allison. "GLE Continues Negotiations for PGDP Depleted Uranium Despite Drop in Market." *Murray State Public Media*, July 31, 2014. <http://wkms.org/post/gle-continues-negotiations-pdgp-depleted-uranium-despite-drop-market>

[12] "Deconversion of Depleted Uranium." Nuclear Regulatory Commission (Updated October 2014). http://www.nrc.gov/materials/fuel-cycle-fac/ur-deconversion.html

[13] Eerkens, Jeff W. "Laser-induced migration and isotope separation of epi-thermal monomers and dimers in supercooled free jets." *Laser and Particle Beams 23* (2005): 225-253.

[14] Eerkens, Jeff; Miller, William H. "Laser Isotope Separation Employing Condensation Repression." *Nuclear Science and Engineering Institute, University of Missouri* (2003). <http://www.osti.gov/energycitations/product.biblio.jsp?osti_id=912774>

[15] Eerkens, Jeff; Kim, Jaewoo. "Isotope Separation by Selective Laser-Assisted Repression of Condensation in Supersonic Free Jets." *AIChE Journal 56, Issue 9* (September 2010): 2331-2337.

[16] Energy Information Agency, Frequently Asked Questions. "How much electricity does an American Home Use." (2013): 1-2. <http://www.eia.gov/tools/faqs/faq.cfm?id=97&t=3>

[17] Energy Information Agency. "Uranium Marketing Annual Report 2013." (May 12, 2014). <http://www.eia.gov/uranium/marketing/>

[18] "Enrichment; Lessons that can be learnt from an Abandoned Project." *Nuclear Engineering International Vol. 45 No. 556* (November 2000): 43-44.

[19] Fargo, Matthew. "The Commercialization of Laser Enrichment." *Center for Strategic and International Studies* (July 7, 2012).

[20] Ferguson, Charles; Boureston, Jack. "Laser Enrichment: Separation Anxiety." *Bulletin of Atomic Scientists 60, Issue 2* (March/April 2005): 14-18. http://www.cfr.org/world/laser-enrichment-separation-anxiety/p7876

[21] "Gas Centrifuge Enrichment Facility Licensing." Nuclear Regulatory Commission (Updated May 2014). http://www.nrc.gov/materials/fuel-cycle-fac/gas-centrifuge.html

[22] GLE, "Revision 7 to Global Laser Enrichment License Application-Public Version." *Submission to Uranium Enrichment Branch of U.S. Nuclear Regulatory Commission.* (August 20, 2012).

[23] "Hearing before the Subcommittee on Energy Research and Development of the Committee on energy and natural resources United States Senate: Status of the DOE's AVLIS Program." *Senate Hearing 102-318* (September 24, 1991): 1-77.

[24] Heller, Arnie. "Laser Technology Follows in Lawrence's Footsteps." *Science and Technology Review*. Lawrence Livermore National Laboratory, (May 2000). <https://str.llnl.gov/str/Hargrove.html>

[25] "History of USEC." *The Paducah Sun, Paducah Kentucky* (January 2004). <http://www.state.nv.us/nucwaste/news2004/nn12034.htm>

[26] Kaoutzanis, Christodoulos. "Megatons to Megawatts: A Mega-Player of U.S. Nuclear Enrichment." *Georgetown International Environmental Law Review 24, Vol. 1* (Fall 2011): 1-33.

[27] Kemp, R. Scott. "The Nonproliferation Emperor has no clothes." *International Security 38, No. 4* (Spring 2014): 39-78.

[28] Kemp, R. Scott. "Class Lectures on Weaponization of Uranium." *MIT NSE* (Spring 2015).

[29] Kiernan, Vincent. "US Enrichment Corp. Shuts Down AVLIS." *Laser Focus World: Washington Report* (August 1999): 80-81.

[30] Khlopkov, Anton. "How the United States Helped Iran Build a Laser Enrichment Laboratory." *The Nonproliferation Review* 20, no. 1 (February 2013): 39-62. doi:10.1080/10736700.2013.769376.

[31] "Laser Enrichment Update: NRC Issues License." *SPIE* (September 2012) <http://optics.org/news/3/9/34>

[32] Lester, Richard. "Class Notes on Fuel Cycle and Enrichment." *22.812 Managing Nuclear Technology,* MIT NSE, (Spring 2015).

[33] "Low Enriched Uranium from France, Germany, the Netherlands, and the United States." *U.S. International Trade Commission* (USITC) *Publication No. 3486* (February 2002): 3-25.

[34] Lyman, John. "Enrichment Separative Capacity for SILEX." Submitted to SP-1 POTAS Project, Los Alamos National Laboratory, *Federation of American Scientists* (2007). http://www.fas.org/sgp/othergov/doe/lanl/docs4/silex.pdf

[35] "On USEC decision to close Portsmouth." *Congressional Record-House Vol. 146* (statement of Secretary of Energy Bill Richardson) (June 21, 2000): 4912-4913.

[36] Podvig, Pavel; Bukharin, Oleg. "Russian Strategic Nuclear Forces." (2001): 98-102.

[37] Rothwell, Geoffrey. "Market Power in Uranium Enrichment." *Science and Global Security Vol. 17* (2009): 132-154.

[38] Serrato, Ruben. "Laser Isotope Separation and the Future of Nuclear Proliferation." (2010): 85-105.

[39] Shropshire, D.E. "Advanced Fuel Cycle Cost Basis." *INL/EXT-07-12107 Idaho National Laboratory* (April 2007): 1-554.

[40] Slakey, Francis; Cohen, Linda. "Stop Laser Enrichment." *Nature Vol. 464* (March 2010): 32-34.

[41] T. Ridge, "Economic Perspective for Uranium Enrichment." *Los Alamos Science Journal Vol. 3 No. 1* (1982): 6-7.

[42] "Uranium Market Data." The Ux Consulting Company LLC (2014) <http://www.uxc.com/>

[43] Zentner M.D. et al. (September 2005). "Nuclear Proliferation Technology Trends Analysis" *Pacific Northwest National Laboratory-14480* (September 2005): 55-59. http://fissilematerials.org/library/zen05.pdf[44] Becker, E.W.-1982, pg.21 SPIE

[45] "Module 3.0: LASER ENRICHMENT METHODS (AVLIS AND MLIS)" U.S. Nuclear Regulatory Commission Technical Training Center Materials, September 2008, pg. 40-46.

[46] Mizin, Victor. "The Russia-Iran Nuclear Connection and U.S. Policy Options." MERIA Journal. Rubin Center for Research in International Affairs. Vol. 8, No. 1. March 7, 2004.

[47] Duz, Sergei, "U.S. uranium laser enrichment technology threatens NPT" Sputnik News. 26 December 2013.

[48] Arisawa, Takashi. "Laser Isotope Separation Study in JAERI." Bulletin of the Research Laboratory for Nuclear Reactors, Tokyo Institute of Technology, Special Issue 1, pg. 147-152 (1992).

[49] Laser Processing of Materials in Japan: Research, Development, and Applications JTIS pg. 27-29.

[50] Central Intelligence Agency "Brazil's Changing Nuclear Goals: Motives and Constraints." Special National Intelligence Estimate, 21 October 1983.

[51] Barletta, Michael, "The Military Nuclear Program in Brazil." Center of International Security and Arms Control, Stanford University, August 1997.

[52] Albright, David; O'Neill, Kevin, "Argentina and Brazil: The Latin American Nuclear Rapproachement." Institute for Science and International Security, May 16, 1996.

[53] Squassoni, Susan; Fite, David. "Brazil's Nuclear History." Arms Control Today Vo. 25 No. 8, Arms Control Association, October 2005.

[54] Diego Santos Vieira de Jesus "THE BRAZILIAN WAY", The Nonproliferation Review, 17:3, 551-567 (2010).

[55] Albright, David, "Update on Lashkar Ab'ad: Iran's Laser Enrichment Capabilities." Institutoe for Science and International Security, 2014.

[56] Muller, Harald; Kokoski, Richard. "The Non-Proliferation Treaty: Political and Technical Prospects and Dangers in 1990." Stockholm International Peace Research Institute (SIPRI), April 1990.

[57] Spector, L.S. "The New Nuclear Nations" Vintage: New York, 1985, pg. 101.

[58] Woddi, T.V.K.; Charlton, W.S.; Nelson, Paul. "India's Nuclear Fuel Cycle: Unraveling the Impact of the U.S.-India Nuclear Accord." Synthesis Lectures on Nuclear Technology and Society, Morgan & Claypool Publishers, 2009.

[59] Ramana, M.V. "India's Uranium Enrichment Program." INESAP Bulletin, 24 December 2004.

[60] Jha, Saurav. "The Thorium Question: An Interview with India's Nuclear Czar" CNN-IBN News Agency, September 2013.

[61] "Israel's Nuclear Weapons Program" December 1997 <www.nuclearweaponarchive.org/Israel/index.html>

[62] Baeckman, Adolf von. "Nuclear Verification in South Africa." International Atomic Energy Agency Bulletin, January 1995.

[63] "South African Nuclear Chronology" Nuclear Threat Initiative, May 2007. <http://www.nti.org/media/pdfs/south_africa_nuclear.pdf?_=1316466791>

[64] Gorwitz, Mark. "The South Korean Laser Isotope Separation Experience." Institute for Science and International Security, 1996.

[65] Gorwitz, Mark. "The South Korean Laser Isotope Separation Experience." Institute for Science and International Security, 2004.

[66] Benedict, Manson; Pigford, Thomas H.; Levi, Hans W. "Nuclear Chemical Engineering" Second Edition, McGraw-Hill Book Company, 1981.

[67] Eerkens, Jozef. W. "Lectures on SILARC" Massachusetts Institute of Technology, March 2015.

[68] Scott, Jeff. "Shock Diamonds and Mach Disks," 17 April 2005. <www.aerospaceweb.org>

[69] Cohen, Karl. "The Theory of Isotope Separation as Applied to the Large-Scale Production of U235." McGraw-Hill Book Company Inc., 1951.

[70] "Guidelines for Transfers of Nuclear-Related Dual-Use Equipment, Materials, Software, and Related Technology." Nuclear Supplier Group, Part 1, pg. 40-45, June 2013.

[71] "Guidelines for Transfers of Nuclear-Related Dual-Use Equipment, Materials, Software, and Related Technology." Nuclear Supplier Group, Part 2, pg. 30-40, June 2013.

[72] "Generating Parahydrogen." Centre for Hyperpolarization, The University of York, 2013. <http://www.york.ac.uk/res/sbd/parahydrogen/generating.html>

[73] Chandler, David. "Long-sought phenomenon finally detected." MIT News Office, July 15, 2015.

[74] "Lasers: Understanding the Basics." Photonics Handbook®, Coherent Inc. Retrieved 28 January 2016.

[75] Eerkens, Jeff W. "Equilibrium dimer concentrations in gases and gas mixtures." Chemical Physics Vol. 269, pg. 189-241, 2001.

[76] Milani, Kevin. "The Scientific History of the Atomic Bomb." Hibbing Community College, <http://www.hcc.mnscu.edu/chem/abomb/page_id_35050.html>

[77] Olander, Donald R. "Two-Up, One-Down Ideal Cascades for Isotope Separation." Nuclear Technology, Vol. 29, April 1976.

[78] Glaser, Alexander. "Characteristics of the Gas Centrifuge for Uranium Enrichment and Their Relevance for Nuclear Weapon Proliferation." Science and Global Security, Vol. 16, pg. 1-25, 2008.

[79] Refractive index database, Xenon, from Bideau-Mehu et al., 1981 <http://refractiveindex.info>

[80] "STAR-CCM+ Convergent Divergent Nozzle Tutorial." CD-adapco® December 30, 2014 <https://www.youtube.com/watch?v=-mjH7gKUO0o>

[81] U.S. Code of Federal Regulations, section 10, part 110-"Export and Import of Nuclear Equipment and Material" Appendix C, <http://www.nrc.gov/reading-rm/doc-collections/cfr/part110/full-text.html#part110-appc>

[82] MONEL® alloy 400, Special Metals Corporation, SMC-053, February 2005. <http://www.specialmetals.com/assets/documents/alloys/monel/monel-alloy-400.pdf>

[83] Schroeder, C.B.; Fawley W.M. "Statistical properties of radiation power levels from a high-gain free-electron laser at and beyond saturation." Vol. 507 Issue 1-2 11 July 2003, pg. 110-114. dx.doi.org/10.1016/s0168-9002(03)00850-7

[84] F. J. Duarte (Ed.), *Tunable Lasers Handbook* (Academic, New York, 1995) Chapter 9.

[85] R.L. Byer; W.R. Trutna. "Multiple-Pass Raman Gain Cell." Applied Optics Vol. 19 No. 2. 15 January 1980.

[86] "Manufacturing Cost Estimation." Cost Estimator Tools, CUSTOMPART.NET, Accessed Jan. 20 2016.

[87] "How Much Does a Construction Project Cost?" Brown-Wegher Construction Estimate for Conventional Warehouse, Accessed Jan. 21 2016. <www.brownwegher.com/cost-of-construction-chart/>

[88] Rothwell, Geoffrey; "The Cost Structure of International Uranium Enrichment Service Supply." Submitted to Science & Global Security, 23 May 2008.

[89] Gaebler, Frank; "Cost effective, high speed metal cutting laser." The Laser User, Issue 67, Summer 2012, pg. 7.